NASA TECHNICAL NOTE

NASA TN D-6594

NASA TN D-6594

HEAT TRANSFER AND BOUNDARY LAYER IN CONICAL NOZZLES

by Donald R. Boldman and Robert W. Graham

Lewis Research Center
Cleveland, Ohio 44135

NATIONAL AERONAUTICS AND SPACE ADMINISTRATION • WASHINGTON, D. C. • FEBRUARY 1972

1. Report No.	2. Government Accession No.	3. Recipient's Catalog No.
NASA TN D-6594		

4. Title and Subtitle	5. Report Date
HEAT TRANSFER AND BOUNDARY LAYER IN CONICAL NOZZLES	February 1972
	6. Performing Organization Code
7. Author(s)	8. Performing Organization Report No.
Donald R. Boldman and Robert W. Graham	E-6228
	10. Work Unit No.
9. Performing Organization Name and Address	132-15
Lewis Research Center National Aeronautics and Space Administration Cleveland, Ohio 44135	11. Contract or Grant No.
	13. Type of Report and Period Covered
12. Sponsoring Agency Name and Address	Technical Note
National Aeronautics and Space Administration Washington, D. C. 20546	14. Sponsoring Agency Code

15. Supplementary Notes

16. Abstract

A review of a comprehensive experimental investigation of the heat transfer and boundary layer in 30°-15° and 60°-15° conical nozzles at Lewis Research Center is presented. The experiments were conducted with air at a stagnation temperature of 539 K (970° R) and throat Reynolds numbers based on a diameter ranging from 6×10^{5} to 5×10^{6}. Nozzle wall surface finish was varied from a smooth machine finish to a 826×10^{-6} cm (325×10^{-6} in.) rms sandblasted finish. Measured heat transfer and wall temperatures are tabulated.

17. Key Words (Suggested by Author(s))

Turbulent boundary layer
Heat transfer
Turbulence
Nozzles
Roughness
Laminarization

18. Distribution Statement

Unclassified - unlimited

19. Security Classif. (of this report)	20. Security Classif. (of this page)	21. No. of Pages	22. Price*
Unclassified	Unclassified	60	$3.00

* For sale by the National Technical Information Service, Springfield, Virginia 22151

HEAT TRANSFER AND BOUNDARY LAYER IN CONICAL NOZZLES

by Donald R. Boldman and Robert W. Graham

Lewis Research Center

SUMMARY

A review of a comprehensive experimental investigation of the heat transfer and boundary layer in 30°-15° and 60°-15° conical nozzles is presented. The experiments were conducted with air at a stagnation temperature of 539 K (970° R) and at throat Reynolds numbers ranging from 6×10^{5} to 5×10^{6}.

Boundary layer surveys in the 30°-15° nozzle suggested that the ratio of energy to momentum thickness at the throat could be large (possibly as high as 10). Under these conditions a simple integral energy analysis provided good estimates of the high Reynolds number heat transfer (±20 percent) at the expense of a pronounced underprediction in nozzle entrance and exit regions. Incorporation of a modified auxiliary equation relating the heat transfer to an energy thickness and acceleration parameter resulted in improved predictions throughout the nozzles.

Hot wire surveys at Mach 0.08 in the 30°-15° nozzle revealed certain differences in the distributions of intermittency factor and turbulence intensity from the corresponding profiles for unaccelerated flows. The distribution of intermittency factor suggested the presence of a boundary layer mass detrainment phenomenon similar to that observed by others in highly accelerated flows.

Pronounced effects of wall surface finish on nozzle heat transfer were observed at sandblasted roughness levels of less than 826×10^{-6} centimeter (325×10^{-6} in.) rms. Roughness altered the Reynolds number range in which "laminarized" heat transfer was observed as well as the levels of heat transfer in the turbulent boundary layer regime.

INTRODUCTION

The fluid mechanics and heat transfer in an accelerated turbulent flow have been found to be distinctively different from the nonaccelerating case. Consequently, in recent years considerable research effort has been devoted to the study of the effects of acceleration on the boundary layer and heat transfer in various internal and external

flows. Internal flow in a converging-diverging (C-D) nozzle has been one of the more important applications. This report will be devoted to a review and summary of the results of references 1 to 9 which were concerned with the heat transfer and boundary layer in smooth and rough wall C-D nozzles. All of the data to be presented were obtained in a facility at the Lewis Research Center which supplied air at a stagnation temperature of 539 K (970° R).

Experimental results to be discussed include effects of independent variations in pipe inlet length, diameter, and cooling on the boundary layer and heat transfer in smooth wall 30°-15° and 60°-15° half angle water-cooled C-D nozzles (refs. 1 to 5). Some effects of nozzle surface finish on the heat transfer will also be discussed (refs. 6 and 7). Data will be presented for a range of stagnation pressures or local Reynolds numbers in order to illustrate a boundary layer reverse transition or "laminarization" phenomenon as was shown in references 5 and 9. Predictions of the observed results in smooth wall nozzles will be based on various options and modifications of the Bartz integral boundary layer theory (ref. 10), applicable to flows in which the boundary layer does not undergo reverse transition. Such predictions have been rendered, for example, in references 1, 4, and 8.

SYMBOLS

A	area
c_f	skin friction coefficient
D	diameter
h_i	heat transfer coefficient based on enthalpy difference
i	enthalpy
K	acceleration parameter, $\frac{\mu_e}{\rho_e u_e^2} \frac{du_e}{dx}$
l_c	length of inlet which is cooled
l_u	length of inlet which is uncooled
M	Mach number
N	interaction exponent
n	denominator in power law exponent
P	pressure
Pr	Prandtl number

q	heat transfer rate
R	radius
Re	Reynolds number
r	recovery factor
St	Stanton number
T	temperature
u	velocity
$\sqrt{\overline{u'^2}}/u_\infty$	turbulence intensity
x	axial distance from geometric throat
x_a	distance along nozzle wall from onset of acceleration
y	distance from wall
$\bar{z}$	axial distance from throat to nozzle entrance (tables II and III)
β	angular positions of heat meters (tables II and III)
γ	intermittency factor
Δ	thermal boundary layer thickness
δ	velocity boundary layer thickness
ϵ_c	contraction area ratio
θ	momentum thickness
μ	viscosity
ρ	density
φ	energy thickness

Subscripts:

ad	adiabatic wall conditions
D	diameter
e	edge of boundary layer
r	properties based on reference enthalpy condition
s	static condition
t	local stagnation condition in boundary layer or throat condition
w	wall condition

0	free stream stagnation condition
∞	free stream condition

APPARATUS

The experimental approach for studying the fluid mechanics and heat transfer in C-D nozzles makes use of the facility described in reference 1. This tunnel-type air facility, shown in figure 1, had provisions for controlling the uniformity of the flow, the turbulence intensity, and the history of the boundary layer development upstream of the nozzle. The apparatus comprises:

(1) A heater to elevate the temperature of the air

(2) A plenum and screens to straighten the flow

(3) A bleed system to initiate the boundary layer at the leading edge of pipe inlets

(4) A pipe inlet which can be tailored by means of length and cooling to produce the desired boundary layer at the nozzle entrance

(5) A smooth or rough wall nozzle instrumented for heat transfer measurements and local surveys of the boundary layer.

This type of facility lends itself not only to varying geometry situations but also to a range of upstream conditions that affect such parameters as Reynolds number and temperature ratio.

Inlet Configurations

In order to examine the effects of inlet boundary layer history on nozzle heat transfer, five pipe inlet configurations were employed. Three of the inlets were uncooled thus initiating the thermal boundary layer at the entrance of the cooled nozzles. The other two inlets had cooled walls. Typical uncooled (adiabatic wall) and cooled inlets are shown in figures 2(a) and (b), respectively. Dimensions for the five inlets are given in table I. All of the inlets were fabricated from stainless-steel pipe which was machined to an inside surface finish of 163×10^{-6} centimeter (64×10^{-6} in.) rms.

The largest inlets had inside diameters of 16.51 centimeters (6.50 in.) which provided a nominal nozzle contraction area ratio ϵ_c of 18.8. A boundary layer survey station (station 1) was located in each of these inlets as shown in figure 2. In order to decrease ϵ_c, the diameter of the uncooled and cooled inlets was reduced to 7.80 centimeters (3.07 in.). These inlets provided a nozzle contraction area ratio of about 4.2.

Water-Cooled Nozzles

Two water-cooled stainless-steel conical nozzles, each having a nominal throat diameter and throat radius of curvature of 3.8 centimeters (1.5 in.) were used in the investigation. The nozzles had half angles of convergence of 30° and 60° and a half angle of divergence of 15° (hereinafter, these nozzles will be identified by their half angles). Coordinates for the 30°-15° and 60°-15° nozzles are presented in tables II and III, respectively. The expansion area ratios for the 30°-15° and 60°-15° nozzles, given by the ratio of exit to throat area, were 25.3 and 3.32, respectively.

In studies of the effects of nozzle surface roughness on the heat transfer (refs. 6 and 7) the wall was roughened by a sandblasting technique which provided a range of roughness levels up to 826×10^{-6} centimeter (325×10^{-6} in.) rms. The sandblasting technique produced a "natural" type of roughness in which the peaks and valleys were joined by a surface having random gradual curvature rather than vertical faces which could be produced by machining methods.

INSTRUMENTATION

The basic instrumentation was concerned with the measurement of local heat flux, temperatures, pressures, and turbulence. The nozzles were instrumented with 0.318-centimeter- (0.125-in.-) diameter Inconel plug heat flux meters of the type discussed in reference 1. A heat meter was located at each of the stations listed in tables II and III. Local values of heat flux and wall temperature were calculated from the measured temperature gradient along the heat meter.

Boundary layer temperature surveys were obtained with miniature probes of the type described in reference 2. These surveys were obtained at station 1 in the 16.51-centimeter- (6.50-in.-) diameter inlets and at stations 4, 12, 16, 18, and 19a in the 30°-15° nozzle. Temperature surveys were also made at station 4 in the 60°-15° nozzle.

The thermocouples in the temperature probes were of the open ball junction type having ball diameters of 0.0076 and 0.13 centimeter (0.003 and 0.005 in.) and sheath diameters of 0.020 and 0.036 centimeter (0.008 and 0.014 in.), respectively. The smaller size temperature probes were used in the transonic and supersonic portions of the 30°-15° nozzle (stations 12, 16, 18, and 19).

Pressure taps along the nozzle wall provided a distribution of static pressure throughout the nozzle. The pressure taps were located at the stations given in tables II and III.

Total pressure measurements across the boundary layer were made with pressure probes of the type described in reference 2. These pressure probes had a rectangular opening with a nominal width of 0.076 centimeter (0.030 in.) and height of 0.005 centimeter (0.002 in.). The boundary layer surveys were made at station 1 in the 16.51-centimeter- (6.50-in.-) diameter inlets and at stations 4, 16, 18, and 19a in the 30°-15° nozzle. Boundary layer total pressure measurements were obtained at station 4 in the 60°-15° nozzle.

A constant temperature hot wire anemometry system was employed in the measurement of the intermittency and turbulence intensity in the boundary layer (ref. 9). The hot wire measurements were obtained at ambient temperature conditions. Hot wire probes were located at station 4 in the 30°-15° nozzle. The sensing element was made of 0.0005-centimeter- (0.0002-in.-) diameter tungsten wire having a length of 0.3 centimeter (0.1 in.). The ends of the tungsten wire were copper plated and soft soldered to needle-point Inconel conductors. Alinement of the wire relative to the nozzle wall was achieved by means of a cathetometer.

PROCEDURE

In the operation of the facility the plenum total pressure was varied between 21 and 207 newtons per square centimeter (30 and 300 psia), respectively. The maximum total temperature was set at 539 K (970° R). The boundary layer bleed control on the pipe inlet was used to initiate the boundary layer at the leading edge of the inlet. Sufficient "soak" time was allowed to bring the entire apparatus to thermal equilibrium prior to the recording of data.

EXPERIMENTAL RESULTS

Static Pressure and Mach Number

The ratios of experimental wall static to total pressure P_s/P_0 and corresponding Mach number M are given in table IV. The value of static pressure at the geometric throat was always lower than the value based on one-dimensional isentropic flow ($P_s/P_0 = 0.5283$) as would be expected. In both nozzles the throat pressure ratio corresponding to a throat radius of curvature equal to the diameter was about 12 percent lower than the value for one-dimensional flow.

Comparison of the pressure ratio in the 16.51-centimeter (6.50-in.) pipe inlet with the values at station 2 in the nozzles reveals the presence of an adverse pressure gradient at the nozzle entrance. An effect of this adverse pressure gradient is to cause

separation of the flow at the nozzle entrance; however, unpublished boundary layer surveys near the intersection of the pipe inlet and 30°-15° nozzle revealed that the separated region is very small (<0.63 cm or 0.25 in.) downstream of the nozzle entrance. Boundary layer measurements were not obtained in the entrance region of the 60°-15° nozzle.

Heat Transfer

Experimental heat transfer distributions in the nozzles are presented in terms of a heat transfer coefficient based on enthalpy difference which is given by the following equation:

$$h_i = \frac{q}{i_{ad} - i_w} \tag{1}$$

where the adiabatic enthalpy is

$$i_{ad} = i_s + r(i_0 - i_s) \tag{2}$$

The recovery factor r for a turbulent boundary layer is equal to $Pr^{1/3}$. The values of h_i and the wall temperatures for all tests with the 16.51-centimeter- (6.50-in.-)diameter inlets have been presented in tables V and VI, which are described in the appendix.

In illustrating the effects of Reynolds number (stagnation pressure) on nozzle heat transfer it was found advantageous to present the results in the form of a nondimensional grouping of Stanton and Prandtl numbers which can be written as

$$St_r Pr^{0.7} = \frac{q}{\rho_r u_\infty (i_{ad} - i_w)} Pr^{0.7} = \frac{h_i Pr^{0.7}}{\rho_r u_\infty} \tag{3}$$

The subscript r denotes that properties were evaluated at the reference enthalpy condition of Eckert (ref. 11) given by

$$i_r = i_s + 0.5(i_w - i_s) + 0.22(i_{ad} - i_s) \tag{4}$$

The Prandtl number in equation (3) was assumed to have a constant value of 0.71. The heat transfer grouping $St_r Pr^{0.7}$ in equation (3) is convenient from the standpoint of

comparing the results with correlations for unaccelerated flows which are usually of the form

$$St_r Pr^{0.7} = f(Re_{D,r}) \tag{5}$$

The Reynolds number $Re_{D,r}$ is given by

$$Re_{D,r} = \frac{\rho_r u_\infty D}{\mu_r} \tag{6}$$

where, again, the properties are based on the reference enthalpy condition of equation (4).

Nozzle heat transfer with uncooled inlets. - An initial phase of the program was to assess the influence of the uncooled inlet geometry on the heat tranfer and boundary layer in the nozzle. At first, only adiabatic inlets of the type shown in figure 2(a) were employed. In reference 2 it was observed that when the length of the 16.51-centimeter-(6.50-in.-) diameter inlet was increased from 43.1 to 337.8 centimeters (17.0 to 133.0 in.), the heat transfer coefficient h_i in the entrance region decreased by approximately 20 percent as shown in figure 3. This change in heat transfer in the vicinity of the nozzle entrance can be estimated by the method of reference 12. The difference in nozzle heat transfer resulting from pronounced changes in uncooled inlet length diminished rapidly as the flow accelerated. In terms of the velocity boundary layer that entered the nozzle, the thickness δ varied from about 1.3 centimeters (0.5 in.) for the short inlet to 8.25 centimeters (3.25 in.) (fully developed) for the long inlet. Nevertheless, this large variation in δ at the nozzle entrance did not significantly alter the heat transfer in the 30°-15° and 60°-15° nozzles.

A related but different question concerns the effect on the heat transfer coefficient in the nozzle when the diameter of the uncooled inlet is reduced. This can be interpreted as a shortening of the nozzle or reduction in the contraction ratio ϵ_c while maintaining a fixed throat geometry and convergence angle. The local mass flux in the nozzle is unchanged in this case. It was shown in reference 1 that upon changing the nozzle contraction ratio in this fashion the nozzle heat transfer can be altered appreciably. This result is illustrated in figure 4. In tests with the 30°-15° nozzles (fig. 4(a)) as well as the 60°-15° nozzle (fig. 4(b)), higher heat transfer coefficients accompanied the reduction in inlet diameter (contraction area ratio). The greatest difference in heat transfer coefficient occurred in the sonic throat of the nozzles. For the 30°-15° nozzle an increase in the peak heat transfer coefficient of 75 percent was observed when the inlet diameter was reduced from 16.5 to 7.8 centimeters (6.5 to 3.1 in.) (fig. 4(a)). This change in inlet

diameter represents a change in contraction area ratio of from 19.0 to 4.2. The corresponding increase in peak heat transfer coefficient in the 60°-15° nozzle was 43 percent (fig. 4(b)).

It was shown that large differences in the velocity boundary layer thickness δ at the nozzle entrance result in only modest changes in the entrance heat transfer (possibly 20 percent, fig. 3) and insignificant changes in throat heat transfer. However, an increase in the thermal boundary layer Δ at the nozzle entrance can produce significant reductions in the heat transfer throughout the nozzle as reported in reference 4. Large values of Δ ($\Delta \approx 1.5$ cm or 0.6 in.) at the nozzle entrance were obtained by means of cooled inlets of the type shown in figure 2(b). An indication of the reduction in local heat transfer accompanying the increase in the entrance value of Δ can be obtained by comparing the results in figures 3 and 5 for corresponding inlet diameters.

The effect of altering the cooled inlet diameter (varying the contraction ratio for a fixed throat diameter) on the heat transfer in the 30°-15° and 60°-15° nozzles was similar to that observed for uncooled inlets (ref. 4). That is, a reduction in cooled inlet diameter produced an increase in the nozzle heat transfer coefficient as shown in figure 5. The increase in peak heat transfer coefficient accompanying a change in inlet diameter of from 16.5 to 7.8 centimeters (6.5 to 3.1 in.) was 57 percent for the 30°-15° nozzle (fig. 5(a)) and 50 percent for the 60°-15° nozzle (fig. 5(b)).

The effects of the different inlet configurations on the peak heat transfer coefficient in the nozzles is summarized in figure 6 with h_i plotted as a function of ϵ_c. As indicated previously, a thickening of the nozzle entrance thermal boundary layer effects a reduction in sonic throat heat transfer coefficient (assuming a fixed nozzle geometry and inlet diameter). Results from reference 1 for the 30°-15° nozzle operating with a small diameter adiabatic inlet ($\epsilon_c = 2.74$) are also presented in figure 6(a). These data tend to suggest a logarithmic variation of peak heat transfer with contraction area ratio, at least for cases in which the thermal boundary layer is initiated at the nozzle entrance.

Effect of nozzle convergence angle. - The effect of convergence angle on nozzle heat transfer has been reported in reference 2. These results, which are shown in figure 7(a) were for the 16.5-centimeter- (6.5-in.-) diameter adiabatic inlet coupled to the 30°-15° and 60°-15° nozzles. The contraction area ratios for the two nozzles were nominally the same. As shown in figure 7(a) the peak heat transfer coefficient in the 60°-15° nozzle was about 40 percent higher than the value for the 30°-15° nozzle.

A similar comparison is presented in figure 7(b) for tests with the same diameter cooled inlet; however, in this case the difference in peak heat transfer coefficient is not as great. The sonic throat value of h_i in the 60°-15° nozzle exceeded that of the 30°-15° nozzle by only about 13 percent. These results are consistent with those of reference 13, in which Back, Cuffel, and Massier compared the performance of 10° and 45° half angle of convergence nozzles operating with cooled inlets. At the high Reynolds number condition, there was essentially no difference in throat heat transfer.

In conclusion, the effects of convergence angle on throat heat transfer can be quite appreciable if the thermal boundary layer is initiated at the nozzle entrance (uncooled inlet coupled to a cooled nozzle). However, if the inlet is cooled in order to produce a thick thermal boundary layer at the nozzle entrance, the convergence angle effects on throat heat transfer can be small or possibly negligible.

Effect of Reynolds number. - Interesting effects resulting from a variation in the Reynolds number have been observed in the nozzle heat transfer studies of references 5 and 13. For a fixed geometry and total temperature, the Reynolds number can be controlled by adjusting the inlet total pressure. When the Reynolds number was reduced appreciably, the phenomena called reverse transition or "laminarization" was observed. During "laminarization," the heat transfer rates in the regions of high acceleration, such as the throat, were observed to approach laminar values. Figure 8 shows typically what happens to the heat transfer at the throat and upstream stations over a range of Reynolds numbers (ref. 5). Results are presented for the 30°-15° nozzle in figure 8(a) and for the 60°-15° nozzle in figure 8(b). The experimental distributions of $St_r Pr^{0.7}$ with $Re_{D,r}$ are compared to the distributions based on unaccelerated flow-type correlations for a turbulent and laminar boundary layer. These relations are as follows for a turbulent boundary layer:

$$St_r Pr^{0.7} = 0.026\, Re_{D,r}^{-0.2} \tag{7}$$

and for a laminar boundary layer

$$St_r Pr^{0.7} = 0.290\, Re_{D,r}^{-0.5} \tag{8}$$

These correlation equations merely provide a convenient representation of the heat transfer level which aids in interpreting the results of figure 8.

As the Reynolds number is reduced, the experimental heat transfer at a given station generally experiences a rather abrupt reduction from the values based on the turbulent boundary layer correlation. This change in $St_r Pr^{0.7}$ occurred in the range of $1.0\times10^6 < Re_{D,r} < 2\times10^6$ as shown in figure 8. The greatest reduction in experimental heat transfer occurred at the throat station at low Reynolds number. Here the heat transfer was within a few percent of the values based on the correlation for a laminar boundary layer.

The effect of inlet thermal boundary layer on the heat transfer at a given station was independent of the Reynolds number. As shown in figure 8, the heat transfer in tests with the uncooled inlet was higher than the corresponding value for a cooled inlet at all Reynolds numbers. It is interesting to note that, at a given station, the change in nozzle heat transfer accompanying the change from an uncooled to a cooled inlet was approxi-

mately the same at low Reynolds numbers ("laminarized" boundary layer) as it was at high Reynolds numbers (turbulent boundary layer).

The Reynolds number corresponding to the onset of "laminarization" was also unaltered by the conditions of the inlet thermal boundary layer. This can be noted by comparing the results for the cooled and uncooled inlets in figure 8. The onset of "laminarization" has often been associated with an acceleration parameter K which is predominantly dependent upon the free stream flow conditions. In this report the value of K was essentially unchanged by changes in the inlet cooling thus possibly explaining the negligible effect on the Reynolds number for "laminarization." Whenever the acceleration parameter exceeds a nominal value of about 3×10^{-6}, a rapid dropoff in the Stanton number occurs. As shown in references 5 and 14 and other sources, this value of K is computed from an inequality involving the momentum thickness Reynolds number. Forward transition (laminar to turbulent) is often associated with a critical momentum Reynolds number Re_θ of 360. It is assumed in the "laminarization" process that the same Re_θ applies to a transition reversal. Obviously, this assumption is questionable for, even in forward transition, the transition Reynolds number can vary by nearly an order of magnitude. However, the concept of a critical value of K is desirable since it provides the designer with a readily calculable quantity (depends only on the free stream flow properties) for approximating the conditions in which "laminarization" has been observed. In reference 5 it was concluded that the critical value of acceleration parameter provides a fair definition of the conditions in which the heat transfer is influenced by "laminarization."

Boundary Layer Profiles

The experimental boundary layer surveys were obtained in both the subsonic and supersonic portions of the nozzle. Boundary layer temperature and velocity profiles were obtained at stations 4, 16, 18, and 19a in the 30°-15° nozzle operating with the 16.51-centimeter- (6.50-in.-) diameter uncooled and cooled inlets. The Mach numbers at these stations were 0.08, 2.1, 3.7, and 4.4, respectively. In addition to these stations, temperature boundary layer surveys were obtained at station 12 (Mach 1.3). The profiles were obtained as close to the geometric throat as possible; however, velocity boundary layer surveys could not be made at Mach 1.3 because of the extremely thin boundary layer in the region of the throat. In this report only the profiles at stations 4, 12, and 19a (subsonic, throat, and supersonic portions of the nozzle, respectively) will be shown. Results for the other stations can be obtained from reference 3.

The experimental data are compared to the profile shapes for nonaccelerated turbulent boundary layers. Profiles may be described in terms of exponential relations, that is,

Velocity:

$$\frac{u}{u_e} = \left(\frac{y}{\delta}\right)^{1/n} \tag{9}$$

Temperature:

$$\frac{T_t - T_w}{T_{t,e} - T_w} = \left(\frac{y}{\Delta}\right)^{1/n} \tag{10}$$

The commonly accepted value of n for turbulent flow is approximately 7. For the experimental boundary layer in accelerated flows it is often difficult to determine the values of δ and Δ which represent the thicknesses of the velocity and thermal layers, respectively. If one follows the general practice, the velocity layer thickness δ is considered to be the distance y where $u = u_e \equiv 0.99\ u_\infty$ and the thermal layer thickness Δ is the distance y where $T_t = T_{t,e} \equiv 0.99\ T_0$. However, there is evidence that the aforementioned edge criterion are not meaningful for boundary layers in accelerating flows (refer to ref. 15). For this reason the profiles are presented as a function of y, rather than a nondimensional distance.

The experimental velocity and temperature profiles are presented in figures 9, 10, and 11 for station 4 (Mach 0.08), station 12 (Mach 1.3), and station 19a (Mach 4.4), respectively. These profiles correspond to tests with the 16.51-centimeter- (6.50-in.-) diameter cooled inlet coupled to the 30°-15° nozzle. The measurements were made at the high Reynolds number conditions corresponding to a stagnation pressure of 207 newtons per square centimeter (300 psia) and stagnation temperature of 539 K (970° R). As explained earlier, velocity boundary layer profiles were not measured at the Mach 1.3 station.

The inner portions of the velocity profiles at Mach 0.08 and Mach 4.4 (figs. 9(a) and 11(a), respectively) are described reasonably well by a one-seventh power variation. The outer portion of these profiles, however, are characterized by a long "wake" region in which local velocities are within a few percent of the free stream value. The results of reference 15 indicate that the outer portions of such velocity distributions can often be treated as inviscid flow. The small radial variation in velocity in this region could be the result of negative mass entrainment in the momentum layer which is predicted by various boundary layer analyses and was shown experimentally in reference 15.

The temperature profiles at Mach 0.08, Mach 1.3, and Mach 4.4 matched the one-seventh power profiles fairly well (figs. 9(b) and 11(b), respectively) over an appreciable distance from the wall. The extent of the one-seventh power variation for the tempera-

ture profiles generally exceeded that for the corresponding velocity profiles as is particularly evident at Mach 0.08 (fig. 9).

Reynolds Number Effects on Boundary Layer Profiles

Several investigators have examined the effect of Reynolds number on the time-averaged velocity and temperature profiles (i.e., refs. 5 and 13). Earlier it was indicated that reducing the Reynolds number could lead to the phenomenon of "laminarization" and substantial reductions in the local heat transfer (see fig. 8).

Both references 5 and 13 reported the results of boundary layer surveys made in the subsonic portion of nozzles. The research nozzle of reference 13 had a 10° half angle of convergence whereas in reference 5, the convergence half angle was 30°. Both references reported that the velocity boundary layer profile approached a laminar shape of the Reynolds number was reduced. Velocity and temperature profiles at the Mach 0.08 station in the 30°-15° nozzle are shown in figure 12 (refer also to ref. 5) for a high and a low Reynolds number operating condition. A definite change in the slope of the velocity profile can be noted in the near wall region at the low Reynolds number condition. However, because of temperature probe size limitations, temperature measurements in the laminarized zone ($y \lesssim 0.010$ cm or 0.004 in.) could not be obtained. Figure 12 reveals that the measured temperature and velocity profiles at $y > 0.010$ centimeter (0.004 in.) are nearly identical at the two Reynolds number levels.

The low Reynolds number profiles correspond to conditions in which the acceleration parameter K exceeds a critical value of about 3×10^{-6} (refer to ref. 5). The value of K for the low Reynolds number data of figure 12 was about 6×10^{-6}. Similar results were evident in measured profiles at $K \approx 2.8$ and 4.1×10^{-6} in the 10°-10° nozzle of reference 13. The results of reference 13 also indicated that further increases in K (reductions in stagnation pressure) brought about a change in the inner portion profile of the temperature profile as well as the velocity. At $K \approx 6.0$ and 8.3×10^{-6}, both the velocity and temperature profiles possessed laminar time-mean characteristics in the region nearest the wall.

It is of interest to examine the temperature profiles near the throat of the nozzle for the operating conditions given in figure 12. These temperature profiles, which were obtained at Mach 1.3, are presented in figure 13. At the low Reynolds number where "laminarization" of the upstream velocity layer was apparent (fig. 12(a)), the throat temperature profile exhibited a slope characteristic of a laminar boundary layer in the region of $y \leq 0.025$ centimeter (0.010 in.). It is rather surprising, however, to note a similar type of profile at the high Reynolds number where the heat transfer was nearly twice the value at low Reynolds number (fig. 8(a)). Based on the critical acceleration

parameter K, the velocity boundary layer at the throat would be turbulent at the high Reynolds number condition. Therefore, it is difficult to explain the laminar-type behavior of the inner portion of the temperature profile, especially since the thermal response in the layer is expected to lag that of the velocity layer (ref. 13). These results tend to emphasize the need for supplementation of the time-mean profiles with detailed turbulence measurements in order to adequately understand the "laminarization" phenomenon.

Experimental Momentum and Energy Thickness Distributions

The deficiency thicknesses of momentum θ and energy φ are given by the following equations:

$$\theta = \int_0^{\delta} \frac{\rho u}{\rho_e u_e}\left(1 - \frac{u}{u_e}\right)dy \tag{11}$$

$$\varphi = \int_0^{\Delta} \frac{\rho u}{\rho_e u_e}\left(1 - \frac{T_t - T_w}{T_{t,e} - T_w}\right)dy \tag{12}$$

The experimental distributions of θ and φ in the 30°-15° nozzle are presented in figures 14 and 15, respectively (ref. 4). These measurements were obtained with the 16.51-centimeter- (6.50-in.-) diameter adiabatic and cooled inlets. Comparison of figures 14 and 15 reveals that the energy thickness φ is generally much greater than the corresponding value of momentum thicknesss θ for a given inlet and stagnation conditions. Also, as would be expected, the local values of energy thickness in the nozzle are greatest for the tests in which a cooled inlet was employed. In tests with the cooled inlet, the throat value of φ was nearly 10 times greater than θ. It will be shown that the energy thickness is an important dimension in the prediction of the local heat transfer in the nozzle.

Some Observations Based on Hot Wire Measurements

In reference 9 a hot wire probe was installed at station 4 (Mach 0.08) in the 30°-15° nozzle in an attempt to obtain better resolution of the velocity profile and gain a better

understanding of the mean turbulence characteristics in the region of $y \leq 0.025$ centimeter (0.01 in.). This portion of the boundary layer is particularly important in assessing the effects of Reynolds number on the profiles. As shown previously the pitot probe measurements of velocity revealed a change in the profile at low Reynolds number (fig. 12(a)) - a condition associated with "laminarization" of the boundary layer.

All of the measurements were obtained at the Mach 0.08 station in the 30°-15° nozzle at a nominal stagnation temperature of 305 K (550° R). This operating temperature simplified the calibration of the wire through the assumption of incompressible flow.

Intermittency Factor and Turbulence Intensity

Measurements of the distribution of intermittency factor γ were obtained by means of an electronics circuit of the type described in reference 16. The intermittency factor is simply the fraction of time that the flow is turbulent. The distribution of intermittency factor at station 4 (Mach 0.08) in the 30°-15° nozzle is shown in figure 16. This profile was measured at the high Reynolds number condition where "laminarization" effects on the time-mean velocity measurements were not evident. It was shown in reference 9 that the profile of intermittency factor in the nozzle is considerably different from that of a nonaccelerated flow which can be approximated by a Gaussian integral type of distribution (refs. 17 and 18).

It was further shown in reference 9 that the distribution of intermittency factor in figure 16 could be described by a composite distribution comprising a Gaussian integral distribution in the near wall region ($y < 0.076$ cm or 0.03 in.) and an integral log-normal distribution in the outer region. Reference 9 should be consulted for details of the analysis.

The composite nature of the intermittency profile suggested the presence of a layer within a layer. The portion of the curve at $y < 0.076$ centimeter (0.03 in.) was expected to reflect the turbulence due to a detrainment of fluid from the boundary layer into the free stream similar to the results of reference 15. The contribution of this outer intermittent region to the turbulent transport of heat in the nozzle is not presently understood.

It is well known that a knowledge of the intermittency is required in order to properly interpret the measurements of turbulence intensity $\sqrt{\overline{u'^2}}/u_{\infty}$ in the boundary layer. This arises from the fact that a hot wire placed in a mixed flow (boundary layer or wall shear flow, detrained or rotational inviscid flow, and free stream flow) reacts alternately to each type of turbulent flow as it sweeps past the wire. At any time the average signal such as turbulence intensity is the result of an averaging of the turbulence in the mixed flow. In order to compare the turbulence intensity in an accelerated flow with the turbulence intensity in an unaccelerated flow, it is necessary to account for the

difference in the mixed flows. As shown in reference 9, the correction of the measured intensity for the mixed flow effects tends to become complicated by the presence of a detrained layer. Since the correction procedure is rather involved, reference 9 should be consulted for additional details. Only the final results of the measured and corrected turbulence intensities will be presented herein.

These results are presented in figure 17 where the turbulence intensity $\sqrt{\overline{u'^2}}/u_\infty$ is plotted as a function of distance from the wall y/δ. The measured and corrected distributions are compared to the distribution for a nonaccelerated flow (ref. 9). The correction for the detraining layer produces an upward displacement of the distribution. The outer portion of the corrected profile, from $y/\delta \geq 0.4$, is of the same order as the distribution for a flat plate. This result suggested that the effects of acceleration on the time-averaged turbulence characteristics in the boundary layer may not be largely affected by favorable acceleration. However, because of the mixing of the rotational inviscid detrained layer with the wall shear layer, the direct measurements of the turbulence intensity produced values appreciably lower than flat plate values at the same nondimensional distance from the wall.

Description of Nozzle Boundary Layer Growth

It was shown in figures 14 and 15 that in the accelerating flow of a cooled nozzle the energy thickness can greatly exceed the momentum thickness. The ratio φ/θ generally attains its greatest value near the throat of the nozzle where the heat flux is a maximum. Bartz (ref. 10) recognized these differences in the growth of the thermal and velocity boundary layers in a nozzle flow and accounted for nonunity values of φ/θ in his integral boundary layer theory by means of an interaction function in the momentum-heat analogy. One option of the integral method is to assume an interaction function equal to unity thereby providing a relatively simple energy method for computing heat transfer. This basic energy method has been applied to a variety of nozzle flows in references 1, 3, and 4 and was shown to yield satisfactory predictions of throat heat transfer. However, upstream and downstream of the throat the energy method of reference 10 tended to underpredict the measured heat transfer. In reference 8, the auxiliary equation relating the heat transfer to an energy thickness Reynolds number was further modified by empirical methods to provide a better description of the heat transfer throughout the nozzle. A discussion of the predictive capabilities of these energy methods will follow.

COMPARISON OF EXPERIMENTAL AND THEORETICAL HEAT TRANSFER

The experimental heat transfer coefficients will be compared to the values based on the unaccelerated flow type of correlation given by equation (7), the integral energy boundary layer analysis of reference 10, and the modified energy method of reference 8. All of these methods are intended for flows in which the boundary layer remains turbulent throughout the nozzle. In the present study, this boundary layer criterion is expected to apply to the high Reynolds number flow obtained at a stagnation pressure of 207 newtons per square meter (300 psia).

Boundary Layer Theory (Ref. 10)

The boundary layer analysis of reference 10 essentially involves the solution of the integral momentum and energy equation and employs Coles friction law, one-seventh power profiles for velocity and temperature difference, and a modified von Karman form of Reynolds analogy. Reference 10 should be consulted for further details concerning the assumptions incorporated in this method. Two basic options are provided in this boundary layer program. These options concern the method of evaluating the skin friction coefficient and, as mentioned previously, the selection of an interaction exponent. This interaction exponent is used to relate the Stanton number for unequal momentum and energy thicknesses to that for equal thicknesses by a factor $(\varphi/\theta)^N$ viz.; $St = f(Re_\varphi)(\varphi/\theta)^N$. The interaction exponent N can be assigned values in the range of 0 to 0.25.

Skin friction coefficient. - The skin friction coefficient c_f was assumed equal to the adiabatic skin friction coefficient obtained when $T_w = T_{ad}$. The value of $c_{f,ad}$ was based on free stream gas properties.

Interaction exponent. - With emphasis on the prediction of throat heat transfer, the best value for the interaction exponent N was determined to be zero. In this special case of N = 0, the integral energy equation can be decoupled and solved independent of the momentum equation. In this "energy calculation method" the heat transfer or Stanton number is related to thickness Reynolds number as follows:

$$St = f(Re_\varphi) = \frac{\frac{c_f(Re_\varphi)}{2}}{1 - 5\left[\frac{c_f(Re_\varphi)}{2}\right]^{1/2}\left[1 - Pr + \ln\left(\frac{6}{5\,Pr + 1}\right)\right]} \tag{13}$$

Modified Energy Method (Ref. 8)

In reference 8, the auxiliary equation of reference 10, equation (13), was modified by empirical considerations to provide a relation between the heat transfer, energy thickness Reynolds number, and an acceleration parameter. The resulting equation was

$$St = 1.6\, f(Re_{\varphi}) \left(1.0 - 0.11 \frac{x_a\, d(u_{\infty} R)}{u_{\infty}\, R\, dx_a} \right) \tag{14}$$

The functions $f(Re_{\varphi})$ in equations (13) and (14) are identical.

Predicted Heat Transfer

Correlation approach. - The heat transfer distributions based on the unaccelerated turbulent flow-type correlation (eq. (7)) indicated pronounced differences from the experimental throat heat transfer as shown in figures 18 and 19. The throat heat transfer coefficients emanating from the correlation equation are nearly a factor of two greater than the experimental values. The correlated heat transfer was independent of the nozzle convergence angle (as noted upon comparison of figs. 18 and 19) and also independent of the inlet cooling (as noted upon comparison of part (a) with part (b) in figs. 18 and 19). Identical peak values of predicted heat transfer in the nozzles were the result of a predominant dependence on the mass flux which was essentially the same for the two configurations. The correlation equation provided ultraconservative estimates of the heat transfer for the cases presented in figures 18 and 19; however, under conditions in which the thermal boundary layer is initiated near the throat of the nozzle the simple correlation approach can produce nonconservative estimates of the throat heat flux (ref. 1). All of this suggested the need for a better method of predicting nozzle heat transfer. In order to account for differences in such things as the nozzle convergence angle or entrance conditions, it was necessary to apply boundary layer methods such as the integral boundary layer theory of reference 10 and the modified analysis of reference 8.

Boundary layer approach. - Predictions of the throat heat transfer based on the integral energy calculation of reference 10 are considerably better than the results from the aforementioned correlation as shown in figures 18 and 19. As discussed previously, these predictions depend on only one boundary layer thickness, namely, the energy thickness φ. Various simplifications of this energy method have been presented in references 1 and 4. In these references the method was applied to a variety of configura-

tions, including chemical rocket nozzles (ref. 4). In general, the predicted throat heat transfer was in good agreement with the data (within about 20 percent). However, the results of reference 4 also revealed that the energy method can underpredict the heat transfer in the nozzle entrance region. In reference 8, an improvement in the predicted subsonic heat transfer was obtained by altering the auxiliary equation of reference 10. Results based on the modified equation (eq. (14)) are presented in figures 18 and 19. With the exception of the 60°-15° nozzle operating with the cooled inlet (fig. 19(b)), the predictions based on the latter method provide equal or slightly better agreement with the data in the nozzle throat and much better agreement in the entrance and exit regions.

SOME EFFECTS OF SURFACE ROUGHNESS ON NOZZLE HEAT TRANSFER

So far all of the discussion has pertained to smooth wall nozzles. The effects of surface roughness on the heat transfer in the 30°-15° and 60°-15° nozzles has been presented in references 6 and 7. A lengthy discussion of the results is beyond the scope of this report; however, the highlights of the work will be mentioned and the heat transfer data will be presented in tables V and VI, which are described in the appendix.

The effects of surface roughness on nozzle heat transfer can best be illustrated by plotting the Stanton-Prandtl number group $St_r Pr^{0.7}$ as a function of Reynolds number $Re_{D,r}$. Results for the throat station of the 30°-15° and 60°-15° nozzles are shown in figure 20. In both the 30°-15° nozzle (fig. 20(a)) and the 60°-15° nozzle (fig. 20(b)), the heat transfer at a given surface roughness was lowest in tests with the cooled inlet. For a given nozzle and inlet, two important effects of roughness on heat transfer can be observed; namely, (1) an increase in roughness at a given Reynolds number produces an increase in heat transfer and (2) an increase in roughness reduces the range of Reynolds number in which "laminarized" levels of heat transfer can be measured. In references 6 and 7 it was further concluded, based on an extensive examination of data at several stations in the nozzles, that in the low Reynolds number ("laminarized") regime the effect of roughness on heat transfer is essentially negligible. In addition, it was noted that in the high Reynolds number (turbulent) regime the heat transfer was not noticeably affected until the roughness exceeded the estimated sublayer height. References 6 and 7 should be consulted for further details.

SUMMARY OF RESULTS

A review of the results of a comprehensive experimental investigation of the heat transfer and boundary layer in 30°-15° and 60°-15° conical nozzles has been presented.

The experiments were conducted with air at a stagnation temperature of 539 K (970° R) and at throat Reynolds numbers ranging from 6×10^5 to 5×10^6. Effects of wall surface finish on nozzle heat transfer were also examined. The principal results of this investigation can be summarized as follows:

1. Altering the length of uncooled pipe inlets with length to diameter ratios greater than 2.6 (changing the turbulent boundary layer momentum thickness at the nozzle entrance) resulted in a negligible effect on the throat heat transfer in 30°-15° and 60°-15° converging-diverging (C-D) nozzles. However, upon cooling the pipe inlets (increasing the thickness of the thermal boundary layer on the nozzle entrance) pronounced reductions in throat heat transfer were observed.

2. When the free stream Reynolds number was varied over an appropriate range, two distinct reductions in heat transfer from the values for unaccelerated flow were observed. The larger of these reductions in heat transfer occurred at Reynolds numbers of about 1×10^6 or less and is believed to be associated with a boundary layer reverse transition or "laminarization" phenomenon. At Reynolds numbers in excess of about 1×10^6 the reduction in throat heat transfer was as large as 50 percent.

3. Hot wire surveys of intermittency factor and turbulence intensity at Mach 0.08 in the 30°-15° nozzle tended to substantiate the presence of a boundary layer mass detrainment phenomenon. The measured values of turbulence intensity were appreciably lower than flat plate values; however, upon incorporating the detrainment concept and correcting the measurements using the intermittency factor, the intensity levels in the nozzle boundary layer approached the classical flat plate results.

4. Satisfactory predictions of nozzle heat transfer were obtained by means of an integral energy boundary layer method. This method was applicable to smooth wall nozzles operating at sufficiently high Reynolds numbers to maintain a turbulent boundary layer throughout the nozzle.

5. The principal effects of increasing the nozzle surface roughness were to increase the heat transfer in the turbulent boundary layer regime and to reduce the Reynolds number range in which "laminarization" occurs.

Lewis Research Center,
National Aeronautics and Space Administration,
Cleveland, Ohio, October 19, 1971,
132-15.

APPENDIX - TABULATED HEAT TRANSFER COEFFICIENTS AND WALL TEMPERATURES

Experimental values of nozzle heat transfer coefficient h_i and wall temperature T_w are tabulated in tables V and VI, respectively. Data are presented for the 30°-15° and 60°-15° nozzles operating with the 16.51-centimeter- (6.50-in.-) diameter adiabatic and cooled inlets. The lengths of these inlets are given in table I (inlets 2 and 3, respectively). In order to preserve clarity in tables V and VI, only the nominal values of stagnation pressure P_0 and stagnation temperature T_0 are shown. However, in using the results it may be desirable to incorporate the exact values of the stagnation conditions which varied slightly from run to run. Therefore table VII is provided for conversion from nominal to exact values of the stagnation conditions.

REFERENCES

1. Boldman, Donald R.; Neumann, Harvey E.; and Schmidt, James F.: Heat Transfer in 30° and 60° Half-Angle of Convergence Nozzles with Various Diameter Uncooled Pipe Inlets. NASA TN D-4177, 1967.

2. Boldman, D. R.; Schmidt, J. F.; and Ehlers, R. C.: Effect of Uncooled Inlet Length and Nozzle Convergence Angle on the Turbulent Boundary Layer and Heat Transfer in Conical Nozzles Operating with Air. J. Heat Transfer, vol. 89, no. 4, Nov. 1967, pp. 341-350.

3. Boldman, Donald R.; and Graham, Robert W.: Heat Transfer and Thermal Boundary Layer in a Conical Nozzle. Paper 69-474, AIAA, June 1969.

4. Graham, Robert W.; and Boldman, Donald R.: The Use of Energy Thickness in Prediction of Throat Heat Transfer in Rocket Nozzles. NASA TN D-5356, 1969.

5. Boldman, Donald R.; Schmidt, James F.; and Gallagher, Anne K.: Laminarization of a Turbulent Boundary Layer as Observed from Heat Transfer and Boundary Layer Measurements in Conical Nozzles. NASA TN D-4788, 1968.

6. Reshotko, Meyer; Boldman, Donald R.; and Ehlers, Robert C.: Heat Transfer in a 60° Half-Angle of Convergence Nozzle with Various Degrees of Roughness. NASA TN D-5887, 1970.

7. Reshotko, M.; Boldman, D. R.; and Ehlers, R. C.: Effect of Roughness on Heat Transfer in Conical Nozzles. Augmentation of Convective Heat and Mass Transfer. A. E. Bergles and R. L. Webb, eds., ASME, 1970, pp. 63-69.

8. Boldman, Donald R.; Schmidt, James F.; and Ehlers, Robert C.: Prediction of Local and Integrated Heat Transfer in Nozzles Using an Integral Turbulent Boundary Layer Method. NASA TN D-6595, 1972.

9. Boldman, Donald R.; Neumann, Harvey E.; and Ehlers, Robert C.: Velocity, Intermittency, and Turbulence Intensity Measurements in the Boundary Layer of an Accelerated Flow. NASA TN D-6043, 1970.

10. Bartz, D. R.: Turbulent Boundary-Layer Heat Transfer from Rapidly Accelerating Flow of Rocket Combustion Gases and of Heated Air. Advances in Heat Transfer. Vol. 2. James P. Hartnett and Thomas F. Irvine, Jr., eds., Academic Press, 1965, pp. 1-108.

11. Eckert, E. R. G.; and Drake, Robert M., Jr.: Heat and Mass Transfer. Second ed., McGraw-Hill Book Co., Inc., 1959.

12. Kays, William M.: Convective Heat and Mass Transfer. McGraw-Hill Book Co., Inc., 1966, p. 242.

13. Back, L. H.; Cuffel, R. F.; and Massier, P. F.: Laminarization of a Turbulent Boundary Layer in Nozzle Flow-Boundary Layer and Heat Transfer Measurements with Wall Cooling. Paper 69-HT-56, ASME, Aug. 1969.

14. Moretti, P. M.; and Kays, W. M.: Heat Transfer Through an Incompressible Turbulent Boundary Layer with Varying Free-Stream Velocity and Varying Surface Temperature. Rep. P.G.-1, Thermosciences Div., Stanford Univ., Nov. 1964.

15. Brinich, Paul F.; and Neumann, Harvey E.: Some Effects of Acceleration on the Turbulent Boundary Layer. AIAA J., vol. 8, no. 5, May 1970, pp. 987-989.

16. Bradbury, L. J. S.: A Simple Circuit for the Measurement of the Intermittency Factor in a Turbulent Flow. Aeronaut. Quart., vol. 15, Aug. 1964, pp. 281-284.

17. Klebanoff, P. S.: Characteristics of Turbulence in a Boundary Layer with Zero Pressure Gradient. NACA Rep. 1247, 1955.

18. Corrsin, Stanley; and Kistler, Alan L.: The Free-Stream Boundaries of Turbulent Flows. NACA TN 3133, 1954.

TABLE I. - DIMENSIONS OF INLETS

Inlet	Diameter, D		Uncooled length, l_u		Cooled length, l_c	
	cm	in.	cm	in.	cm	in.
1	16.51	6.50	337.8	133.0	----	----
2	16.51	6.50	43.1	17.0	----	----
3	16.51	6.50	34.0	13.4	61.5	24.2
4	7.80	3.07	45.7	18.0	----	----
5	7.80	3.07	-----	-----	45.7	18.0

TABLE II. - INSTRUMENTATION FOR 30°-15° NOZZLES

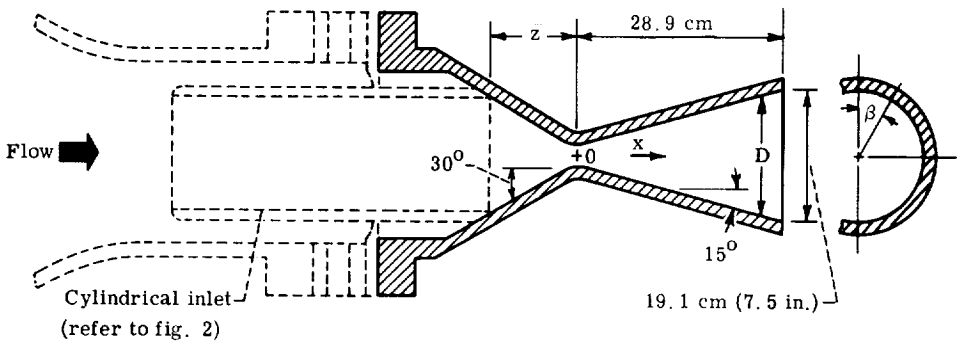

Inlet	Diameter, D		Axial distance, $\bar{z}$		Contraction area ratio, ϵ_c
	cm	in.	cm	in.	
1, 2, and 3	16.51	6.50	12.032	4.737	18.98
4 and 5	7.80	3.07	4.255	1.675	4.23

Station	Angular position, β, deg		Axial distance, x		Diameter, D		Ratio of axial distance to throat diameter, x/D_t	Area ratio, A/A_t
	Pressure tap	Heat flux meter	cm	in.	cm	in.		
2	231	51	-11.468	-4.515	15.875	6.250	-3.026	17.548
3	129	309	-8.928	-3.515	12.934	5.092	-2.356	11.648
4	180	0	-6.380	-2.512	9.992	3.934	-1.684	6.952
5	231	51	-5.481	-2.158	8.961	3.528	-1.446	5.591
6	283	103	-4.602	-1.812	7.945	3.128	-1.214	4.395
7	334	154	-3.708	-1.460	6.914	2.722	-.979	3.328
8	26	206	-2.819	-1.110	5.883	2.316	-.744	2.410
9	77	257	-1.557	-.613	4.470	1.760	-.411	1.392
10	129	309	-.445	-.175	3.835	1.510	-.117	1.024
11	180	0	0	0	3.790	1.492	0	1.000
12	231	51	.330	.130	3.815	1.502	.087	1.013
13	283	103	.648	.255	3.912	1.540	.171	1.065
14	334	154	.996	.392	4.074	1.604	.263	1.156
15	26	206	1.610	.634	4.399	1.732	.425	1.348
16	77	257	3.101	1.221	5.187	2.042	.818	1.873
17	180	0	6.949	2.736	7.259	2.858	1.834	3.669
18	↓	↓	13.889	5.468	10.978	4.322	3.665	8.391
19			20.831	8.201	14.712	5.792	5.497	15.070
19a			24.181	9.520	16.520	6.504	6.381	19.003
20			28.021	11.032	18.593	7.320	7.394	24.071

TABLE III. - INSTRUMENTATION FOR 60°-15° NOZZLE

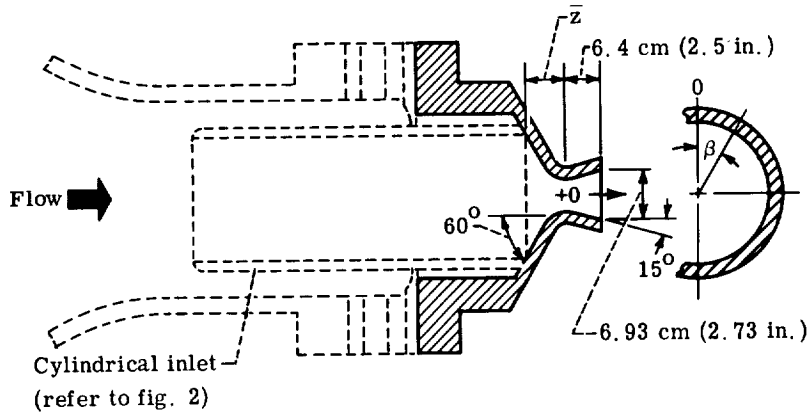

Inlet	Diameter, D		Axial distance, $\bar{z}$		Contraction area ratio, ϵ_c
	cm	in.	cm	in.	
1, 2, and 3	16.51	6.50	5.852	2.304	18.80
4 and 5	7.80	3.07	3.338	1.314	4.19

Station	Angular position, β, deg		Axial distance, x		Diameter, D		Ratio of axial distance to throat diameter, x/D_t	Area ratio, A/A_t
	Pressure tap	Heat flux meter	cm	in.	cm	in.		
2	180	0	-5.296	-2.085	14.580	5.740	-1.391	14.663
3	77	257	-4.450	-1.752	11.643	4.584	-1.169	9.352
4	129	209	-4.153	-1.635	10.612	4.178	-1.091	7.769
5	180	0	-3.848	-1.515	9.555	3.762	-1.011	6.299
6	231	51	-3.063	-1.206	6.939	2.732	-.805	3.322
7	283	103	-2.591	-1.020	5.865	2.309	-.680	2.373
8	334	154	-1.476	-.581	4.409	1.736	-.388	1.341
9	26	206	-.371	-.146	3.851	1.516	-.097	1.023
10	77	257	0	0	3.807	1.499	0	1.000
11	129	309	.381	.150	3.863	1.521	.100	1.030
12	180	0	.704	.277	3.975	1.565	.185	1.090
13	231	51	1.016	.400	4.122	1.623	.267	1.172
14	283	103	1.580	.622	4.422	1.741	.415	1.349
15	334	154	3.071	1.209	5.215	2.053	.807	1.876
16	26	206	5.436	2.140	6.464	2.545	1.428	2.883

TABLE IV. - EXPERIMENTAL STATIC- TO TOTAL-PRESSURE RATIOS AND MACH NUMBER

(a) Nozzles

Station	30°-15° nozzle			60°-15° nozzle		
	Area ratio, A/A_t	Pressure ratio, P_s/P_0	Mach number M	Area ratio, A/A_t	Pressure ratio, P_s/P_0	Mach number M
2	17.548	0.99946	0.02778	14.663	0.9996	0.02391
3	11.648	.99847	.04677	9.352	.99907	.03646
4	6.952	.99565	.07894	7.769	.99826	.04988
5	5.591	.99325	.09841	6.299	.99691	.06651
6	4.395	.98887	.12655	3.322	.9811	.16533
7	3.328	.9804	.16840	2.373	.9560	.25436
8	2.410	.9624	.23463	1.341	.8227	.53547
9	1.392	.8399	.50553	1.023	.5680	.93649
10	1.024	.5733	.92813	1.000	.4681	1.10044
11	1.000	.4600	1.11446	1.030	.3383	1.34716
12	1.013	.3733	1.27507	1.090	.2612	1.52889
13	1.065	.2785	1.48469	1.172	.2222	1.63844
14	1.156	.2084	1.68124	1.349	.1765	1.79082
15	1.348	.1820	1.77070	1.876	.1103	2.09448
16	1.873	.1125	2.08183	2.883	.0545	2.54588
17	3.669	.0375	2.78852	------	-------	-------
18	8.391	.0094	3.73770	------	-------	-------
19	15.070	.0038	4.42415	------	-------	-------
19a	19.00	.0027	4.70038	------	-------	-------
20	24.071	.0024	4.79800	------	-------	-------

(b) Pipe inlets

Inlet	Diameter, D		Nominal area ratio, A/A_t	Pressure ratio, P_s/P_0	Mach number M
	cm	in.			
1, 2, and 3	16.51	6.50	18.89	[a]0.99932	0.03117
4 and 5	7.80	3.07	4.21	[b].9866	.13896

[a]Measured at station 1, inlet 2.

[b]Denotes value based on one-dimensional flow.

TABLE V. - EXPERIMENTAL HEAT TRANSFER COEFFICIENTS IN 30°-15° AND 60°-15° NOZZLES

[Stagnation temperature T_0 = 539 K (970° R).]

(a) 30°-15° nozzle, adiabatic inlet (inlet 2, table I)

(a-1) SI units

Station	Axial distance, x, cm	Diameter, D, cm	Stagnation pressure, P_0, N/cm^2											
			206.8				110.3				75.8			
			Nozzle roughness level, cm rms											
			Smooth	305×10^{-6}	445×10^{-6}	826×10^{-6}	Smooth	305×10^{-6}	445×10^{-6}	826×10^{-6}	Smooth	305×10^{-6}	445×10^{-6}	826×10^{-6}
			Heat transfer coefficient based on enthalpy, h_i, g/(cm^2)(sec)											
2	-11.468	15.875	0.0717	0.0759	0.0809	0.0844	0.0463	0.0472	0.0506	0.0512	0.0368	0.0368	0.0393	0.0386
3	-8.928	12.934	.0823	.0872	.1216	.1434	.0422	.0453	.0509	.0724	.0326	.0341	.0355	.0420
4	-6.380	9.992	.1294	.1441	.1687	.1800	.0543	.0638	.0928	.1019	.0329	.0374	.0470	.0652
5	-5.481	8.961	.1455	.1631	.1919	.2130	.0717	.0801	.1083	.1202	.0411	.0423	.0636	.0823
6	-4.602	7.945	.1638	.1898	.2081	.2306	.0886	.0970	.1216	.1350	.0492	.0520	.0809	.0949
7	-3.708	6.914	.1891	.2074	.2383	.2278	.1097	.1244	.1406	.1589	.0633	.0710	.0998	.1146
8	-2.819	5.883	.2390	.2918	.3051	.3410	.1420	.1659	.1842	.2046	.0914	.1076	.1343	.1498
9	-1.557	4.470	.3122	.3867	.3888	.4373	.1969	.2292	.2447	.2693	.1378	.1680	.1856	.2011
10	-.455	3.835	.3382	.3909	.3993	.4457	.2172	.2510	.2566	.2749	.1624	.1912	.1997	.2109
11	0	3.790	.3347	.3958	.4007	.4204	.2039	.2397	.2615	.2707	.1575	.1870	.1997	.2081
12	.330	3.815	.2587	.3839	.3811	.4148	.1765	.2257	.2419	.2573	.1385	.1730	.1835	.1919
13	.648	3.912	.2383	.3206	.3340	.3628	.1631	.1898	.2095	.2264	.1280	.1448	.1596	.1715
14	.996	4.074	.2229	.3030	.3150	.3354	.1610	.1751	.1940	.2060	.1230	.1336	.1455	.1547
15	1.610	4.399	.2299	.2861	.2890	.3227	.1455	.1624	.1751	.1926	.1097	.1202	.1294	.1413
16	3.101	5.187	.1955	.2369	.2482	.2791	.1125	.1321	.1441	.1624	.0830	.0963	.1034	.1153
17	6.949	7.259	.0970	.1174	.1216	.1448	.0539	.0653	.0667	.0780	.0411	.0476	.0474	.0531
18	13.889	10.978	.0412	.0427	.0433	.0478	.0238	.0236	.0246	.0262	.0174	.0172	.0175	.0188
19	20.831	14.712	.0214	.0210	.0212	.0225	.0120	.0120	.0120	.0127	.0089	.0084	.0089	.0103
20	28.021	18.593	.0174	.0169	.0180	.0221	.0139	.0129	.0155	.0132	.0153	.0136	.0150	.0166

Station	Axial distance, x, cm	Diameter, D, cm	Stagnation pressure, P_0, N/cm^2											
			51.7				31.0				20.7			
			Nozzle roughness level, cm rms											
			Smooth	305×10^{-6}	445×10^{-6}	826×10^{-6}	Smooth	305×10^{-6}	445×10^{-6}	826×10^{-6}	Smooth	305×10^{-6}	445×10^{-6}	826×10^{-6}
			Heat transfer coefficient based on enthalpy, h_i, g/(cm^2)(sec)											
2	-11.468	15.875	0.0289	0.0295	0.0307	0.0305	0.0214	0.0210	0.0224	0.0219	0.0161	0.0165	0.0174	0.0176
3	-8.928	12.934	.0257	.0267	------	.0299	.0193	.0202	.0198	.0212	.0148	.0155	.0155	.0170
4	-6.380	9.992	.0236	.0262	.0283	.0318	.0174	.0186	.0198	.0199	.0138	.0146	.0153	.0159
5	-5.481	8.961	.0278	.0276	.0302	.0371	.0195	.0193	.0202	.0211	.0152	.0153	.0158	.0166
6	-4.602	7.945	.0290	.0288	.0343	.0506	.0199	.0194	.0201	.0208	.0156	.0153	.0156	.0165
7	-3.708	6.914	.0315	.0312	.0501	.0773	.0207	.0207	.0220	.0244	.0161	.0153	.0165	.0176
8	-2.819	5.883	.0402	.0453	.0809	.1090	.0242	.0241	.0275	.0413	.0187	.0186	.0229	.0223
9	-1.557	4.470	.0560	.0801	.1357	.1526	.0284	.0298	.0547	.0907	.0217	.0221	.0249	.0448
10	-.455	3.835	.0745	.1294	.1519	.1610	.0290	.0410	.0907	.1034	.0211	.0205	.0311	.0652
11	0	3.790	.1019	.1385	.1526	.1617	.0295	.0431	.0963	.1062	.0193	.0228	.0451	.0717
12	.330	3.815	.0738	.1266	.1364	.1476	.0273	.0537	.0837	.0949	.0191	.0193	.0489	.0623
13	.648	3.912	.0695	.1055	.1188	.1322	.0226	.0498	.0759	.0851	.0167	.0191	.0467	.0582
14	.996	4.074	.0685	.0984	.1083	.1174	.0192	.0408	.0688	.0766	.0136	.0146	.0413	.0538
15	1.610	4.399	.0780	.0900	.0949	.1062	.0365	.0513	.0612	.0685	.0204	.0221	.0399	.0485
16	3.101	5.187	.0631	.0717	.0752	.0844	.0330	.0459	.0489	.0533	.0155	.0112	.0337	.0370
17	6.949	7.259	.0300	.0366	.0346	.0369	.0191	.0229	.0227	.0231	.0039	.0151	.0160	.0162
18	13.889	10.978	.0129	.0131	.0129	.0138	.0085	.0082	.0103	.0117	.0059	.0075	.0108	------
19	20.831	14.712	.0068	.0065	.0115	.0124	.0086	.0077	.0098	.0115	.0066	.0083	.0097	.0098
20	28.021	18.593	.0122	.0118	.0136	.0152	.0102	.0098	.0120	.0108	.0134	.0112	.0110	.0017

TABLE V. - Continued. EXPERIMENTAL HEAT TRANSFER COEFFICIENTS IN 30°-15° AND 60°-15° NOZZLES

[Stagnation temperature T_0 - 539 K (970° R).]

(a) Concluded. 30°-15° nozzle, adiabatic inlet (inlet 2, table I)

(a-2) U.S. customary units

Station	Axial distance, x, in.	Diameter, D, in.	Stagnation pressure, P_0, psia: 300				160				110			
			Nozzle roughness level, in. rms: Smooth	120×10^{-6}	175×10^{-6}	325×10^{-6}	Smooth	120×10^{-6}	175×10^{-6}	325×10^{-6}	Smooth	120×10^{-6}	175×10^{-6}	325×10^{-6}
			Heat transfer coefficient based on enthalpy, h_1, lbm/(in.^{2})(sec)											
2	-4.515	6.250	1.02×10^{-3}	1.08×10^{-3}	1.15×10^{-3}	1.20×10^{-3}	0.659×10^{-3}	0.672×10^{-3}	0.719×10^{-3}	0.728×10^{-3}	0.523×10^{-3}	0.523×10^{-3}	0.559×10^{-3}	0.549×10^{-3}
3	-3.515	5.092	1.17	1.24	1.73	2.04	.600	.644	.724	1.03	.464	.485	.505	.598
4	-2.512	3.934	1.84	2.05	2.40	2.56	.772	.907	1.32	1.45	.468	.532	.668	.928
5	-2.158	3.528	2.07	2.32	2.73	3.03	1.02	1.14	1.54	1.71	.585	.602	.905	1.17
6	-1.812	3.128	2.33	2.70	2.96	3.28	1.26	1.38	1.73	1.92	.700	.740	1.15	1.35
7	-1.460	2.722	2.69	2.95	3.39	3.74	1.56	1.77	2.00	2.26	.901	1.01	1.42	1.63
8	-1.110	2.316	3.40	4.15	4.34	4.85	2.02	2.36	2.62	2.91	1.30	1.53	1.91	2.13
9	-.613	1.760	4.44	5.50	5.53	6.22	2.80	3.26	3.48	3.83	1.96	2.39	2.64	2.86
10	-.175	1.510	4.81	5.56	5.68	6.34	3.09	3.57	3.65	3.91	2.31	2.72	2.84	3.00
11	0	1.492	4.76	5.63	5.70	5.98	2.90	3.41	3.72	3.85	2.24	2.66	2.84	2.96
12	.130	1.502	3.68	5.46	5.42	5.90	2.51	3.21	3.44	3.66	1.97	2.46	2.61	2.73
13	.255	1.540	3.39	4.56	4.75	5.16	2.32	2.70	2.98	3.22	1.82	2.06	2.27	2.44
14	.392	1.604	3.17	4.31	4.48	4.77	2.29	2.49	2.76	2.93	1.75	1.90	2.07	2.20
15	.634	1.732	3.27	4.07	4.11	4.59	2.07	2.31	2.49	2.74	1.56	1.71	1.84	2.01
16	1.221	2.042	2.78	3.37	3.53	3.97	1.60	1.88	2.05	2.31	1.18	1.37	1.47	1.64
17	2.736	2.858	1.38	1.67	1.73	2.06	.767	.929	.948	1.11	.585	.677	.674	.755
18	5.468	4.322	.586	.608	.616	.680	.339	.335	.350	.373	.248	.245	.249	.268
19	8.201	5.792	.305	.298	.301	.320	.170	.170	.170	.181	.126	.120	.126	.147
20	11.032	7.320	.248	.241	.256	.315	.197	.184	.221	.188	.218	.193	.214	.236

Station	Axial distance, x, in.	Diameter, D, in.	Stagnation pressure, P_0, psia: 75				45				30			
			Nozzle roughness level, in. rms: Smooth	120×10^{-6}	175×10^{-6}	825×10^{-6}	Smooth	120×10^{-6}	175×10^{-6}	325×10^{-6}	Smooth	120×10^{-6}	175×10^{-6}	325×10^{-6}
			Heat transfer coefficient based on enthalpy, h_1, lbm/(in.^{2})(sec)											
2	-4.515	6.250	0.411×10^{-3}	0.419×10^{-3}	0.436×10^{-3}	0.434×10^{-3}	0.304×10^{-3}	0.299×10^{-3}	0.319×10^{-3}	0.311×10^{-3}	0.229×10^{-3}	0.235×10^{-3}	0.248×10^{-3}	0.250×10^{-3}
3	-3.515	5.092	.366	.380	----------	.425	.274	.287	.281	.302	.211	.221	.221	.242
4	-2.512	3.934	.335	.372	.402	.452	.247	.264	.282	.283	.196	.208	.218	.226
5	-2.158	3.528	.396	.393	.430	.527	.277	.275	.288	.300	.216	.217	.225	.236
6	-1.812	3.128	.413	.410	.488	.720	.283	.276	.286	.296	.222	.217	.222	.235
7	-1.460	2.722	.448	.444	.713	1.10	.295	.294	.313	.347	.229	.217	.234	.251
8	-1.110	2.316	.572	.644	1.15	1.55	.344	.343	.391	.588	.266	.264	.326	.317
9	-.613	1.760	.796	1.14	1.93	2.17	.404	.424	.778	1.29	.309	.314	.354	.637
10	-.175	1.510	1.06	1.84	2.16	2.29	.413	.583	1.29	1.47	.300	.291	.443	.927
11	0	1.492	1.45	1.97	2.17	2.30	.419	.613	1.37	1.51	.274	.324	.641	1.02
12	.130	1.502	1.05	1.80	1.94	2.10	.388	.764	1.19	1.35	.272	.275	.695	.886
13	.255	1.540	.988	1.50	1.69	1.88	.321	.708	1.08	1.21	.238	.271	.664	.828
14	.392	1.604	.975	1.40	1.54	1.67	.273	.581	.979	1.09	.193	.208	.588	.765
15	.634	1.732	1.11	1.28	1.35	1.51	.519	.730	.870	975	.290	.315	.568	.690
16	1.221	2.042	.898	1.02	1.07	1.20	.470	.653	.695	758	.220	.159	.480	.526
17	2.736	2.858	.426	.521	.492	.525	.271	.326	.323	329	.056	.215	.228	.231
18	5.468	4.322	.184	.187	.184	.196	.121	.117	.146	.167	.084	.107	.153	----------
19	8.201	5.792	.096	.093	.163	.176	.122	.109	.139	.163	.094	.118	.138	.139
20	11.032	7.320	.173	.168	.194	.216	.145	.140	.171	.154	.191	.159	.156	.024

TABLE V. - Continued. EXPERIMENTAL HEAT TRANSFER COEFFICIENTS IN 30°-15° AND 60°-15° NOZZLES

[Stagnation temperature T_0 = 539 K (970° R).]

(b) 60°-15° nozzle, adiabatic inlet (inlet 2, table I)

(b-1) SI units

Station	Axial distance, x, cm	Diameter, D, cm	Stagnation pressure, P_0, N/cm^2											
			206.8				110.3				75.8			
			Nozzle roughness level, cm rms											
			Smooth	305×10^{-6}	445×10^{-6}	826×10^{-6}	Smooth	305×10^{-6}	445×10^{-6}	826×10^{-6}	Smooth	305×10^{-6}	445×10^{-6}	826×10^{-6}
			Heat transfer coefficient based on enthalpy, h_i, $g/(cm^2)(sec)$											
2	-5.296	14.580	0.0720	0.0691	0.0689	0.0734	0.0480	0.0444	0.0435	0.0435	0.0374	0.0341	0.0333	0.0333
3	-4.450	11.643	.0783	.0867	.0986	.1279	.0513	.0513	.0532	.0590	.0408	.0387	.0406	.0425
4	-4.153	10.612	.0825	.0986	.1286	.1741	.0527	.0536	.0572	.0837	.0417	.0402	.0423	.0492
5	-3.848	9.555	.0909	.1251	.1796	.2083	.0556	.0580	.0724	.1097	.0439	.0420	.0481	.0619
6	-3.063	6.939	.1573	.2880	.3152	.3516	.0703	.1223	.1863	.2208	.0549	.0643	.1026	.1554
7	-2.591	5.865	.2342	.3761	.4124	.4523	.0787	.2081	.2496	.2833	.0596	.1012	.1694	.2067
8	-1.476	4.409	.3963	.4732	.5068	.5781	.1146	.2869	.3185	.3586	.0653	.1962	.2320	.2686
9	-.371	3.851	.4404	.4725	.5166	.5515	.1737	.2932	.3276	.3452	.0759	.2144	.2419	.2573
10	0	3.807	.4299	.4530	.4914	.5396	.1898	.2854	.3122	.3382	.0872	.2074	.2292	.2482
11	.381	3.863	.3754	.3970	.4362	.4816	.1610	.2496	.2763	.3030	.0633	.1814	.2032	.2215
12	.704	3.975	.3607	.3914	.4243	.4578	.1631	.2341	.2594	.2728	.0654	.1680	.1877	.2046
13	1.016	4.122	.3376	.3551	.3921	.4243	.1582	.2109	.2404	.2538	.0572	.1526	.1751	.1884
14	1.580	4.422	.2852	.2999	.3439	.3803	.1568	.1758	.2039	.2208	.0631	.1287	.1462	.1603
15	3.071	5.215	.2139	.2272	.2726	.3111	.1343	.1308	.1547	.1772	.0900	.1012	.1083	.1266

Station	Axial distance, x, cm	Diameter, D, cm	Stagnation pressure, P_0, N/cm^2											
			51.7				31.0				20.7			
			Nozzle roughness level, cm rms											
			Smooth	305×10^{-6}	445×10^{-6}	826×10^{-6}	Smooth	305×10^{-6}	445×10^{-6}	826×10^{-6}	Smooth	305×10^{-6}	445×10^{-6}	826×10^{-6}
			Heat transfer coefficient based on enthalpy, h_i, $g/(cm^2)(sec)$											
2	-5.296	14.580	0.0291	0.0265	0.0256	0.0250	0.0207	0.0193	0.0179	0.0179	0.0159	0.0149	0.0141	0.0143
3	-4.450	11.643	.0314	.0310	.0315	.0319	.0234	.0228	.0230	.0231	.0181	.0180	.0185	.0175
4	-4.153	10.612	.0322	.0322	.0325	.0343	.0240	.0240	.0238	.0243	.0186	.0189	.0188	.0185
5	-3.848	9.555	.0340	.0343	.0362	.0394	.0252	.0257	.0264	.0271	.0198	.0203	.0211	.0207
6	-3.063	6.939	.0431	.0450	.0574	.0979	.0328	.0339	.0364	.0453	.0258	.0266	.0278	.0302
7	-2.591	5.865	.0470	.0531	.0909	.1440	.0358	.0359	.0416	.0773	.0279	.0286	.0291	.0394
8	-1.476	4.409	.0503	.0951	.1601	.1964	.0380	.0371	.0609	.1244	.0296	.0297	.0305	.0769
9	-.371	3.851	.0471	.0888	.1727	.1887	.0394	.0333	.0970	.1216	.0261	.0263	.0291	.0776
10	0	3.807	.0530	.0804	.1601	.1817	.0313	.0318	.0949	.1160	.0238	.0244	.0269	.0762
11	.381	3.863	.0403	.1069	.1426	.1622	.0276	.0284	.0837	.1055	.0208	.0208	.0233	.0706
12	.704	3.975	.0368	.1160	.1321	.1468	.0259	.0283	.0801	.0956	.0332	.0196	.0304	.0633
13	1.016	4.122	.0354	.1048	.1230	.1356	.0225	.0255	.0766	.0865	.0168	.0171	.0310	.0570
14	1.580	4.422	.0277	.0930	.1028	.1146	.0188	.0228	.0645	.0731	.0140	.0134	.0347	.0482
15	3.071	5.215	.0208	.0727	.0755	.0888	.0131	.0135	.0479	.0548	.0091	.0097	.0156	.0356

TABLE V. - Continued. EXPERIMENTAL HEAT TRANSFER COEFFICIENTS IN 30°-15° AND 60°-15° NOZZLES

[Stagnation temperature T_0 - 539 K (970° R).]

(b) Concluded. 60°-15° nozzle, adiabatic inlet (inlet 2, table I)

(b-2) U.S. customary units

Station	Axial distance, x, in.	Diameter, D, in.	Stagnation pressure, P_0, psia											
			300				160				110			
			Nozzle roughness level, in. rms											
			Smooth	120×10^{-6}	175×10^{-6}	325×10^{-6}	Smooth	120×10^{-6}	175×10^{-6}	325×10^{-6}	Smooth	120×10^{-6}	175×10^{-6}	325×10^{-6}
			Heat transfer coefficient based on enthalpy, h_i, lbm/(in.^{2})(sec)											
2	-2.085	5.740	1.03×10^{-3}	0.988×10^{-3}	0.985×10^{-3}	1.05×10^{-3}	0.683×10^{-3}	0.631×10^{-3}	0.619×10^{-3}	0.619×10^{-3}	0.532×10^{-3}	0.485×10^{-3}	0.473×10^{-3}	0.473×10^{-3}
3	-1.752	4.584	1.12	1.24	1.41	1.83	.730	.730	.757	.839	.580	.550	.577	.604
4	-1.635	4.178	1.18	1.41	1.84	2.49	.749	.762	.813	1.19	.593	.572	.602	.700
5	-1.515	3.762	1.30	1.79	2.57	2.98	.791	.825	1.03	1.56	.624	.597	.684	.880
6	-1.206	2.732	2.25	4.12	4.51	5.03	1.00	1.74	2.65	3.14	.781	.915	1.46	2.21
7	-1.020	2.309	3.35	5.38	5.90	6.47	1.12	2.96	3.55	4.03	.848	1.44	2.41	2.94
8	-.581	1.736	5.67	6.77	7.25	8.27	1.63	4.08	4.53	5.10	.929	2.79	3.30	3.82
9	-.146	1.516	6.30	6.76	7.39	7.89	2.47	4.17	4.66	4.91	1.08	3.05	3.44	3.66
10	0	1.499	6.15	6.48	7.03	7.72	2.70	4.06	4.44	4.81	1.24	2.95	3.26	3.53
11	.150	1.521	5.37	5.68	6.24	6.89	2.29	3.55	3.93	4.31	.901	2.58	2.89	3.15
12	.277	1.565	5.16	5.60	6.07	6.55	2.32	3.33	3.69	3.88	.930	2.39	2.67	2.91
13	.400	1.623	4.83	5.08	5.61	6.07	2.25	3.00	3.42	3.61	.814	2.17	2.49	2.68
14	.622	1.741	4.08	4.29	4.92	5.44	2.23	2.50	2.90	3.14	.897	1.83	2.08	2.28
15	1.209	2.053	3.06	3.25	3.90	4.45	1.91	1.86	2.20	2.52	1.28	1.44	1.54	1.80

Station	Axial distance, x, in.	Diameter, D, in.	Stagnation pressure, P_0, psia											
			75				45				30			
			Nozzle roughness level, in. rms											
			Smooth	120×10^{-6}	175×10^{-6}	325×10^{-6}	Smooth	120×10^{-6}	175×10^{-6}	325×10^{-6}	Smooth	120×10^{-6}	175×10^{-6}	325×10^{-6}
			Heat transfer coefficient based on enthalpy, h_i, lbm/(in.^{2})(sec)											
2	-2.085	5.740	0.417×10^{-3}	0.379×10^{-3}	0.366×10^{-3}	0.358×10^{-3}	0.295×10^{-3}	0.275×10^{-3}	0.255×10^{-3}	0.255×10^{-3}	0.227×10^{-3}	0.213×10^{-3}	0.202×10^{-3}	0.204×10^{-3}
3	-1.752	4.584	.449	.444	.450	.456	.333	.324	.327	.328	.259	.258	.265	.251
4	-1.635	4.178	.460	.461	.465	.490	.341	.341	.338	.345	.266	.270	.269	.264
5	-1.515	3.762	.486	.490	.518	.563	.359	.365	.376	.386	.283	.290	.302	.296
6	-1.206	2.732	.617	.644	.821	1.40	.466	.482	.518	.644	.369	.381	.398	.432
7	-1.020	2.309	.673	.759	1.30	2.06	.509	.511	.592	1.10	.399	.409	.416	.564
8	-.581	1.736	.719	1.36	2.29	2.81	.540	.527	.866	1.77	.424	.425	.436	1.10
9	-.146	1.516	.674	1.27	2.47	2.70	.560	.473	1.38	1.73	.373	.376	.416	1.11
10	0	1.499	.758	1.15	2.29	2.60	.445	.453	1.35	1.65	.340	.349	.385	1.09
11	.150	1.521	.576	1.53	2.04	2.32	.393	.404	1.19	1.50	.298	.297	.334	1.01
12	.277	1.565	.526	1.66	1.89	2.10	.368	.403	1.14	1.36	.475	.281	.435	.906
13	.400	1.623	.506	1.50	1.76	1.94	.320	.363	1.09	1.23	.241	.244	.444	.815
14	.622	1.741	.396	1.33	1.47	1.64	.268	.324	.917	1.04	.201	.192	.497	.689
15	1.209	2.053	.298	1.04	1.08	1.27	.186	.192	.682	.779	.130	.138	.223	.510

TABLE V. - Continued. EXPERIMENTAL HEAT TRANSFER COEFFICIENTS IN 30°-15° AND 60°-15° NOZZLES

[Stagnation temperature T_0 = 539 K (970° R).]

(c) 30°-15° nozzle, cooled inlet (inlet 3, table I)

(c-1) SI units

Station	Axial distance x, cm	Diameter, D, cm	Stagnation pressure, P_0, N/cm^2											
			206.8				110.3				75.8			
			Nozzle roughness level, cm rms											
			Smooth	305×10^{-6}	445×10^{-6}	826×10^{-6}	Smooth	305×10^{-6}	445×10^{-6}	826×10^{-6}	Smooth	305×10^{-6}	445×10^{-6}	826×10^{-6}
			Heat transfer coefficient based on enthalpy, h_i, g/(cm^2)(sec)											
2	-11.468	15.875	0.0448	0.0500	0.0596	0.0510	0.0286	0.0328	0.0372	0.0293	0.0222	0.0242	0.0291	0.0224
3	-8.928	12.934	.0598	.0650	.0949	.0963	.0322	.0342	.0406	.0508	.0241	.0248	.0281	.0293
4	-6.380	9.992	.0970	.1118	.1413	.1244	.0461	.0531	.0759	.0731	.0276	.0307	.0391	.0508
5	-5.481	8.961	.1097	.1216	.1575	.1413	.0572	.0629	.0893	.0830	.0331	.0347	.0534	.0592
6	-4.602	7.945	.1174	.1301	.1498	.1526	.0678	.0745	.0914	.0935	.0392	.0429	.0639	.0692
7	-3.708	6.914	.1336	.1476	.1779	.1730	.0809	.0879	.1062	.1090	.0498	.0558	.0787	.0822
8	-2.819	5.883	.1715	.1969	.2151	.2137	.1069	.1223	.1371	.1371	.0695	.0858	.1026	.1048
9	-1.577	4.470	.2088	.2419	.2629	.2503	.1371	.1589	.1744	.1666	.0970	.1195	.1357	.1301
10	-.455	3.835	.2348	.2608	.2897	.2594	.1554	.1751	.1912	.1751	.1181	.1357	.1505	.1399
11	0	3.790	.2299	.2812	.3072	.2629	.1448	.1863	.2053	.1779	.1104	.1399	.1617	.1392
12	.330	3.815	.1828	.2496	.2784	.2447	.1336	.1624	.1800	.1617	.1034	.1223	.1392	.1280
13	.648	3.912	.1701	.2060	.2180	.2285	.1237	.1364	.1476	.1533	.0928	.1048	.1167	.1195
14	.996	4.074	.1708	.1821	.2095	.2215	.1153	.1251	.1385	.1448	.0893	.0970	.1069	.1132
15	1.610	4.399	.1610	.1905	.1990	.2109	.1062	.1188	.1266	.1329	.0816	.0900	.0963	.1019
16	3.101	5.187	.1399	.1680	.1793	.1856	.0886	.0998	.1076	.1146	.0671	.0738	.0801	.0851
17	6.949	7.259	.0893	.0949	.1062	.1097	.0526	.0545	.0582	.0610	.0373	.0385	.0423	.0422
18	13.889	10.978	.0356	.0376	.0394	.0417	.0201	.0213	.0226	.0224	.0146	.0151	.0157	.0195
19	20.831	14.712	.0193	.0191	.0198	.0200	.0106	.0106	.0111	.0222	.0074	.0074	.0082	.0213
20	20.021	18.593	.0141	.0160	.0162	.0326	.0095	.0122	.0162	.0285	.0101	.0130	.0145	.0258

Station	Axial distance, x, cm	Diameter, D, cm	Stagnation pressure, P_0, N/cm^2											
			51.7				31.0				20.7			
			Nozzle roughness level, cm rms											
			Smooth	305×10^{-6}	445×10^{-6}	826×10^{-6}	Smooth	305×10^{-6}	445×10^{-6}	826×10^{-6}	Smooth	305×10^{-6}	445×10^{-6}	826×10^{-6}
			Heat transfer coefficient based on enthalpy, h_i, g/(cm^2)(sec)											
2	-11.468	15.875	0.0174	0.0206	0.0226	0.0174	0.0126	0.0142	0.0161	0.0127	0.0097	0.0110	0.0121	0.0097
3	-8.928	12.934	.0185	.0193	.0212	.0195	.0132	.0138	.0150	.0138	.0103	.0108	.0113	.0104
4	-6.380	9.992	.0194	.0223	.0236	.0250	.0135	.0155	.0165	.0148	.0105	.0119	.0127	.0112
5	-5.481	8.961	.0217	.0221	.0261	.0301	.0148	.0152	.0166	.0157	.0116	.0120	.0127	.0118
6	-4.602	7.945	.0227	.0231	.0304	.0406	.0155	.0154	.0164	.0169	.0122	.0122	.0127	.0127
7	-3.708	6.914	.0252	.0257	.0430	.0565	.0161	.0157	.0181	.0205	.0126	.0124	.0136	.0143
8	-2.819	5.883	.0333	.0399	.0662	.0773	.0193	.0200	.0240	.0367	.0152	.0157	.0168	.0174
9	-1.557	4.470	.0434	.0650	.1026	.1005	.0219	.0236	.0466	.0652	.0173	.0179	.0207	.0289
10	-.455	3.835	.0599	.0984	.1167	.1090	.0225	.0337	.0703	.0752	.0170	.0177	.0276	.0453
11	0	3.790	.0629	.1097	.1244	.1104	.0210	.0356	.0794	.0759	.0147	.0201	.0409	.0498
12	.330	3.815	.0622	.0928	.1076	.0998	.0193	.0420	.0679	.0688	.0139	.0165	.0408	.0442
13	.648	3.912	.0538	.0780	.0900	.0942	.0172	.0385	.0593	.0651	.0127	.0160	.0385	.0431
14	.996	4.074	.0531	.0731	.0830	.0879	.0151	.0325	.0546	.0603	.0112	.0121	.0347	.0400
15	1.610	4.399	.0572	.0666	.0731	.0773	.0273	.0401	.0488	.0531	.0144	.0201	.0330	.0363
16	3.101	5.187	.0498	.0550	.0593	.0627	.0265	.0351	.0392	.0417	.0113	.0092	.0273	.0285
17	6.949	7.259	.0292	.0292	.0299	.0297	.0175	.0188	.0196	.0192	.0070	.0124	.0139	.0169
18	13.889	10.978	.0107	.0112	.0117	.0213	.0068	.0070	.0087	.0197	.0073	.0083	.0100	.0158
19	20.831	14.712	.0055	.0061	.0100	.0216	.0068	.0073	.0084	.0180	.0065	.0078	.0087	.0134
20	28.021	18.593	.0097	.0116	.0129	.0240	.0084	.0098	.0109	.0200	.0111	.0101	.0101	.0180

TABLE V. - Continued. EXPERIMENTAL HEAT TRANSFER COEFFICIENTS IN 30°-15° AND 60°-15° NOZZLES

[Stagnation temperature T_0 539 K (970° R).]

(c) Concluded. 30°-15° nozzle, cooled inlet (inlet 3, table I)

(c-2) U.S. customary units

Station	Axial distance, x, in.	Diameter, D, in.	Stagnation pressure, P_0, psia											
			300				160				110			
			Nozzle roughness level, in. rms											
			Smooth	120×10^{-6}	175×10^{-6}	325×10^{-6}	Smooth	120×10^{-6}	175×10^{-6}	325×10^{-6}	Smooth	120×10^{-6}	175×10^{-6}	325×10^{-6}
			Heat transfer coefficient based on enthalpy, h_i, lbm/(in.^{2})(sec)											
2	-4.515	6.250	0.637×10^{-3}	0.711×10^{-3}	0.847×10^{-3}	0.726×10^{-3}	0.407×10^{-3}	0.466×10^{-3}	0.529×10^{-3}	0.417×10^{-3}	0.316×10^{-3}	0.344×10^{-3}	0.414×10^{-3}	0.318×10^{-3}
3	-3.515	5.092	.850	.924	1.35	1.37	.458	.486	.577	.722	.343	.353	.399	.417
4	-2.512	3.934	1.38	1.59	2.01	1.77	.655	.755	1.08	1.04	.393	.437	.556	.722
5	-2.158	3.528	1.56	1.73	2.24	2.01	.814	.894	1.27	1.18	.471	.493	.760	.842
6	-1.812	3.128	1.67	1.85	2.13	2.17	.965	1.06	1.30	1.33	.557	.610	.909	.984
7	-1.460	2.722	1.90	2.10	2.53	2.46	1.15	1.25	1.51	1.55	.709	.794	1.12	1.17
8	-1.110	2.316	2.44	2.80	3.06	3.04	1.52	1.74	1.95	1.95	.989	1.22	1.46	1.49
9	-.613	1.760	2.97	3.44	3.74	3.56	1.95	2.26	2.48	2.37	1.38	1.70	1.93	1.85
10	-.175	1.510	3.34	3.71	4.12	3.69	2.21	2.49	2.72	2.49	1.68	1.93	2.14	1.99
11	0	1.492	3.27	4.00	4.37	3.74	2.06	2.65	2.92	2.53	1.57	1.99	2.30	1.98
12	.130	1.502	2.60	3.55	3.96	3.48	1.90	2.31	2.56	2.30	1.47	1.74	1.98	1.82
13	.255	1.540	2.42	2.93	3.10	3.25	1.76	1.94	2.10	2.18	1.32	1.49	1.66	1.70
14	.392	1.604	2.43	2.59	2.98	3.15	1.64	1.78	1.97	2.06	1.27	1.38	1.52	1.61
15	.634	1.732	2.29	2.71	2.83	3.00	1.51	1.69	1.80	1.89	1.16	1.28	1.37	1.45
16	1.221	2.042	1.99	2.39	2.55	2.64	1.26	1.42	1.53	1.63	.955	1.05	1.14	1.21
17	2.736	2.858	1.27	1.35	1.51	1.56	.748	.775	.828	.868	.531	.547	.601	.601
18	5.468	4.322	.507	.535	.560	.593	.286	.303	.321	.319	.207	.215	.224	.277
19	8.201	5.792	.275	.272	.282	.285	.151	.151	.158	.316	.105	.105	.116	.303
20	11.032	7.320	.200	.227	.231	.464	.135	.174	.231	.406	.143	.185	.206	.367

Station	Axial distance, x, in.	Diameter, D, in.	Stagnation pressure, P_0, psia											
			75				45				30			
			Nozzle roughness level, in. rms											
			Smooth	120×10^{-6}	175×10^{-6}	325×10^{-6}	Smooth	120×10^{-6}	175×10^{-6}	325×10^{-6}	Smooth	120×10^{-6}	175×10^{-6}	325×10^{-6}
			Heat transfer coefficient based on enthalpy, h_i, lbm/(in.^{2})(sec)											
2	-4.515	6.250	0.248×10^{-3}	0.293×10^{-3}	0.322×10^{-3}	0.247×10^{-3}	0.179×10^{-3}	0.202×10^{-3}	0.229×10^{-3}	0.181×10^{-3}	0.138×10^{-3}	0.156×10^{-3}	0.172×10^{-3}	0.138×10^{-3}
3	-3.515	5.092	.263	.275	.301	.278	.188	.196	.213	.196	.146	.154	.161	.148
4	-2.512	3.934	.276	.317	.336	.356	.192	.220	.235	.211	.149	.169	.180	.160
5	-2.158	3.528	.308	.315	.371	.428	.211	.216	.236	.224	.165	.170	.180	.168
6	-1.812	3.128	.323	.329	.433	.577	.220	.219	.233	.241	.173	.174	.180	.181
7	-1.460	2.722	.358	.365	.611	.804	.229	.224	.257	.291	.179	.177	.194	.203
8	-1.110	2.316	.473	.568	.941	1.10	.275	.285	.342	.522	.216	.224	.239	.248
9	-.613	1.760	.618	.924	1.46	1.43	.312	.336	.663	.928	.246	.255	.295	.411
10	-.175	1.510	.852	1.40	1.66	1.55	.320	.479	1.00	1.07	.242	.252	.393	.645
11	0	1.492	.894	1.56	1.77	1.57	.298	.506	1.13	1.08	.209	.286	.582	.709
12	.130	1.502	.885	1.32	1.53	1.42	.274	.597	.966	.979	.198	.235	.580	.629
13	.255	1.540	.765	1.11	1.28	1.34	.244	.548	.844	.926	.180	.228	.548	.613
14	.392	1.604	.755	1.04	1.18	1.25	.215	.462	.777	.858	.160	.172	.494	.569
15	.634	1.732	.814	.947	1.04	1.10	.389	.571	.694	.755	.205	.286	.469	.516
16	1.221	2.042	.709	.782	.844	.892	.377	.499	.557	.593	.161	.131	.388	.405
17	2.736	2.858	.416	.416	.425	.423	.249	.267	.279	.273	.100	.176	.197	.241
18	5.468	4.322	.152	.159	.167	.303	.097	.100	.123	.280	.104	.118	.142	.225
19	8.201	5.792	.078	.087	.142	.307	.097	.104	.120	.256	.093	.111	.123	.191
20	11.032	7.320	.138	.165	.184	.341	.119	.140	.155	.284	.158	.144	.144	.256

TABLE V. - Continued. EXPERIMENTAL HEAT TRANSFER COEFFICIENTS IN 30°-15° AND 60°-15° NOZZLES

[Stagnation temperature T_0 = 539 K (970° R).]

(d) 60°-15° nozzle, cooled inlet (inlet 3, table I)

(d-1) SI units

Station	Axial distance, x, cm	Diameter, D, cm	Stagnation pressure, P_0, N/cm^2											
			206.8				110.3				75.8			
			Nozzle roughness level, cm rms											
			Smooth	305×10^{-6}	445×10^{-6}	826×10^{-6}	Smooth	305×10^{-6}	445×10^{-6}	826×10^{-6}	Smooth	305×10^{-6}	445×10^{-6}	826×10^{-6}
			Heat transfer coefficient based on enthalpy, h_i, $g/(cm^2)(sec)$											
2	-5.296	14.580	0.0498	0.0505	0.0500	0.0641	0.0328	0.0319	0.0309	0.0392	0.0249	0.0243	0.0236	0.0296
3	-4.450	11.643	.0581	.0634	.0776	.0881	.0380	.0379	.0386	.0437	.0301	.0293	.0295	.0321
4	-4.153	10.612	.0648	.0741	.0979	.1328	.0408	.0412	.0427	.0619	.0318	.0316	.0317	.0396
5	-3.848	9.555	.0741	.0951	.1258	.1657	.0456	.0458	.0558	.0865	.0355	.0342	.0364	.0494
6	-3.063	6.939	.1209	.1915	.2055	.2586	.0571	.0893	.1118	.1624	.0446	.0499	.0752	.1188
7	-2.591	5.865	.1706	.2419	.2572	.2838	.0631	.1441	.1673	.1863	.0473	.0773	.1202	.1427
8	-1.476	4.409	.2488	.2845	.3041	.3278	.0928	.1877	.2053	.2285	.0514	.1350	.1575	.1744
9	-.371	3.851	.2649	.2936	.3104	.3327	.1589	.1990	.2102	.2215	.0634	.1491	.1652	.1737
10	0	3.807	.2558	.2810	.2992	.3341	.1498	.1898	.1990	.2222	.0639	.1434	.1547	.1715
11	.381	3.863	.2377	.2649	.2845	.3320	.1413	.1737	.1863	.2201	.0595	.1301	.1434	.1723
12	.704	3.975	.2433	.2558	.2656	.3411	.1561	.1624	.1737	.2165	.0907	.1209	.1315	.1631
13	1.016	4.122	.2272	.2328	.2426	.3229	.1392	.1469	.1582	.1997	.0557	.1097	.1209	.1519
14	1.580	4.422	.2006	.2139	.2279	.2670	.1266	.1322	.1441	.1645	.0650	.0991	.1076	.1244
15	3.071	5.215	.1664	.1817	.1936	.2202	.1062	.1097	.1160	.1322	.0633	.0801	.0851	.0970

Station	Axial distance, x, cm	Diameter, D, cm	Stagnation pressure, P_0, N/cm^2											
			51.7				31.0				20.7			
			Nozzle roughness level, cm rms											
			Smooth	305×10^{-6}	445×10^{-6}	826×10^{-6}	Smooth	305×10^{-6}	445×10^{-6}	826×10^{-6}	Smooth	305×10^{-6}	445×10^{-6}	826×10^{-6}
			Heat transfer coefficient based on enthalpy, h_i, $g/(cm^2)(sec)$											
2	-5.296	14.580	0.0185	0.0185	0.0178	0.0224	0.0130	0.0131	0.0127	0.0157	0.0101	0.0101	0.0097	0.0118
3	-4.450	11.643	.0227	.0227	.0228	.0243	.0164	.0167	.0165	.0171	.0127	.0129	.0128	.0130
4	-4.153	10.612	.0243	.0244	.0242	.0287	.0176	.0178	.0174	.0199	.0140	.0140	.0135	.0151
5	-3.848	9.555	.0275	.0269	.0272	.0331	.0203	.0198	.0196	.0228	.0161	.0156	.0152	.0173
6	-3.063	6.939	.0350	.0346	.0412	.0248	.0263	.0252	.0266	.0361	.0210	.0201	.0201	.0245
7	-2.591	5.865	.0368	.0410	.0691	.1014	.0276	.0281	.0328	.0537	.0220	.0228	.0231	.0303
8	-1.476	4.409	.0384	.0706	.1125	.1328	.0291	.0295	.0509	.0879	.0231	.0236	.0243	.0549
9	-.371	3.851	.0394	.0651	.1209	.1328	.0265	.0268	.0745	.0886	.0209	.0212	.0240	.0599
10	0	3.807	.0375	.0577	.1132	.1300	.0238	.0254	.0703	.0851	.0182	.0191	.0212	.0568
11	.381	3.863	.0324	.0804	.1042	.1286	.0220	.0227	.0640	.0837	.0167	.0166	.0190	.0556
12	.704	3.975	.0560	.0853	.0965	.1202	.0267	.0223	.0603	.0780	.0173	.0153	.0246	.0516
13	1.016	4.122	.0311	.0783	.0881	.1111	.0198	.0207	.0567	.0710	.0143	.0135	.0242	.0473
14	1.580	4.422	.0305	.0727	.0783	.0909	.0161	.0155	.0501	.0586	.0124	.0113	.0296	.0394
15	3.071	5.215	.0175	.0583	.0594	.0699	.0115	.0136	.0383	.0439	.0084	.0076	.0168	.0292

TABLE V. - Concluded. EXPERIMENTAL HEAT TRANSFER COEFFICIENTS IN 30°-15° AND 60°-15° NOZZLES

[Stagnation temperature T_0 = 539 K (970° R).]

(d) Concluded. 60°-15° nozzle, cooled inlet (inlet 3, table I)

(d-2) U.S. customary units

Station	Axial distance, x, in.	Diameter, D, in.	Stagnation pressure, P_0, psia											
			300				160				110			
			Nozzle roughness level, in. rms											
			Smooth	120×10^{-6}	175×10^{-6}	325×10^{-6}	Smooth	120×10^{-6}	175×10^{-6}	325×10^{-6}	Smooth	120×10^{-6}	175×10^{-6}	325×10^{-6}
			Heat transfer coefficient based on enthalpy, h_1, lbm/(in.^{2})(sec)											
2	-2.085	5.740	0.712×10^{-3}	0.722×10^{-3}	0.715×10^{-3}	0.917×10^{-3}	0.467×10^{-3}	0.454×10^{-3}	0.440×10^{-3}	0.557×10^{-3}	0.354×10^{-3}	0.346×10^{-3}	0.335×10^{-3}	0.421×10^{-3}
3	-1.752	4.584	.831	.907	1.11	1.26	.540	.539	.549	.621	.428	.417	.419	.456
4	-1.635	4.178	.927	1.06	1.40	1.90	.581	.586	.607	.881	.452	.449	.451	.563
5	-1.515	3.762	1.06	1.36	1.80	2.37	.649	.651	.793	1.23	.505	.487	.518	.702
6	-1.206	2.732	1.73	2.74	2.94	3.70	.812	1.27	1.59	2.31	.635	.710	1.07	1.69
7	-1.020	2.309	2.44	3.46	3.68	4.06	.898	2.05	2.38	2.65	.673	1.10	1.71	2.03
8	-.581	1.736	3.56	4.07	4.35	4.69	1.32	2.67	2.92	3.25	.731	1.92	2.24	2.48
9	-.146	1.516	3.79	4.20	4.44	4.76	2.26	2.83	2.99	3.15	.902	2.12	2.35	2.47
10	0	1.499	3.66	4.02	4.28	4.78	2.13	2.70	2.83	3.16	.909	2.04	2.20	2.44
11	.150	1.521	3.40	3.79	4.07	4.75	2.01	2.47	2.65	3.13	.846	1.85	2.04	2.45
12	.277	1.565	3.48	3.66	3.80	4.88	2.22	2.31	2.47	3.08	1.29	1.72	1.87	2.32
13	.400	1.623	3.25	3.33	3.47	4.62	1.98	2.09	2.25	2.84	.793	1.56	1.72	2.16
14	.622	1.741	2.87	3.06	3.26	3.82	1.80	1.88	2.05	2.34	.924	1.41	1.53	1.77
15	1.209	2.053	2.38	2.60	2.77	3.15	1.51	1.56	1.65	1.88	.901	1.14	1.21	1.38

Station	Axial distance, x, in.	Diameter, D, in.	Stagnation pressure, P_0, psia											
			75				45				30			
			Nozzle roughness level, in. rms											
			Smooth	120×10^{-6}	175×10^{-6}	325×10^{-6}	Smooth	120×10^{-6}	175×10^{-6}	325×10^{-6}	Smooth	120×10^{-6}	175×10^{-6}	325×10^{-6}
			Heat transfer coefficient based on enthalpy, h_1, lbm/(in.^{2})(sec)											
2	-2.085	5.740	0.265×10^{-3}	0.265×10^{-3}	0.255×10^{-3}	0.320×10^{-3}	0.185×10^{-3}	0.187×10^{-3}	0.180×10^{-3}	0.223×10^{-3}	0.145×10^{-3}	0.144×10^{-3}	0.138×10^{-3}	0.169×10^{-3}
3	-1.752	4.584	.325	.325	.326	.347	.233	.238	.235	.243	.181	.185	.183	.186
4	-1.635	4.178	.347	.349	.346	.411	.251	.253	.248	.263	.201	.200	.193	.216
5	-1.515	3.762	.393	.385	.389	.474	.289	.281	.279	.324	.231	.223	.218	.247
6	-1.206	2.732	.501	.495	.589	1.07	.374	.359	.378	.513	.301	.288	.288	.350
7	-1.020	2.309	.527	.587	.988	1.45	.393	.400	.467	.764	.315	.326	.331	.433
8	-.581	1.736	.550	1.01	1.61	1.90	.414	.419	.724	1.25	.331	.337	.347	.785
9	-.146	1.516	.563	.931	1.73	1.90	.377	.381	1.06	1.26	.299	.303	.344	.857
10	0	1.499	.537	.825	1.62	1.86	.338	.361	1.00	1.21	.261	.273	.303	.812
11	.150	1.521	.463	1.15	1.49	1.84	.313	.323	.911	1.19	.239	.237	.272	.796
12	.277	1.565	.801	1.22	1.38	1.72	.380	.317	.858	1.11	.247	.219	.352	.738
13	.400	1.623	.445	1.12	1.26	1.59	.281	.294	.807	1.01	.204	.193	.346	.676
14	.622	1.741	.436	1.04	1.12	1.30	.229	.220	.713	.834	.177	.162	.423	.563
15	1.209	2.053	.251	.834	.850	1.00	.163	.193	.545	.625	.120	.109	.241	.418

TABLE VI. - EXPERIMENTAI WALL TEMPERATURES IN 30^{O}-15^{O} AND 60^{O}-15^{O} NOZZLES

[Stagnation temperature T_0 = 539 K (970^{O} R).]

(a) 30^{O}-15^{O} nozzle, adiabatic wall (inlet 2, table I)

(a-1) SI units

Station	Axial distance, x, cm	Diameter, D, cm	Stagnation pressure, P_0, N/cm^2											
			206.8				110.3				75.8			
			Nozzle roughness level, cm rms											
			Smooth	305×10^{-6}	445×10^{-6}	826×10^{-6}	Smooth	305×10^{-6}	445×10^{-6}	826×10^{-6}	Smooth	305×10^{-6}	445×10^{-6}	826×10^{-6}
			Wall temperature, T_w, K											
2	-11.468	15.875	406.6	412.3	408.1	411.1	379.1	387.0	380.3	381.6	365.7	373.6	366.0	365.0
3	-8.928	12.934	415.7	416.2	429.8	439.4	374.6	381.9	379.2	398.0	359.2	366.2	359.5	367.9
4	-6.380	9.992	446.6	446.5	449.8	453.4	393.9	402.7	414.8	421.0	367.9	374.7	377.1	396.0
5	-5.481	8.961	449.4	452.9	456.8	461.8	403.0	413.9	424.1	430.0	371.2	379.3	393.1	408.2
6	-4.602	7.945	448.1	459.1	460.9	466.3	412.1	424.4	430.1	436.3	377.6	387.7	405.7	416.3
7	-3.708	6.914	454.8	463.8	466.4	471.0	422.7	435.6	437.2	443.9	389.7	403.1	417.2	425.7
8	-2.819	5.883	463.9	475.8	474.6	478.6	434.8	448.3	447.1	452.3	406.9	423.2	428.6	435.0
9	-1.557	4.470	479.5	486.8	484.7	488.4	454.3	465.3	462.5	466.5	433.4	447.6	447.9	452.4
10	-.455	3.835	481.0	483.9	483.1	486.4	457.2	464.9	463.6	466.7	440.4	451.0	451.0	454.7
11	0	3.790	478.8	481.3	479.1	480.8	454.6	460.2	459.4	461.3	440.0	446.9	445.8	449.2
12	.330	3.815	468.9	477.8	476.3	479.5	445.0	456.6	456.1	459.6	429.8	442.8	442.3	447.0
13	.648	3.912	459.8	470.7	469.9	472.8	437.4	450.3	449.1	452.8	422.5	434.5	435.4	440.6
14	.996	4.074	451.7	464.6	463.4	466.2	432.0	441.5	440.6	444.4	417.7	426.6	425.8	430.9
15	1.610	4.399	452.5	460.7	458.2	462.3	427.5	437.6	433.3	438.5	412.0	420.7	417.2	423.6
16	3.101	5.187	444.2	448.9	447.3	452.2	416.6	422.5	419.5	425.7	400.9	404.8	401.6	408.8
17	6.949	7.259	411.0	414.3	411.2	419.2	380.7	386.9	379.8	388.7	365.7	371.6	362.6	370.1
18	18.889	10.978	365.8	364.4	352.2	358.6	338.8	340.1	328.2	331.4	327.9	329.6	316.9	319.2
19	20.831	14.712	330.0	332.7	320.1	320.9	311.9	317.6	305.0	303.9	304.6	311.3	299.1	299.4
20	28.021	18.593	321.6	325.7	316.1	319.1	311.7	320.9	311.3	308.3	314.2	319.4	310.4	310.4

Station	Axial distance, x, cm	Diameter, D, cm	Stagnation pressure, P_0, N/cm^2											
			51.7				31.0				20.7			
			Nozzle roughness level, cm rms											
			Smooth	305×10^{-6}	445×10^{-6}	826×10^{-6}	Smooth	305×10^{-6}	445×10^{-6}	826×10^{-6}	Smooth	305×10^{-6}	445×10^{-6}	826×10^{-6}
			Wall temperature, T_w, K											
2	-11.468	15.875	354.9	361.1	353.5	352.1	339.8	346.6	338.2	336.5	328.5	336.9	327.6	326.6
3	-8.928	12.934	348.1	353.6	346.5	349.2	333.4	341.9	332.4	333.4	324.2	332.3	323.1	324.1
4	-6.380	9.992	352.0	356.1	350.3	356.7	335.4	341.8	333.3	333.4	325.4	332.5	323.1	323.2
5	-5.481	8.961	350.2	356.5	354.0	364.3	333.1	341.6	333.2	334.7	323.7	332.3	322.9	324.3
6	-4.602	7.945	348.9	356.4	359.7	379.3	330.7	339.4	333.0	334.6	321.0	330.3	321.9	323.6
7	-3.708	6.914	352.3	359.9	377.2	401.1	331.3	340.3	335.6	340.1	321.6	330.6	322.9	324.7
8	-2.819	5.883	361.3	373.7	398.0	414.9	335.2	344.7	340.3	358.3	324.8	334.2	326.3	328.2
9	-1.557	4.470	383.9	404.8	430.1	435.9	345.4	355.8	376.4	405.0	333.2	341.2	337.3	363.2
10	-.455	3.835	399.7	431.3	436.6	440.0	348.3	371.1	406.4	415.3	333.9	340.6	351.2	387.3
11	0	3.790	417.2	430.8	431.3	434.8	350.3	368.9	404.0	410.7	330.0	341.0	361.0	386.2
12	.330	3.815	395.0	424.9	427.3	432.8	343.3	381.1	399.7	408.2	327.5	336.6	368.6	383.7
13	.648	3.912	389.7	416.7	420.3	425.9	334.4	377.0	393.9	401.6	320.9	335.3	365.8	377.9
14	.996	4.074	387.7	409.3	410.2	415.6	328.8	365.4	384.0	391.4	316.3	326.6	356.4	369.5
15	1.610	4.399	393.7	402.6	400.3	406.9	352.4	375.0	375.2	382.0	327.6	336.8	352.6	361.3
16	3.101	5.187	385.9	389.1	384.4	390.5	351.8	367.1	361.7	365.5	320.1	319.1	343.1	346.6
17	6.949	7.259	353.7	357.5	347.9	352.0	333.3	340.9	329.9	331.2	295.6	325.4	317.6	317.8
18	13.889	10.978	318.8	322.2	308.5	309.7	307.1	311.8	303.4	305.6	299.8	310.6	303.7	282.9
19	20.831	14.712	298.8	307.2	303.8	303.0	302.4	309.5	300.3	301.3	297.8	310.3	299.9	297.6
20	28.021	18.593	309.5	315.7	308.3	307.7	304.9	312.8	304.9	299.7	310.8	314.6	302.7	280.9

TABLE VI. - Continued. EXPERIMENTAL WALL TEMPERATURES IN 30°-15° AND 60°-15° NOZZLES

[Stagnation temperature T_0 = 539 K (970° R).]

(a) Concluded. 30°-15° nozzle, adiabatic wall (inlet 2, table I)

(a-2) U.S. customary units

Station	Axial distance, x, in.	Diameter, D, in.	Stagnation pressure, P_0, psia											
			300				160				110			
			Nozzle roughness level, in. rms											
			Smooth	120×10^{-6}	175×10^{-6}	325×10^{-6}	Smooth	120×10^{-6}	175×10^{-6}	325×10^{-6}	Smooth	120×10^{-6}	175×10^{-6}	325×10^{-6}
			Wall temperature, T_w, $^{\circ}$R											
2	-4.515	6.250	731.8	742.1	734.6	739.9	682.4	696.6	684.5	686.9	658.2	672.5	658.8	657.0
3	-3.515	5.092	748.3	749.2	773.7	791.0	674.2	687.5	682.6	716.4	646.5	659.1	647.1	662.3
4	-2.512	3.934	803.9	803.7	809.6	816.2	709.1	724.8	746.6	757.8	662.2	674.4	678.7	712.8
5	-2.158	3.528	808.9	815.3	822.3	831.1	725.4	745.1	763.3	774.0	668.2	682.7	707.5	734.7
6	-1.812	3.128	806.5	826.4	829.6	839.3	741.7	763.9	774.1	785.4	679.7	697.8	730.2	749.4
7	-1.460	2.722	818.6	834.8	839.5	847.8	760.8	784.0	787.0	799.0	701.5	725.5	750.9	766.3
8	-1.110	2.316	835.0	856.4	854.3	861.5	782.6	806.9	804.8	814.1	732.4	761.8	771.5	783.0
9	-.613	1.760	863.1	876.2	872.4	879.1	817.8	837.6	832.5	839.7	780.1	805.7	806.2	814.4
10	-.175	1.510	865.8	871.1	869.6	875.6	823.0	836.8	834.5	840.0	792.8	811.8	811.8	818.4
11	0	1.492	861.8	866.3	862.3	865.5	818.3	828.3	826.9	830.4	792.0	804.5	802.4	808.6
12	.130	1.502	844.1	860.1	857.4	863.1	801.0	821.9	820.9	827.3	773.6	797.0	796.2	804.6
13	.255	1.540	827.7	847.2	845.8	851.1	787.3	810.5	808.3	815.1	760.5	782.1	783.7	793.0
14	.392	1.604	813.1	836.3	834.2	839.2	777.6	794.7	793.1	800.0	751.9	767.8	766.5	775.7
15	.634	1.732	814.5	829.2	824.7	832.2	769.5	787.7	779.9	789.3	741.6	757.2	750.9	762.4
16	1.221	2.042	799.5	808.0	805.2	813.9	749.8	760.5	755.1	766.2	721.6	728.7	722.8	735.8
17	2.736	2.858	739.8	745.7	740.2	754.6	685.2	696.5	683.6	699.7	658.2	668.9	652.6	666.1
18	5.468	4.322	658.4	656.0	634.0	645.4	609.9	612.2	590.8	596.6	590.3	593.3	570.4	574.5
19	8.201	5.792	594.0	598.9	576.1	577.6	561.5	571.7	549.0	547.1	548.3	560.3	538.4	538.9
20	11.032	7.320	578.8	586.3	569.0	574.4	561.1	577.6	560.4	554.9	565.6	574.9	558.7	558.7

Station	Axial distance, x, in.	Diameter, D, in.	Stagnation pressure, P_0, psia											
			75				45				30			
			Nozzle roughness level, in. rms											
			Smooth	120×10^{-6}	175×10^{-6}	325×10^{-6}	Smooth	120×10^{-6}	175×10^{-6}	325×10^{-6}	Smooth	120×10^{-6}	175×10^{-6}	325×10^{-6}
			Wall temperature, T_w, $^{\circ}$R											
2	-4.515	6.250	638.8	650.0	636.3	633.8	611.6	623.8	608.8	605.7	591.3	606.4	589.6	587.9
3	-3.515	5.092	626.5	636.5	623.7	628.6	600.1	615.4	598.4	600.1	583.5	598.1	581.5	583.3
4	-2.512	3.934	633.6	641.0	630.6	642.1	603.8	615.3	599.9	600.1	585.7	598.5	581.5	581.7
5	-2.158	3.528	630.4	641.7	637.2	655.7	599.6	614.8	599.8	602.4	582.6	598.2	581.2	583.8
6	-1.812	3.128	628.1	641.5	647.4	682.7	595.2	610.9	599.4	602.2	577.8	594.6	579.4	582.5
7	-1.460	2.722	634.2	647.8	679.0	722.0	596.4	612.6	604.0	612.1	578.9	595.1	581.3	584.4
8	-1.110	2.316	650.4	672.7	716.4	746.8	603.4	620.5	612.6	644.9	584.6	601.5	587.4	590.7
9	-.613	1.760	691.0	728.6	774.2	784.6	621.8	640.5	677.6	729.0	599.8	614.2	607.2	653.7
10	-.175	1.510	719.4	776.3	785.9	792.0	626.9	668.0	731.6	747.6	601.1	613.0	632.1	697.2
11	0	1.492	750.9	775.4	776.4	782.7	630.5	664.1	727.2	739.3	594.1	613.8	649.8	695.1
12	.130	1.502	711.0	764.9	769.2	779.1	618.0	686.0	719.5	734.8	589.5	605.8	663.4	690.6
13	.255	1.540	701.4	750.1	756.5	766.6	601.9	678.6	709.1	722.9	577.6	603.5	658.5	680.3
14	.392	1.604	697.9	736.8	738.3	748.0	591.9	657.8	691.2	704.6	569.4	587.8	641.6	665.1
15	.634	1.732	708.7	724.7	720.6	732.4	634.4	675.0	675.4	687.7	589.6	606.3	634.6	650.4
16	1.221	2.042	694.6	700.4	691.9	702.9	633.3	660.8	651.1	657.9	576.2	574.4	617.6	623.9
17	2.736	2.858	636.7	643.5	626.3	633.6	599.9	613.7	593.8	596.2	532.0	585.7	571.7	572.0
18	5.468	4.322	573.9	580.0	555.3	557.4	552.7	561.2	546.1	550.1	539.7	559.0	546.7	509.3
19	8.201	5.792	537.9	553.0	546.8	545.4	544.4	557.1	540.6	542.4	536.0	558.5	539.8	535.6
20	11.032	7.320	557.1	568.2	555.0	553.9	548.8	563.1	548.8	539.4	559.5	566.2	544.9	505.7

TABLE VI. - Continued. EXPERIMENTAL WALL TEMPERATURES IN 30°-15° AND 60°-15° NOZZLES

[Stagnation temperature T_0 = 539 K (970° R).]

(b) 60°-15° nozzle, adiabatic inlet (inlet 2, table I)

(b-1) SI units

Station	Axial distance, x, cm	Diameter, D, cm	Stagnation pressure, P_0, N/cm^2											
			206.8				110.3				75.8			
			Nozzle roughness level, cm rms											
			Smooth	305×10^{-6}	445×10^{-6}	826×10^{-6}	Smooth	305×10^{-6}	445×10^{-6}	826×10^{-6}	Smooth	305×10^{-6}	445×10^{-6}	826×10^{-6}
			Wall temperature, T_w, K											
2	-5.296	14.580	398.9	382.8	395.1	399.1	375.3	356.7	368.6	369.3	362.9	343.4	355.1	356.6
3	-4.450	11.643	399.8	394.7	413.6	428.1	375.0	362.8	376.7	382.9	363.3	348.2	362.3	366.1
4	-4.153	10.612	403.4	401.9	428.3	444.7	376.9	364.4	379.8	401.6	364.9	349.2	363.7	372.9
5	-3.848	9.555	408.4	417.4	445.8	454.7	379.6	369.4	392.2	417.5	367.2	352.4	369.2	385.1
6	-3.063	6.939	440.1	466.3	477.1	481.4	392.4	416.7	448.7	457.4	378.4	377.3	414.6	439.1
7	-2.591	5.865	463.3	479.8	488.5	491.8	401.4	449.0	465.3	470.6	385.1	405.9	444.6	455.8
8	-1.476	4.409	484.6	486.8	494.7	498.1	420.9	463.9	475.8	479.4	388.9	443.7	460.8	467.4
9	-.371	3.851	484.1	482.0	489.8	491.5	440.8	460.7	471.5	473.1	394.3	444.8	457.7	460.8
10	0	3.807	480.7	478.5	486.3	488.6	442.9	457.8	468.1	470.4	400.3	441.6	453.6	457.3
11	.381	3.863	473.8	470.9	479.8	482.3	434.1	449.2	461.0	463.4	384.4	432.7	446.3	450.2
12	.704	3.975	468.2	465.7	474.2	476.2	431.2	441.3	453.3	454.8	382.9	424.1	437.9	442.0
13	1.016	4.122	463.4	460.7	470.8	472.9	427.5	435.4	449.4	450.9	375.0	418.2	433.8	437.3
14	1.580	4.422	454.2	450.6	462.2	465.9	424.8	423.1	437.8	441.6	377.9	405.9	420.9	426.6
15	3.071	5.215	440.1	434.3	448.1	453.6	413.7	399.7	420.7	426.8	392.9	388.7	401.4	410.2

Station	Axial distance, x, cm	Diameter, D, cm	Stagnation pressure, P_0, N/cm^2											
			51.7				31.0				20.7			
			Nozzle roughness level, cm rms											
			Smooth	305×10^{-6}	445×10^{-6}	826×10^{-6}	Smooth	305×10^{-6}	445×10^{-6}	826×10^{-6}	Smooth	305×10^{-6}	445×10^{-6}	826×10^{-6}
			Wall temperature, T_w, K											
2	-5.296	14.580	352.2	332.4	343.3	344.5	338.6	319.9	434.2	332.3	330.4	311.2	322.8	326.2
3	-4.450	11.643	351.8	337.6	350.2	352.4	339.7	324.7	437.4	339.1	331.6	316.1	328.7	330.6
4	-4.153	10.612	353.6	338.6	351.2	354.9	341.3	326.1	437.8	340.5	333.1	317.1	329.2	332.1
5	-3.848	9.555	355.7	342.1	355.2	361.6	343.4	329.1	439.4	345.0	334.9	319.9	332.5	335.8
6	-3.063	6.939	366.5	356.9	381.2	412.1	353.1	340.8	446.2	369.6	343.7	330.6	343.9	350.7
7	-2.591	5.865	372.8	366.8	408.7	435.4	358.8	345.2	448.9	398.9	348.6	334.3	347.3	363.4
8	-1.476	4.409	375.2	399.8	440.8	451.1	360.4	346.2	452.2	425.1	349.9	335.4	349.3	396.6
9	-.371	3.851	369.8	393.5	440.1	444.6	354.8	338.7	447.5	419.9	343.3	328.5	344.1	394.9
10	0	3.807	374.5	385.9	435.3	441.1	349.1	336.8	439.3	416.2	339.1	325.1	341.2	392.3
11	.381	3.863	362.4	402.6	428.1	433.9	345.3	332.1	424.0	410.2	335.4	319.7	336.4	387.6
12	.704	3.975	355.8	403.1	419.7	424.7	341.0	329.8	412.8	400.9	339.7	315.8	344.1	379.2
13	1.016	4.122	353.7	397.2	415.2	419.9	335.9	325.9	406.3	395.4	327.7	311.8	345.3	373.8
14	1.580	4.422	343.2	387.4	402.1	408.5	329.8	320.1	393.1	384.1	322.6	303.9	347.2	363.9
15	3.071	5.215	332.5	369.4	382.4	391.6	320.4	303.9	372.2	366.8	313.6	294.6	319.2	348.8

TABLE VI. - Continued. EXPERIMENTAL WALL TEMPERATURES IN 30°-15° AND 60°-15° NOZZLES

[Stagnation temperature T_0 539 K (970° R).]

(b) Concluded. 60°-15° nozzle, adiabatic inlet (inlet 2, table I)

(b-2) U.S. customary units

Station	Axial distance, x, in.	Diameter, D, in.	Stagnation pressure, P_0, psia											
			300				160				110			
			Nozzle roughness level, in. rms											
			Smooth	120×10^{-6}	175×10^{-6}	325×10^{-6}	Smooth	120×10^{-6}	175×10^{-6}	325×10^{-6}	Smooth	120×10^{-6}	175×10^{-6}	325×10^{-6}
			Wall temperature, T_w, $^{\circ}$R											
2	-2.085	5.740	718.1	689.1	711.1	718.3	675.5	642.1	663.5	664.8	653.2	618.1	639.1	641.9
3	-1.752	4.584	719.7	710.5	744.5	770.5	675.0	653.0	678.0	689.2	653.9	626.8	652.2	659.0
4	-1.635	4.178	726.1	723.4	771.0	800.4	678.5	655.9	683.7	722.9	656.9	628.5	654.7	671.2
5	-1.515	3.762	735.2	751.3	802.4	818.4	683.2	665.0	705.9	751.5	661.0	634.4	664.6	693.2
6	-1.206	2.732	792.2	839.4	858.7	866.6	706.3	750.1	807.7	823.4	681.2	679.2	746.2	790.3
7	-1.020	2.309	833.9	863.6	879.3	885.3	722.6	808.2	837.5	847.0	693.2	730.7	800.2	820.4
8	-.581	1.736	872.2	876.3	890.5	896.6	757.7	835.0	856.5	862.9	700.0	798.7	829.5	841.4
9	-.146	1.516	871.4	867.6	881.6	884.7	793.4	829.3	848.7	851.6	709.7	800.6	823.8	829.4
10	0	1.499	865.3	861.3	875.4	879.5	797.3	824.1	842.5	846.8	720.6	794.8	816.5	823.1
11	.150	1.521	852.9	847.7	863.6	868.1	781.4	808.6	829.8	834.2	692.0	778.8	803.4	810.3
12	.277	1.565	842.8	838.2	853.6	857.2	776.2	794.4	815.9	818.7	689.2	763.4	788.3	795.6
13	.400	1.623	834.2	829.3	847.5	851.2	769.5	783.8	808.9	811.6	675.0	752.7	780.9	787.2
14	.622	1.741	817.6	811.0	832.0	838.6	764.7	761.5	788.1	794.8	680.2	730.6	757.6	767.8
15	1.209	2.053	792.1	781.8	806.6	816.4	744.7	719.4	757.3	768.3	707.3	699.6	722.6	738.3

Station	Axial distance, x, in.	Diameter, D, in.	Stagnation pressure, P_0, psia											
			75				45				30			
			Nozzle roughness level, in. rms											
			Smooth	120×10^{-6}	175×10^{-6}	325×10^{-6}	Smooth	120×10^{-6}	175×10^{-6}	325×10^{-6}	Smooth	120×10^{-6}	175×10^{-6}	325×10^{-6}
			Wall temperature, T_w, $^{\circ}$R											
2	-2.085	5.740	634.0	598.3	617.9	620.1	609.4	575.9	781.5	598.2	594.7	560.2	581.1	587.1
3	-1.752	4.584	633.3	607.7	630.4	634.4	611.4	584.5	787.4	610.4	596.8	568.9	591.7	595.0
4	-1.635	4.178	636.5	609.5	632.1	638.9	614.4	586.9	788.1	612.9	599.5	570.8	592.5	597.8
5	-1.515	3.762	640.2	615.8	639.4	650.8	618.1	592.3	791.0	621.0	602.8	575.8	598.5	604.4
6	-1.206	2.732	659.7	642.4	686.2	741.8	635.6	613.5	803.1	665.3	618.7	595.0	619.1	631.2
7	-1.020	2.309	671.1	660.2	735.7	783.8	645.9	621.3	808.0	718.0	627.5	601.7	625.1	654.2
8	-.581	1.736	675.3	719.7	793.4	811.9	648.8	623.2	814.0	765.2	629.9	603.8	628.7	713.8
9	-.146	1.516	665.6	708.3	792.2	800.2	638.7	609.7	805.5	755.9	617.9	591.3	619.3	710.8
10	0	1.499	674.1	694.6	783.5	794.0	628.3	606.3	790.8	749.2	610.4	585.2	614.1	706.2
11	.150	1.521	652.3	724.7	770.5	781.0	621.5	597.8	763.2	738.3	603.7	575.4	605.5	697.7
12	.277	1.565	640.4	725.6	755.4	764.4	613.8	593.6	743.0	721.6	611.4	568.5	619.4	682.6
13	.400	1.623	636.7	714.9	747.4	755.8	604.6	586.6	731.3	711.8	589.8	561.3	621.6	672.8
14	.622	1.741	617.7	697.3	723.7	735.3	593.7	576.1	707.6	691.4	580.6	547.1	624.9	655.1
15	1.209	2.053	598.5	664.9	688.3	704.8	576.7	547.0	669.9	660.2	564.5	530.3	574.6	627.8

TABLE VI. - Continued. EXPERIMENTAL WALL TEMPERATURES IN 30°-15° AND 60°-15° NOZZLES

[Stagnation temperature T_0 = 539 K (970° R).]

(c) 30°-15° nozzle, cooled inlet (inlet 3, table I)

(c-1) SI units

Station	Axial distance, x, cm	Diameter, D, cm	Stagnation pressure, P_0, N/cm^2											
			206.8				110.3				75.8			
			Nozzle roughness level, cm rms											
			Smooth	305×10^{-6}	445×10^{-6}	826×10^{-6}	Smooth	305×10^{-6}	445×10^{-6}	826×10^{-6}	Smooth	305×10^{-6}	445×10^{-6}	826×10^{-6}
			Wall temperature, T_w, K											
2	-11.468	15.875	376.2	391.8	396.6	384.8	365.9	366.7	369.8	356.7	354.8	352.8	356.8	342.0
3	-8.928	12.934	389.3	401.8	418.3	417.0	367.9	367.6	372.9	380.2	354.9	352.2	354.1	352.3
4	-6.380	9.992	419.6	434.2	443.1	434.1	387.6	392.3	409.0	403.1	364.3	364.0	374.1	381.3
5	-5.481	8.961	423.8	437.1	447.1	440.1	396.2	399.9	416.1	409.6	368.9	368.9	388.6	389.9
6	-4.602	7.945	427.7	440.2	445.3	444.3	405.4	407.7	417.2	416.8	376.9	377.7	396.3	397.8
7	-3.708	6.914	434.6	446.4	451.2	451.7	415.1	417.5	423.6	425.9	388.1	391.5	406.2	408.1
8	-2.819	5.883	444.4	456.9	458.3	456.1	425.2	429.3	432.7	430.5	401.3	408.1	415.3	413.6
9	-1.557	4.470	456.9	467.6	468.6	465.2	441.8	445.1	447.2	443.4	422.4	428.7	432.9	428.8
10	-.455	3.835	457.3	467.0	470.0	463.6	443.3	446.6	450.2	443.7	428.2	432.6	437.8	430.4
11	0	3.790	457.7	468.2	469.9	461.2	440.2	447.7	450.6	441.2	426.3	431.8	437.8	427.4
12	.330	3.815	445.9	461.4	464.0	457.9	434.2	440.6	444.2	437.6	419.7	425.4	431.3	424.5
13	.648	3.912	441.3	453.0	453.7	452.4	429.4	431.9	434.1	432.6	414.9	417.4	420.8	418.7
14	.996	4.074	436.7	444.7	447.4	447.6	423.2	423.6	426.3	426.2	410.2	409.6	412.5	412.1
15	1.610	4.399	434.5	443.9	443.3	443.4	419.8	419.9	420.2	419.9	406.1	404.6	405.2	404.9
16	3.101	5.187	424.8	432.8	434.1	434.4	408.6	406.7	408.3	409.4	395.4	391.3	392.1	393.1
17	6.949	7.259	397.8	406.8	408.9	407.3	379.2	379.0	379.3	378.2	366.9	363.1	363.4	360.2
18	13.889	10.978	350.5	359.3	357.0	354.6	341.3	338.2	333.5	329.3	331.6	326.4	321.5	323.9
19	20.831	14.712	321.6	330.4	326.3	320.6	322.4	315.4	311.0	322.4	316.1	308.7	304.7	320.2
20	28.021	18.593	316.7	326.2	321.5	336.9	322.0	316.8	318.4	331.4	322.6	317.4	315.2	326.8

Station	Axial distance, x, cm	Diameter, D, cm	Stagnation pressure, P_0, N/cm^2											
			51.7				31.0				20.7			
			Nozzle roughness level, cm rms											
			Smooth	305×10^{-6}	445×10^{-6}	826×10^{-6}	Smooth	305×10^{-6}	445×10^{-6}	826×10^{-6}	Smooth	305×10^{-6}	445×10^{-6}	826×10^{-6}
			Wall temperature, T_e, K											
2	-11.468	15.875	344.8	344.1	344.5	330.5	333.6	331.2	330.7	318.6	326.6	322.5	320.7	309.7
3	-8.928	12.934	343.9	341.1	341.3	333.5	332.6	329.3	328.4	319.1	325.6	321.4	319.1	310.0
4	-6.380	9.992	348.8	347.8	348.8	345.4	335.8	334.1	333.2	322.6	328.1	325.0	322.9	312.4
5	-5.481	8.961	349.8	347.7	352.3	354.1	336.1	333.2	332.1	324.9	328.4	324.3	322.2	314.2
6	-4.602	7.945	351.8	348.1	357.2	367.2	336.6	332.1	331.0	326.7	329.2	323.8	320.9	315.0
7	-3.708	6.914	355.8	353.2	372.7	385.0	337.8	333.0	333.7	334.4	330.2	324.6	322.2	318.5
8	-2.819	5.883	363.2	366.3	388.9	394.7	340.7	336.3	338.6	351.8	332.7	327.0	323.9	319.4
9	-1.557	4.470	380.7	394.1	416.2	412.8	348.2	345.8	371.4	385.9	338.3	333.0	334.7	342.7
10	-.455	3.835	393.4	414.2	423.7	415.8	349.3	359.6	395.8	393.4	337.6	332.7	349.6	364.2
11	0	3.790	396.3	417.3	423.0	413.6	347.6	359.5	397.3	390.9	333.8	335.5	360.6	365.4
12	.330	3.815	393.2	409.8	416.3	410.6	343.7	368.7	391.5	388.3	331.7	331.2	363.9	362.8
13	.648	3.912	386.8	400.7	406.4	404.9	339.4	365.6	383.6	383.0	329.3	330.6	359.7	359.2
14	.996	4.074	383.6	393.6	397.7	397.4	334.3	355.4	374.9	375.9	325.8	321.1	351.7	353.0
15	1.610	4.399	387.7	388.7	389.6	388.9	352.3	363.1	367.6	367.4	331.5	333.0	347.9	347.1
16	3.101	5.187	380.6	376.1	376.0	376.2	351.8	355.6	355.4	354.0	326.2	314.9	339.3	335.8
17	6.949	7.259	354.4	350.3	348.7	343.5	336.6	334.6	331.8	326.7	315.6	321.8	319.4	320.9
18	13.889	10.978	323.9	318.2	312.8	325.9	315.5	309.9	306.1	323.1	315.5	310.8	308.1	314.7
19	20.831	14.712	311.7	305.4	307.3	320.3	313.4	307.2	303.8	313.6	312.3	307.3	303.3	305.8
20	28.021	18.593	320.6	314.6	311.8	323.8	317.4	311.1	308.2	317.0	321.1	310.8	306.1	313.1

TABLE VI. - Continued. EXPERIMENTAL WALL TEMPERATURES IN 30°-15° AND 60°-15° NOZZLES

[Stagnation temperature T_0 = 539 K (970° R).]

(c) Concluded. 30°-15° nozzle, cooled inlet (inlet 3, table I)

(c-2) U.S. customary units

Station	Axial distance, x, in.	Diameter, D, in.	Stagnation pressure, P_0, psia											
			300				160				110			
			Nozzle roughness level, in. rms											
			Smooth	120×10^{-6}	175×10^{-6}	325×10^{-6}	Smooth	120×10^{-6}	175×10^{-6}	325×10^{-6}	Smooth	120×10^{-6}	175×10^{-6}	325×10^{-6}
			Wall temperature, T_w, $^{\circ}$R											
2	-4.515	6.250	677.1	705.2	713.8	692.6	658.6	660.0	665.7	642.0	638.6	635.1	642.2	615.6
3	-3.515	5.092	700.7	723.3	753.0	750.6	662.3	661.6	671.2	684.4	638.8	633.9	637.4	634.2
4	-2.512	3.934	755.3	781.6	797.5	781.3	697.6	706.1	736.2	725.6	655.8	655.2	673.4	686.3
5	-2.158	3.528	762.9	786.8	804.8	792.2	713.2	719.8	749.0	737.3	664.2	664.0	699.4	701.9
6	-1.812	3.128	769.8	792.4	801.5	799.7	729.8	733.8	751.0	750.2	678.5	679.8	713.4	716.0
7	-1.460	2.722	782.3	803.6	812.2	813.1	747.1	751.5	762.5	766.6	698.5	704.7	731.2	734.5
8	-1.110	2.316	800.0	822.4	824.9	820.9	765.3	772.7	778.9	774.9	722.3	734.5	747.6	744.4
9	-.613	1.760	822.5	841.6	843.5	837.3	795.2	801.2	804.9	798.2	760.4	771.7	779.3	771.9
10	-.175	1.510	823.2	840.6	846.0	834.5	798.0	803.9	810.3	798.7	770.7	778.7	788.0	774.7
11	0	1.492	823.8	842.8	845.9	830.1	792.4	805.9	811.0	794.2	767.3	777.3	788.1	769.3
12	.130	1.502	802.7	830.6	835.2	824.3	781.5	793.0	799.6	787.6	755.5	765.8	776.3	764.1
13	.255	1.540	794.4	815.4	816.7	814.4	773.0	777.4	781.4	778.7	746.9	751.3	757.5	753.7
14	.392	1.604	786.1	800.4	805.3	805.6	761.8	762.5	767.3	767.2	738.4	737.3	742.5	741.7
15	.634	1.732	782.1	799.0	797.9	798.2	755.6	755.9	756.4	755.8	731.0	728.3	729.3	728.9
16	1.221	2.042	764.7	779.0	781.4	782.0	735.5	732.0	734.9	737.0	711.7	704.3	705.8	707.6
17	2.736	2.858	716.0	732.2	736.0	733.1	682.5	682.2	682.7	680.7	660.4	653.6	654.2	648.4
18	5.468	4.322	630.9	646.8	642.6	638.2	614.3	608.7	600.3	592.8	596.9	587.6	578.7	583.1
19	8.201	5.792	578.8	594.7	587.3	577.1	580.3	567.8	559.8	580.4	568.9	555.7	548.5	576.4
20	11.032	7.320	570.0	587.1	578.7	606.5	579.6	570.2	573.1	596.6	580.7	571.3	567.4	588.2

Station	Axial distance, x, in.	Diameter, D, in.	Stagnation pressure, P_0, psia											
			75				45				30			
			Nozzle roughness level, in. rms											
			Smooth	120×10^{-6}	175×10^{-6}	325×10^{-6}	Smooth	120×10^{-6}	175×10^{-6}	325×10^{-6}	Smooth	120×10^{-6}	175×10^{-6}	325×10^{-6}
			Wall temperature, T_w, K											
2	-4.515	6.250	620.7	619.4	620.1	594.9	600.5	596.2	595.2	573.5	587.8	580.5	577.3	557.5
3	-3.515	5.092	619.1	614.0	614.4	600.3	598.6	592.8	591.1	574.4	586.1	578.6	574.3	558.0
4	-2.512	3.934	627.8	626.1	627.9	621.7	604.4	601.3	599.8	580.6	590.5	585.0	581.2	562.3
5	-2.158	3.528	629.6	625.9	634.1	637.3	604.9	599.8	597.8	584.9	591.2	583.8	580.0	565.6
6	-1.812	3.128	633.3	626.6	642.9	660.9	605.8	597.7	595.8	588.1	592.6	582.9	577.7	567.0
7	-1.460	2.722	640.5	635.8	670.9	693.0	608.1	599.4	600.6	602.0	594.4	584.2	579.9	573.3
8	-1.110	2.316	653.8	659.4	700.0	710.5	613.2	605.3	609.5	633.3	598.8	588.6	583.0	574.9
9	-.163	1.760	685.2	709.4	749.1	743.1	626.7	622.4	668.6	694.6	609.0	599.4	602.5	616.9
10	-.175	1.510	708.2	745.5	762.6	748.5	628.7	647.2	712.4	708.1	607.7	598.9	629.2	655.6
11	0	1.492	713.3	751.2	761.4	744.4	625.6	647.1	715.1	703.6	600.8	603.9	649.1	657.8
12	.130	1.502	707.7	737.7	749.4	739.1	618.6	663.7	704.7	699.0	597.1	596.1	655.0	653.0
13	.255	1.540	696.2	721.2	731.5	728.8	610.9	658.1	690.5	689.4	592.8	595.0	647.5	646.5
14	.392	1.604	690.4	708.5	715.9	715.4	601.8	639.7	674.9	676.7	586.4	578.0	633.0	635.4
15	.634	1.732	697.8	699.6	701.3	700.1	634.1	653.6	661.6	661.3	596.7	599.4	626.3	624.7
16	1.221	2.042	685.0	677.0	676.8	677.1	633.2	640.1	639.7	637.2	587.2	566.8	610.7	604.4
17	2.736	2.858	637.9	630.5	627.7	618.3	605.8	602.2	597.3	588.0	568.1	579.3	574.9	577.7
18	5.468	4.322	583.0	572.8	563.0	586.7	567.9	557.8	551.0	581.5	567.9	559.4	554.5	566.4
19	8.201	5.792	561.0	549.7	553.1	576.5	564.2	552.9	546.9	564.4	562.1	553.1	545.9	550.4
20	11.032	7.320	577.1	566.3	561.3	582.9	571.3	560.0	554.8	570.6	578.0	559.4	550.9	563.6

TABLE VI. - Continued. EXPERIMENTAL WALL TEMPERATURES IN 30°-15° AND 60°-15° NOZZLES

[Stagnation temperature T_0 = 539 K (970° R).]

(d) 60°-15° nozzle, cooled inlet (inlet 3, table I)

(d-1) SI units

Station	Axial distance, x, cm	Diameter, D, cm	Stagnation pressure, P_0, N/cm^2											
			206.8				110.3				75.8			
			Nozzle roughness level, cm rms											
			Smooth	305×10^{-6}	445×10^{-6}	826×10^{-6}	Smooth	305×10^{-6}	445×10^{-6}	826×10^{-6}	Smooth	305×10^{-6}	445×10^{-6}	826×10^{-6}
			Wall temperature, T_w, K											
2	-5.296	14.580	388.8	377.9	384.4	399.4	366.0	351.8	358.6	371.5	353.3	338.9	346.3	358.4
3	-4.450	11.643	396.3	391.2	407.0	413.9	372.0	359.7	367.8	375.1	359.6	345.7	354.2	360.4
4	-4.153	10.612	400.3	397.1	417.3	439.2	374.0	360.8	370.5	395.8	361.6	346.4	355.4	371.9
5	-3.848	9.555	406.3	410.9	431.5	448.1	378.7	366.4	384.3	410.6	365.7	350.9	361.8	380.4
6	-3.063	6.939	434.1	454.3	459.9	470.5	390.6	408.6	429.9	445.9	376.6	374.6	402.9	427.9
7	-2.591	5.865	454.2	464.6	468.6	475.5	899.1	432.9	445.0	453.6	381.2	395.5	425.3	438.3
8	-1.476	4.409	471.1	472.2	475.9	480.7	419.6	448.1	456.1	462.7	385.7	429.2	441.4	448.8
9	-.371	3.851	469.6	468.8	473.0	475.7	443.0	446.9	453.6	456.7	393.1	431.0	440.2	443.9
10	0	3.807	467.7	466.4	470.4	474.2	441.3	444.6	450.1	455.8	395.1	428.8	436.3	443.1
11	.381	3.863	461.1	459.9	464.1	474.2	435.9	436.5	443.0	454.2	392.0	420.9	428.7	440.9
12	.704	3.975	457.9	455.2	458.5	468.8	436.2	430.7	437.3	448.2	407.4	414.8	422.8	433.8
13	1.016	4.122	453.9	450.5	454.6	464.5	429.8	425.4	432.9	442.8	384.1	409.4	418.6	428.9
14	1.580	4.422	445.1	441.6	446.4	454.2	421.9	414.0	423.1	430.9	386.4	397.8	406.9	416.1
15	3.071	5.215	431.8	430.7	436.4	443.3	408.2	401.8	409.9	418.2	381.8	384.6	392.9	402.3

Station	Axial distance, x, cm	Diameter, D, cm	Stagnation pressure, P_0, N/cm^2											
			51.7				31.0				20.7			
			Nozzle roughness level, cm rms											
			Smooth	305×10^{-6}	445×10^{-6}	826×10^{-6}	Smooth	305×10^{-6}	445×10^{-6}	826×10^{-6}	Smooth	305×10^{-6}	445×10^{-6}	826×10^{-6}
			Wall temperature, T_w, K											
2	-5.296	14.580	342.5	328.1	335.3	346.6	330.8	315.7	323.9	334.1	324.6	308.5	316.7	326.1
3	-4.450	11.643	348.4	334.1	342.4	348.6	336.4	321.2	329.8	336.1	329.5	313.4	321.9	328.2
4	-4.153	10.612	350.4	334.9	343.4	355.2	338.3	322.2	330.7	340.2	331.1	314.4	322.8	331.1
5	-3.848	9.555	354.2	339.1	347.5	360.7	341.9	325.6	334.1	344.4	334.6	317.5	325.7	334.7
6	-3.063	6.939	364.6	354.4	372.4	401.9	351.4	337.4	349.3	364.3	343.3	328.2	336.9	347.5
7	-2.591	5.865	369.1	360.0	393.9	418.9	356.1	339.6	354.7	382.8	347.4	330.3	339.2	354.9
8	-1.476	4.409	370.9	390.5	422.3	433.9	357.1	342.8	376.9	409.1	348.4	333.0	342.3	382.3
9	-.371	3.851	368.8	384.2	423.2	430.0	350.3	336.9	394.2	406.4	341.9	327.2	340.2	384.6
10	0	3.807	369.7	377.1	418.9	428.4	348.4	335.3	391.4	404.7	339.7	324.0	335.8	382.8
11	.381	3.863	363.4	393.4	411.2	425.6	345.8	330.3	383.7	401.8	336.4	318.9	337.1	380.1
12	.704	3.975	383.4	395.4	405.9	418.3	350.2	330.1	380.0	394.8	335.2	316.7	339.6	374.0
13	1.016	4.122	358.7	390.6	401.9	413.1	340.2	327.7	377.7	389.4	331.2	313.4	340.3	369.2
14	1.580	4.422	353.2	380.6	389.7	400.0	332.1	314.3	366.4	376.9	325.4	305.8	342.7	358.6
15	3.071	5.215	333.8	367.8	375.1	385.7	322.3	309.7	353.9	362.9	316.4	298.2	325.0	346.2

TABLE VI. - Concluded. EXPERIMENTAL WALL TEMPERATURES in 30°-15° AND 60°-15° NOZZLES

[Stagnation temperature T_0 539 K (970° R).]

(d) Concluded. 60°-15° nozzle, cooled inlet (inlet 3, table I)

(d-2) U.S. customary units

Station	Axial distance, x, in.	Diameter, D, in.	Stagnation pressure, P_0, psia											
			300				160				110			
			Nozzle roughness level, in. rms											
			Smooth	120×10^{-6}	175×10^{-6}	325×10^{-6}	Smooth	120×10^{-6}	175×10^{-6}	325×10^{-6}	Smooth	120×10^{-6}	175×10^{-6}	325×10^{-6}
			Wall temperature, T_w, $^{\circ}$R											
2	-2.085	5.740	699.8	680.2	691.9	719.0	658.8	633.3	645.4	668.7	635.9	610.1	623.4	645.1
3	-1.752	4.584	713.4	704.2	732.6	745.0	669.6	647.4	662.0	675.1	647.3	622.3	637.5	648.8
4	-1.635	4.178	720.6	714.7	751.1	790.6	673.2	649.5	666.9	712.5	650.8	623.6	639.8	669.4
5	-1.515	3.762	731.4	739.7	776.7	806.6	681.6	659.5	691.8	739.1	658.2	631.6	651.3	684.8
6	-1.206	2.732	781.4	817.7	827.9	846.9	703.1	735.5	773.9	802.6	677.9	674.3	725.2	770.2
7	-1.020	2.309	817.6	836.2	843.4	855.9	718.4	779.3	801.0	816.4	686.1	711.9	765.6	789.0
8	-.581	1.736	847.9	850.0	856.7	865.2	755.2	806.6	821.0	832.9	694.3	772.5	794.6	807.9
9	-.146	1.516	845.2	843.9	851.4	856.2	797.4	804.4	816.5	822.1	707.6	775.8	792.4	799.1
10	0	1.499	841.8	839.5	846.7	853.6	794.3	800.2	810.2	820.4	711.1	771.8	785.3	797.5
11	.150	1.521	829.9	827.9	835.3	853.6	784.7	785.7	797.4	817.6	705.6	757.6	771.6	793.7
12	.277	1.565	824.3	819.3	825.3	843.9	785.1	775.2	787.1	806.7	733.4	746.7	761.0	780.8
13	.400	1.623	817.0	810.9	818.3	836.1	773.6	765.7	779.3	797.0	691.4	736.9	753.5	772.0
14	.622	1.741	801.1	794.8	803.6	817.6	759.5	745.2	761.5	775.7	695.6	716.0	732.5	749.0
15	1.209	2.053	777.3	775.3	785.5	797.9	734.7	723.2	737.8	752.8	687.2	692.3	707.2	724.1

Station	Axial distance, x, in.	Diameter, D, in.	Stagnation pressure, P_0, psia											
			75				45				30			
			Nozzle roughness level, in. rms											
			Smooth	120×10^{-6}	175×10^{-6}	325×10^{-6}	Smooth	120×10^{-6}	175×10^{-6}	325×10^{-6}	Smooth	120×10^{-6}	175×10^{-6}	325×10^{-6}
			Wall temperature, T_w, $^{\circ}$R											
2	-2.085	5.740	616.5	590.5	603.5	623.9	595.5	568.3	582.9	601.3	584.2	555.3	570.1	586.9
3	-1.752	4.584	627.2	601.3	616.4	627.5	605.5	578.2	593.7	604.9	593.1	564.1	579.5	590.8
4	-1.635	4.178	630.7	602.8	618.2	639.3	609.0	579.9	595.3	612.3	596.0	566.0	581.0	596.0
5	-1.515	3.762	637.6	610.4	625.5	649.2	615.5	586.0	601.3	620.0	602.3	571.5	586.3	602.4
6	-1.206	2.732	656.2	637.9	670.4	723.5	632.5	607.4	628.7	655.7	617.9	590.8	606.4	625.5
7	-1.020	2.309	664.4	648.0	709.0	754.1	641.0	611.3	638.5	689.0	625.4	594.6	610.5	638.9
8	-.581	1.736	667.6	702.9	760.2	781.0	642.8	617.0	678.4	736.3	627.1	599.4	616.2	688.2
9	-.146	1.516	663.9	691.5	761.7	774.0	630.6	606.4	709.6	731.5	615.4	589.0	612.4	692.2
10	0	1.499	665.5	678.7	754.1	771.2	627.1	603.5	704.6	728.5	611.4	583.2	604.4	689.1
11	.150	1.521	654.1	708.2	740.2	766.0	622.5	594.6	690.7	723.3	605.6	574.0	606.7	684.1
12	.277	1.565	690.1	711.7	730.7	753.0	630.4	594.1	684.1	710.6	603.4	570.0	611.3	673.2
13	.400	1.623	645.7	703.1	723.4	743.5	612.3	589.9	679.8	701.0	596.1	564.2	612.5	664.6
14	.622	1.741	635.8	685.1	701.4	720.0	597.8	565.7	659.5	678.5	585.7	550.5	616.9	645.4
15	1.209	2.053	660.8	662.0	675.2	694.2	580.1	557.4	637.0	653.2	569.6	536.8	585.0	623.1

TABLE VII. - STAGNATION PRESSURES AND TEMPERATURES FOR DATA IN TABLES V AND VI

(a) 30°-15° nozzle, adiabatic inlet (inlet 2, table I)

Nozzle roughness		Stagnation pressure, P_0		Stagnation temperature, T_0	
cm rms	in. rms	N/cm^2	psia	K	$^{\circ}R$
Smooth	Smooth	206.8	299.9	539.3	970.8
305×10^{-6}	120×10^{-6}	206.7	299.8	539.5	971.1
445	175	207.1	300.3	540.1	972.2
826	325	206.9	300.0	539.5	971.0
Smooth	Smooth	109.6	159.0	539.6	971.3
305×10^{-6}	120×10^{-6}	110.2	159.8	539.9	971.8
445	175	110.5	160.3	538.9	969.9
826	325	110.7	160.5	538.7	969.7
Smooth	Smooth	75.8	109.9	537.9	968.3
305×10^{-6}	120×10^{-6}	75.7	109.8	539.3	970.8
445	175	75.4	109.3	538.9	969.9
826	325	75.5	109.5	540.1	972.2
Smooth	Smooth	51.9	75.3	540.4	972.8
305×10^{-6}	120×10^{-6}	51.8	75.1	539.0	970.2
445	175	51.6	74.8	539.1	970.3
826	325	52.1	75.5	539.1	970.4
Smooth	Smooth	30.9	44.8	539.0	970.2
305×10^{-6}	120×10^{-6}	30.9	44.8	539.8	971.7
445	175	30.9	44.8	539.1	970.4
826	325	30.9	44.8	539.7	971.4
Smooth	Smooth	20.1	29.1	538.3	969.0
305×10^{-6}	120×10^{-6}	20.3	29.4	539.2	970.5
445	175	20.2	29.3	538.8	969.8
826	325	20.5	29.8	539.5	971.2

TABLE VII. - Continued. STAGNATION PRESSURES AND TEMPERATURES FOR DATA IN TABLES V AND VI

(b) 60°-15° nozzle, adiabatic inlet (inlet 2, table I)

Nozzle roughness		Stagnation pressure, P_0		Stagnation temperature, T_0	
cm rms	in. rms	N/cm^2	psia	K	$^{\circ}R$
Smooth	Smooth	206.8	299.9	539.2	970.6
305×10^{-6}	120×10^{-6}	206.5	299.6	538.6	969.4
445	175	206.7	299.8	539.4	971.0
826	325	206.6	299.6	539.2	970.5
Smooth	Smooth	110.6	160.4	539.2	970.6
305×10^{-6}	120×10^{-6}	110.1	159.8	538.5	969.3
445	175	110.9	160.9	539.3	970.7
826	325	110.3	160.0	539.1	970.4
Smooth	Smooth	75.8	110.0	539.2	970.6
305×10^{-6}	120×10^{-6}	75.2	109.0	539.4	971.0
445	175	75.7	109.9	539.8	971.7
826	325	75.9	110.1	540.0	972.0
Smooth	Smooth	52.0	75.4	539.2	970.6
305×10^{-6}	120×10^{-6}	51.7	75.0	539.3	970.7
445	175	51.6	74.9	540.1	972.2
826	325	51.7	75.0	539.2	970.5
Smooth	Smooth	30.6	44.4	539.2	970.6
305×10^{-6}	120×10^{-6}	30.8	44.6	538.7	969.6
445	175	30.6	44.4	539.2	970.6
826	325	31.0	45.0	539.1	970.3
Smooth	Smooth	20.3	29.4	539.2	970.6
305×10^{-6}	120×10^{-6}	20.6	29.8	539.9	971.9
445	175	20.6	29.9	539.8	971.6
826	325	20.6	29.9	539.3	970.8

TABLE VII. - Continued. STAGNATION PRESSURES AND TEMPERATURES FOR DATA IN TABLES V AND VI

(c) 30°-15° nozzle, cooled inlet (inlet 3, table I)

Nozzle roughness		Stagnation pressure, P_0		Stagnation temperature, T_0	
cm fms	in. rms	N/cm^2	psia	K	$^{\circ}R$
Smooth	Smooth	205.6	298.3	537.9	968.3
305×10^{-6}	120×10^{-6}	206.6	299.7	539.9	971.9
445	175	206.8	299.9	539.1	970.4
826	325	207.0	300.2	539.0	970.3
Smooth	Smooth	109.8	159.3	540.0	972.0
305×10^{-6}	120×10^{-6}	109,8	159.2	539.7	971.5
445	175	109.6	158.9	539.4	970.8
826	325	110.1	159.7	539.6	971.3
Smooth	Smooth	75.4	109.3	539.1	970.3
305×10^{-6}	120×10^{-6}	75.3	109.2	539.3	970.8
445	175	75.4	109.4	539.4	970.9
826	325	76.1	110.3	539.2	970.6
Smooth	Smooth	51.6	74.9	539.9	971.8
305×10^{-6}	120×10^{-6}	51.1	74.2	539.4	970.9
445	175	51.7	74.9	539.3	970.8
826	325	51.5	74.7	539.5	971.1
Smooth	Smooth	30.3	44.0	538.7	969.7
305×10^{-6}	120×10^{-6}	30.1	43.7	539.3	970.8
445	175	31.0	44.9	539.2	970.5
826	325	30.8	44.7	538.9	970.0
Smooth	Smooth	20.2	29.3	539.3	970.8
305×10^{-6}	120×10^{-6}	20.2	29.2	539.5	971.1
445	175	20.3	29.4	539.0	970.2
826	325	20.2	29.2	538.8	969.8

TABLE VII. - Concluded. STAGNATION PRESSURES AND TEMPERATURES FOR DATA IN TABLES V AND VI

(d) 60°-15° nozzle, cooled inlet (inlet 3, table I)

Nozzle roughness		Stagnation pressure, P_0		Stagnation temperature, T_0	
cm rms	in. rms	N/cm^2	psia	K	$^{\circ}R$
Smooth	Smooth	207.1	300.4	539.6	971.3
305×10^{-6}	120×10^{-6}	205.9	298.7	540.7	973.3
445	175	206.6	299.7	539.3	970.7
826	325	207.0	300.3	539.4	970.8
Smooth	Smooth	110.2	159.8	540.3	972.6
305×10^{-6}	120×10^{-6}	110.1	159.7	538.9	970.0
445	175	110.1	159.7	538.8	969.9
826	325	109.8	159.3	539.6	971.2
Smooth	Smooth	76.4	110.8	539.1	970.3
305×10^{-6}	120×10^{-6}	75.5	109.5	540.0	971.9
445	175	75.7	109.7	538.7	969.7
826	325	75.8	109.9	538.8	969.8
Smooth	Smooth	50.8	73.7	539.7	971.5
305×10^{-6}	120×10^{-6}	51.2	74.3	540.2	972.3
445	175	51.5	74.7	539.2	970.6
826	325	51.9	75.3	539.5	971.1
Smooth	Smooth	30.3	44.0	539.7	971.4
305×10^{-6}	120×10^{-6}	30.5	44.2	538.7	969.7
445	175	30.5	44.2	539.3	970.8
826	325	30.9	44.8	539.6	971.3
Smooth	Smooth	20.2	29.3	539.7	971.5
305×10^{-6}	120×10^{-6}	20.4	29.6	538.8	969.9
445	175	20.2	29.2	539.8	971.6
826	325	20.2	29.3	539.0	970.3

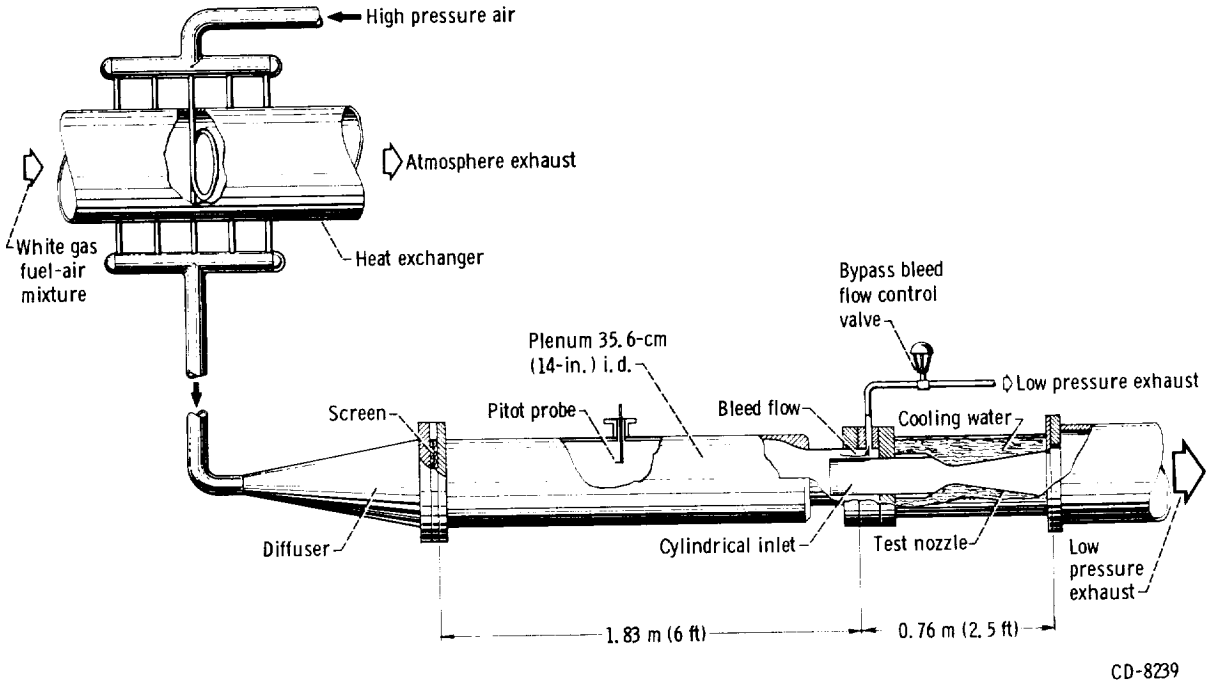

Figure 1. - Nozzle heat transfer facility.

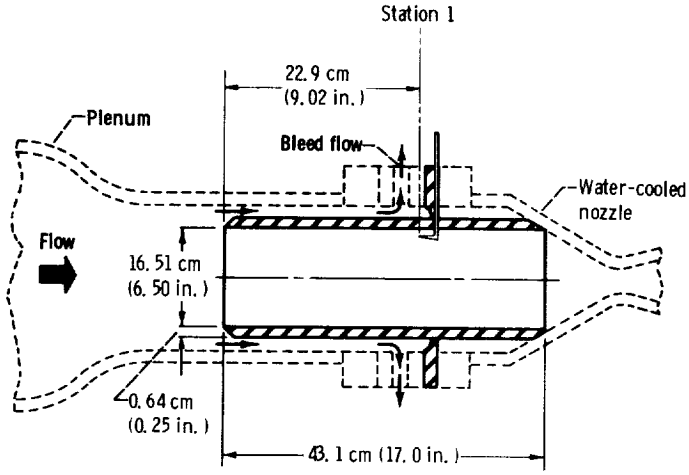

(a) Uncooled (adiabatic wall) inlet (inlet 2, table I).

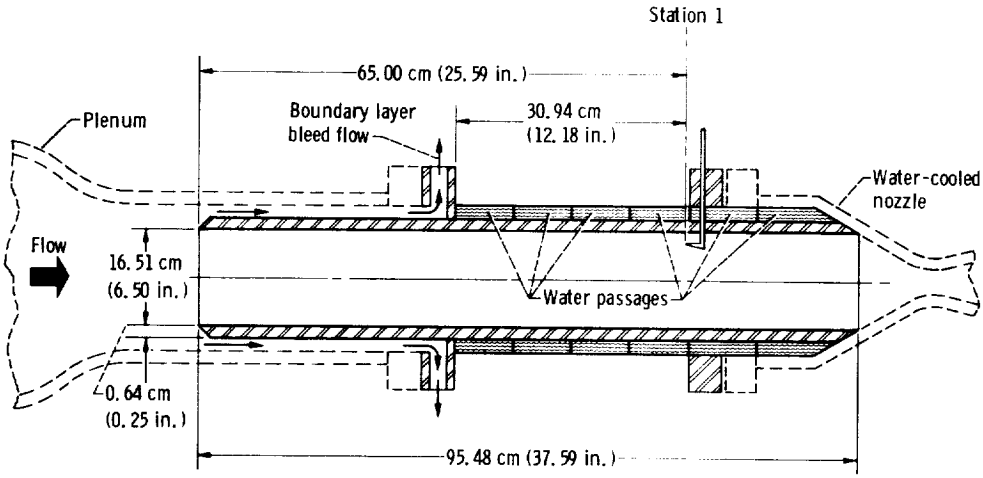

(b) Cooled inlet (inlet 3, table I).

Figure 2. - Uncooled and cooled pipe inlets. 16.51-centimeter- (6.50-in.) inside diameter inlet.

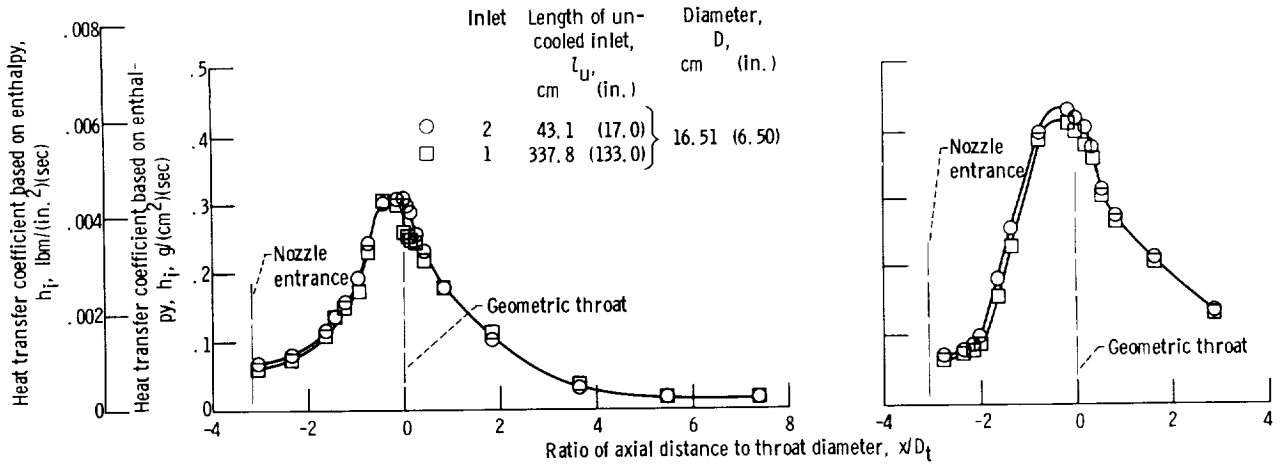

(a) 30^0 - 15^0 nozzle; throat diameter D_t = 3.790 centimeters (1.492 in.); contraction area ratio ϵ_c = 18.98.

(b) 60^0 - 15^0 nozzle; throat diameter D_t = 3.807 centimeters (1.499 in.); contraction area ratio ϵ_c = 18.80.

Figure 3. - Nozzle heat transfer with different length uncooled inlets. Free stream stagnation pressure P_0 = 207 newtons per square centimeter (300 psia); free stream stagnation temperature T_0 = 539 K (970^0 R).

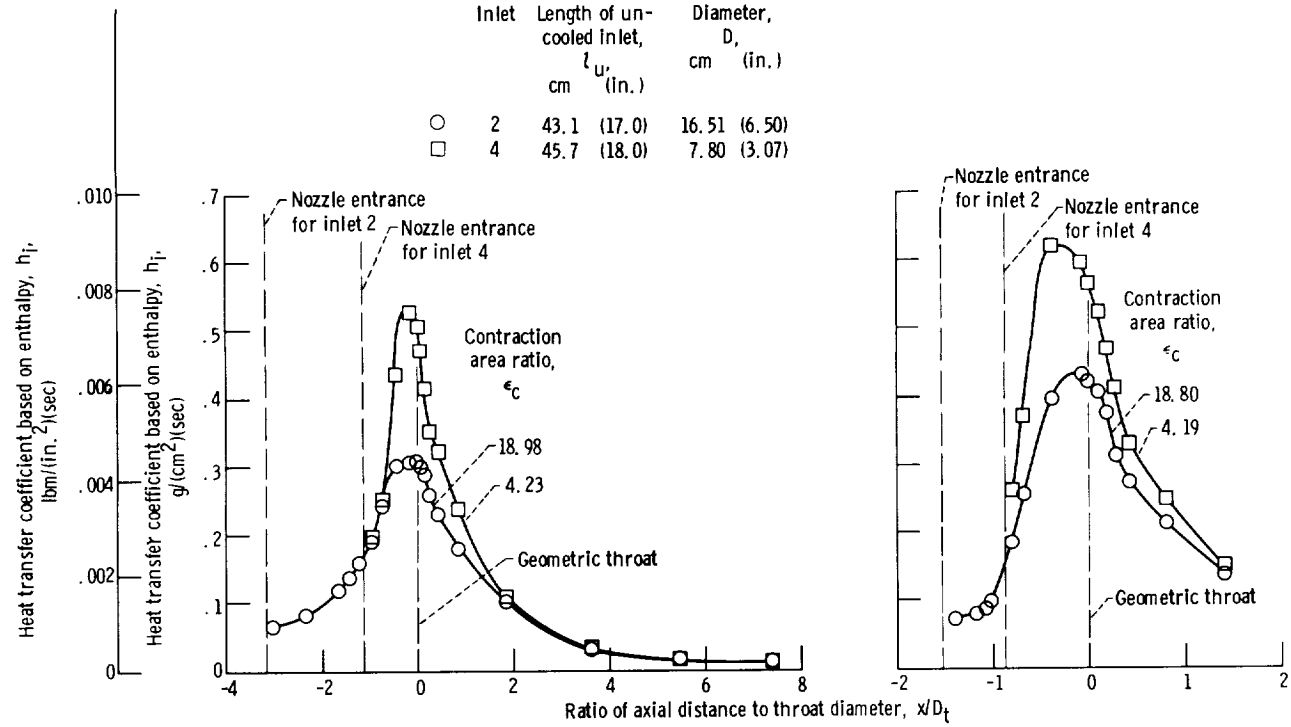

(a) 30^0 - 15^0 nozzle, uncooled (adiabatic wall) inlets; throat diameter D_t = 3.790 centimeters (1.492 in.).

(b) 60^0 - 15^0 nozzle, uncooled (adiabatic wall) inlets; throat diameter D_t = 3.807 centimeters (1.499 in.).

Figure 4. - Nozzle heat transfer with different diameter uncooled inlets (different contraction area ratios). Free stream stagnation pressure P_0 = 207 newtons per square centimeter (300 psia); free stream stagnation temperature T_0 = 539 K (970^0 R).

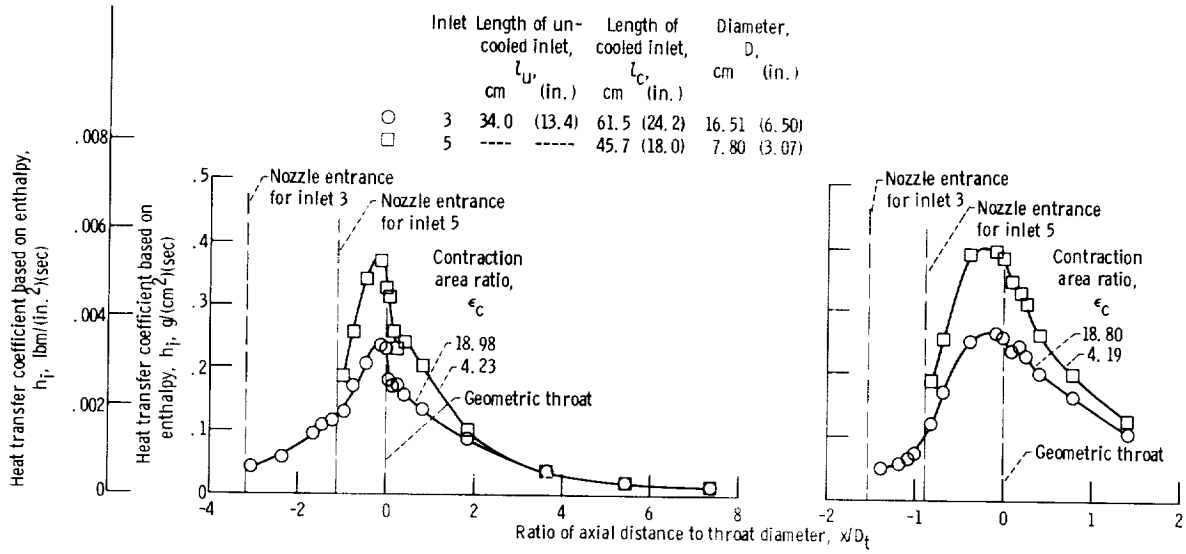

(a) 30^0 - 15^0 nozzle, cooled inlets; throat diameter D_t = 3.790 centimeters (1.492 in.).

(b) 60^0 - 15^0 nozzle, cooled inlets; throat diameter D_t = 3.807 centimeters (1.499 in.).

Figure 5. - Nozzle heat transfer with different diameter cooled inlets (different contraction area ratios). Free stream stagnation pressure P_0 = 207 newtons per square centimeter (300 psia); free stream stagnation temperature T_0 = 539 K (970^0 R).

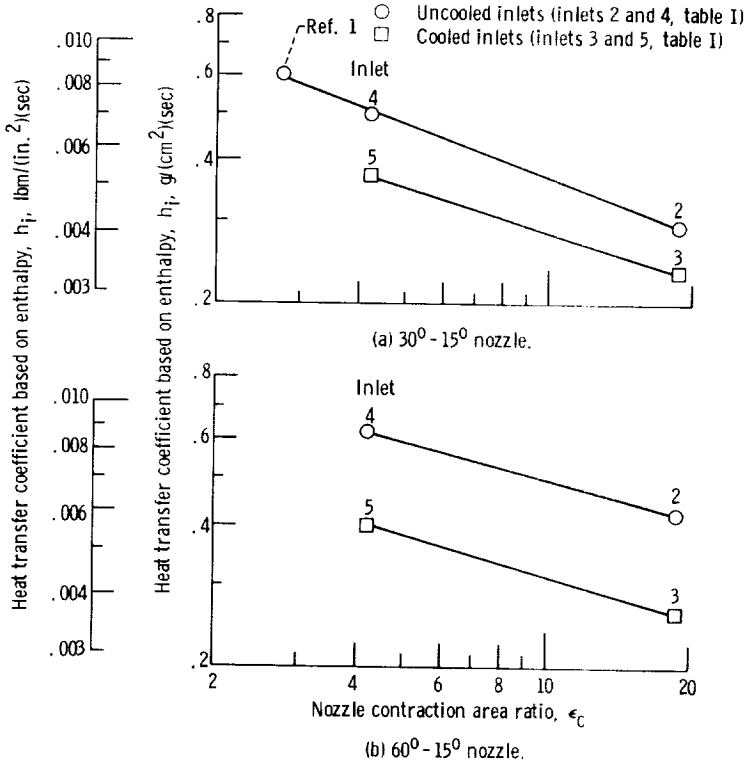

(a) 30^0 - 15^0 nozzle.

(b) 60^0 - 15^0 nozzle.

Figure 6. - Nozzle peak heat transfer coefficients corresponding to tests with different inlets. Free stream stagnation pressure P_0 = 207 newtons per square centimeter (300 psia); free stream stagnation temperature T_0 = 539 K (970^0 R).

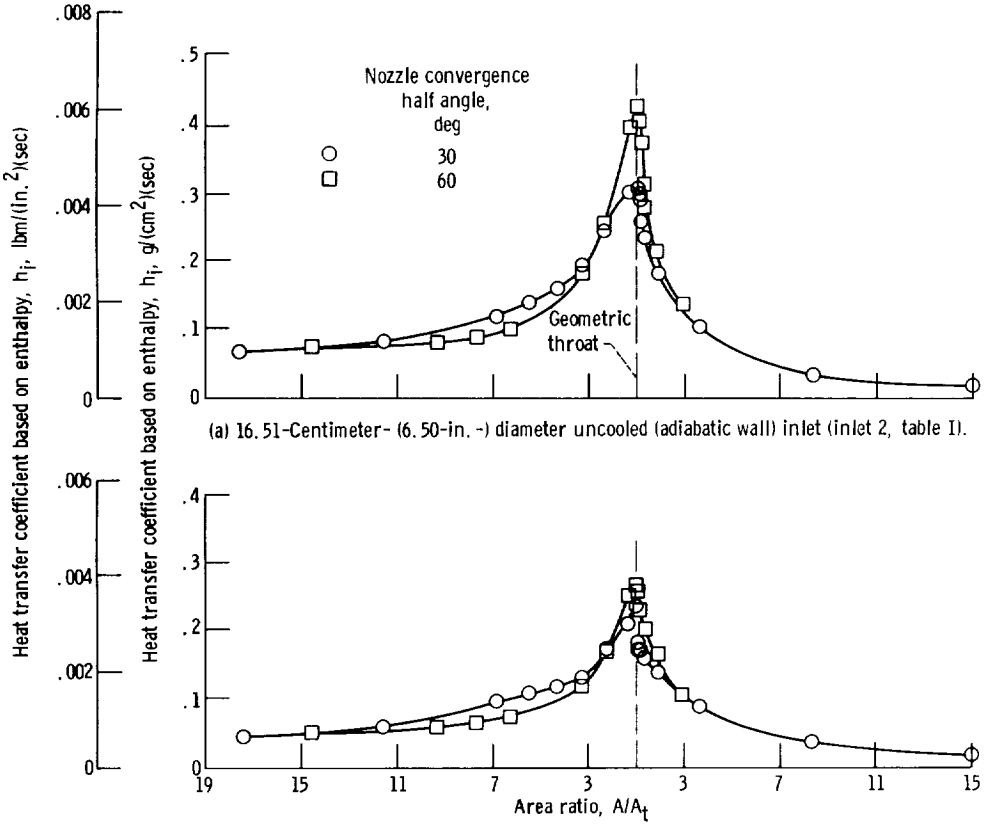

(a) 16.51-Centimeter- (6.50-in.-) diameter uncooled (adiabatic wall) inlet (inlet 2, table I).

(b) 16.51-Centimeter- (6.50-in.-) diameter cooled inlet (inlet 3, table I).

Figure 7. - Nozzle heat transfer with different convergence half angles. Free stream stagnation pressure P_0 = 207 newtons per square centimeter (300 psia); free stream stagnation temperature T_0 = 539 K (970° R); contraction area ratio $\epsilon_c \approx 19$.

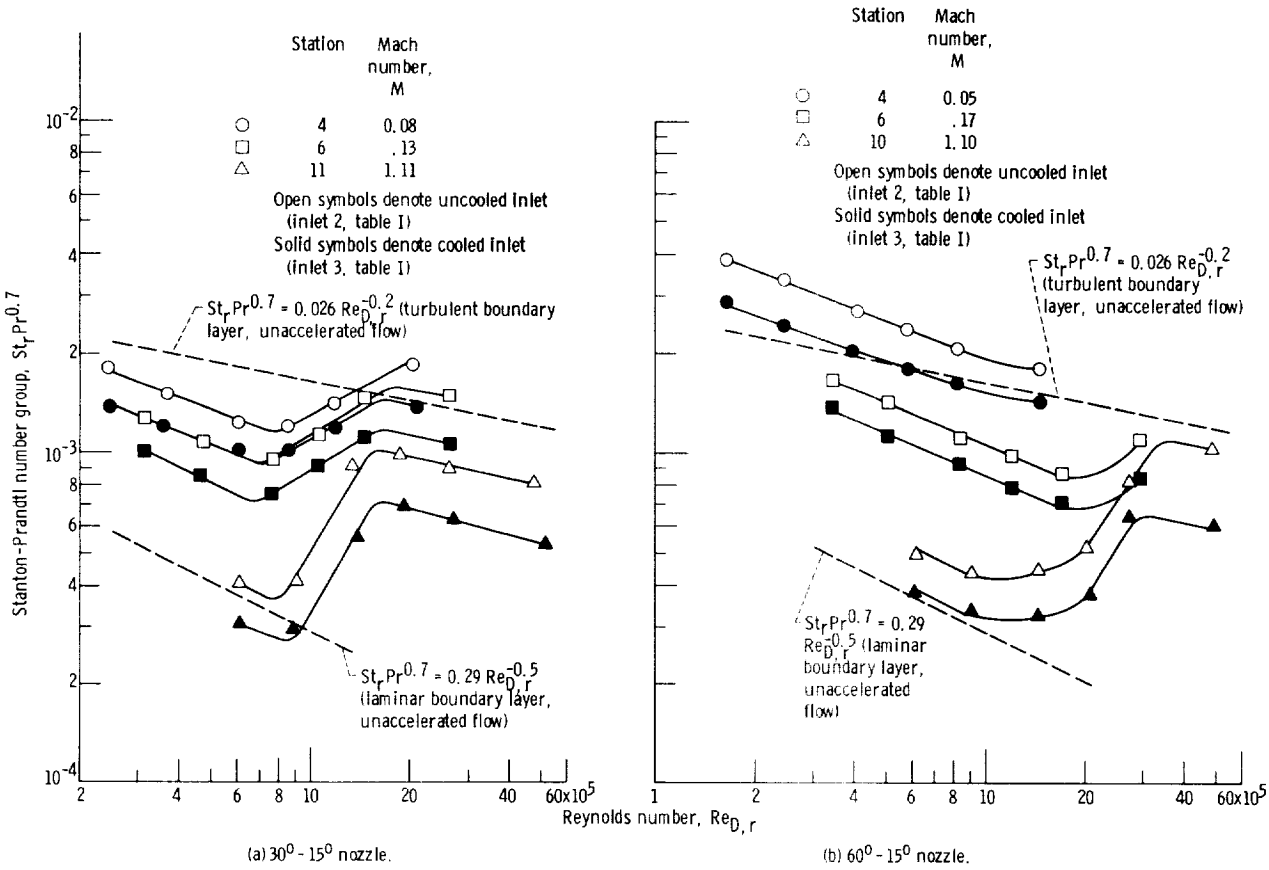

(a) 30^0 - 15^0 nozzle.

(b) 60^0 - 15^0 nozzle.

Figure 8. - Effect of Reynolds number (stagnation pressure) on heat transfer in tests with uncooled (adiabatic wall) and cooled inlets. Free stream stagnation temperature T_0 = 539 K (970^0 R); contraction area ratio $\epsilon_c \approx 19$.

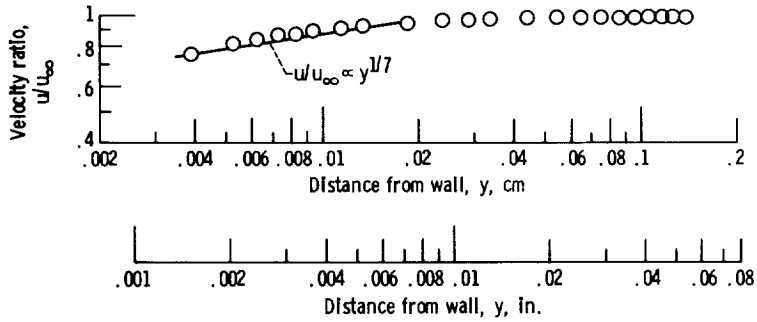

(a) Logarithmic variation of velocity ratio u/u_∞ with distance y.

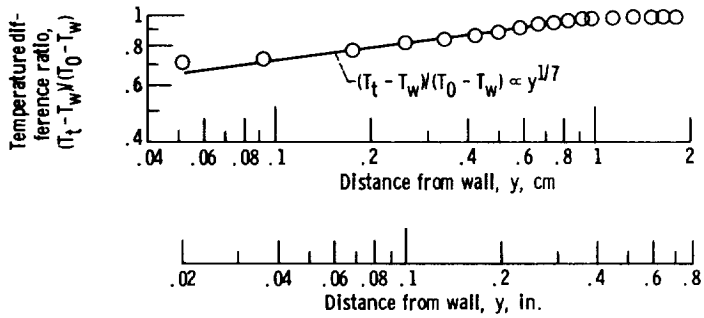

(b) Logarithmic variation of temperature difference ratio $(T_t - T_w)/(T_0 - T_w)$ with distance y.

Figure 9. - Velocity and temperature profiles at Mach 0.08 in 30^0 - 15^0 nozzle operating with 16.51-centimeter- (6.50-in. -) diameter cooled inlet (inlet 3, table I). Free stream stagnation pressure P_0 = 207 newtons per square centimeter (300 psia); free stream stagnation temperature T_0 = 539 K (970^0 R); free stream velocity u_∞ = 36.6 meters per second (120 ft/sec).

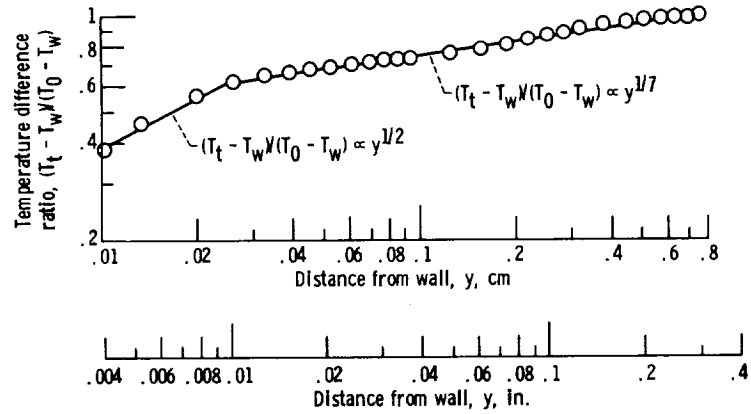

Figure 10. - Temperature profile at Mach 1.3 in 30^0 - 15^0 nozzle operating with 16.51 centimeter- (6.50-in. -) diameter cooled inlet (inlet 3, table I). Free stream stagnation pressure P_0 = 207 newtons per square centimeter (300 psia); free stream stagnation temperature T_0 = 539 K (970^0 R).

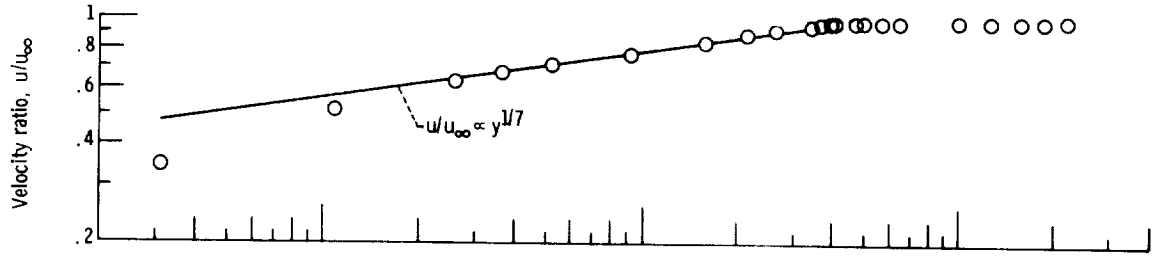

(a) Logarithmic variation of velocity ratio u/u_∞ with distance y.

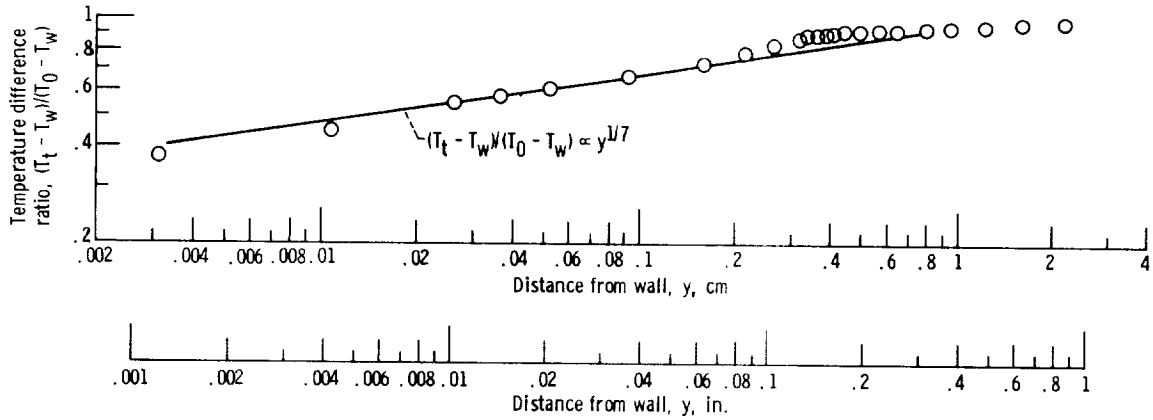

(b) Logarithmic variation of temperature difference ratio $(T_t - T_w)/(T_0 - T_w)$ with distance y.

Figure 11. - Velocity and temperature profiles at Mach 4.4 in 30^0 - 15^0 nozzle operating with 16.51-centimeter- (6.50-in.-) diameter cooled inlet (inlet 3, table I). Free stream stagnation pressure P_0 = 207 newtons per square centimeter (300 psia); free stream stagnation temperature T_0 = 539 K (970^0 R); free stream velocity u_∞ = 933 meters per second (3060 ft/sec).

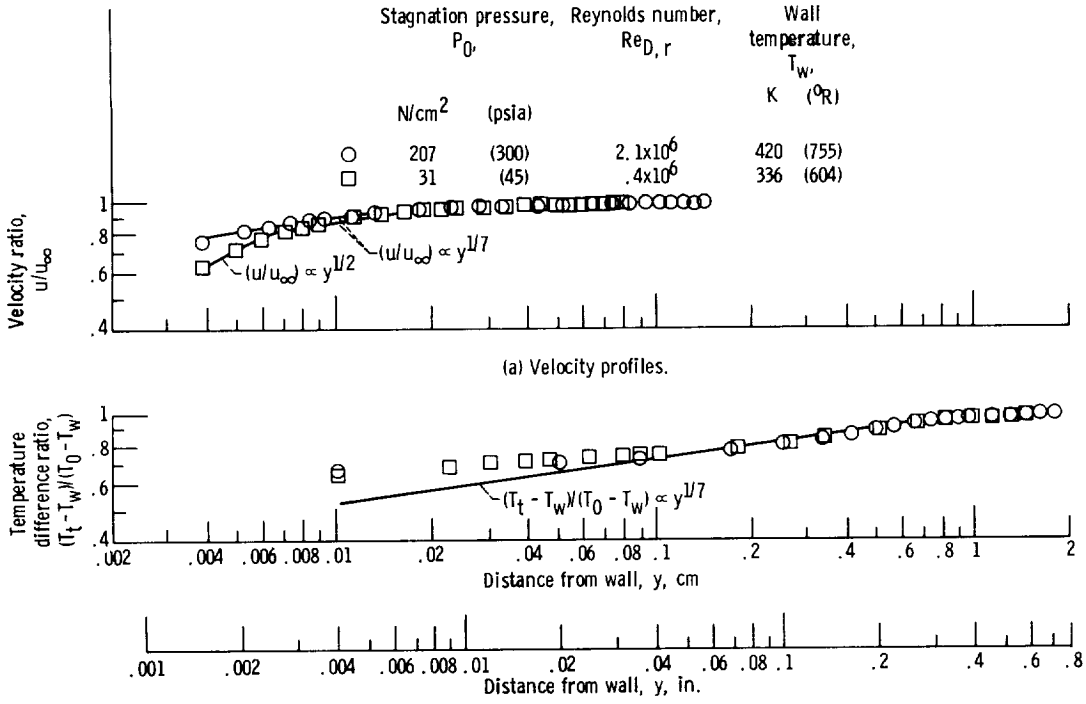

(a) Velocity profiles.

(b) Temperature profiles.

Figure 12. - Effect of Reynolds number (stagnation pressure) on velocity and temperature profiles in 30^0 - 15^0 nozzle operating with 16.51-centimeter- (6.50-in.-) diameter cooled inlet (inlet 3, table I). Free stream stagnation temperature T_0 = 539 K (970^0 R); Mach number M = 0.08; free stream velocity u_∞ = 36.6 meters per second (120 ft/sec).

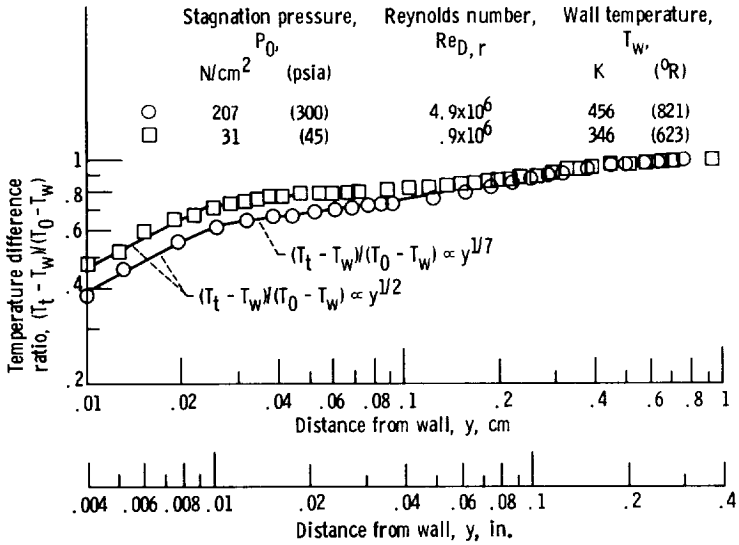

Figure 13. - Effect of Reynolds number (stagnation pressure) on temperature profiles near throat of 30^0 - 15^0 nozzle operating with 16.51-centimeter- (6.50-in.-) diameter cooled inlet (inlet 3, table I). Free stream stagnation temperature T_0 = 539 K (970^0 R); Mach number M = 1.3.

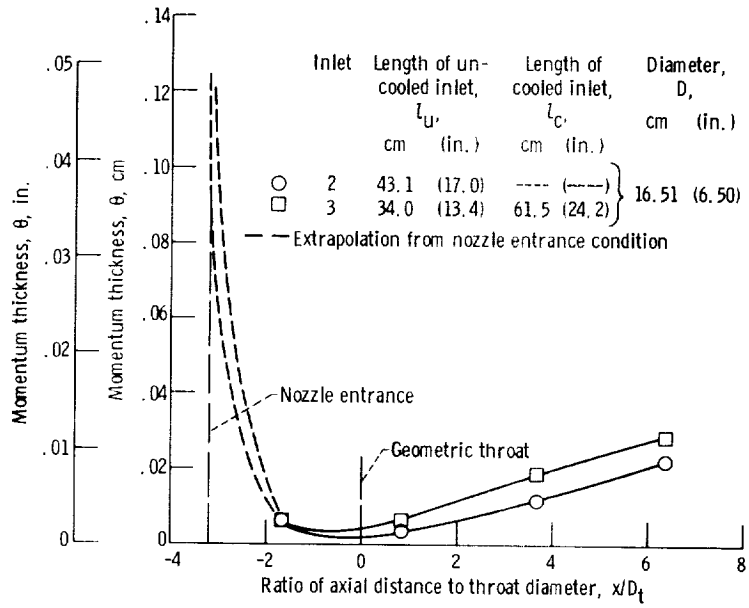

Figure 14. - Momentum thickness distributions in 30^0 - 15^0 nozzle. Free stream stagnation pressure P_0 = 207 newtons per square centimeter (300 psia); free stream stagnation temperature T_0 = 539 K (970^0 R); contraction area ratio ϵ_c = 18.98.

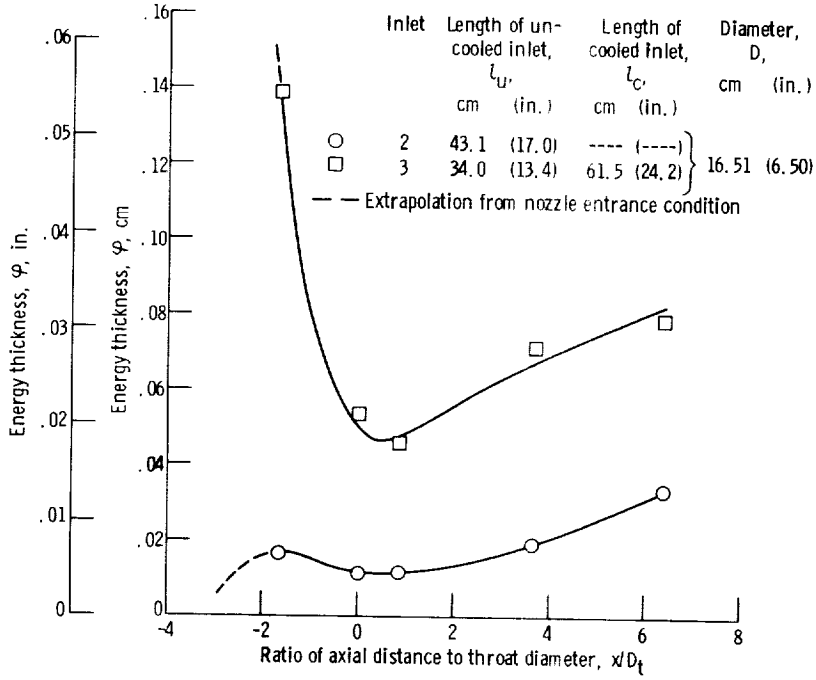

Figure 15. - Energy thickness distributions in 30^0 - 15^0 nozzle. Free stream stagnation pressure P_0 = 207 newtons per square centimeter (300 psia); free stream stagnation temperature T_0 = 539 K (970^0 R); contraction area ratio ϵ_c = 18.98.

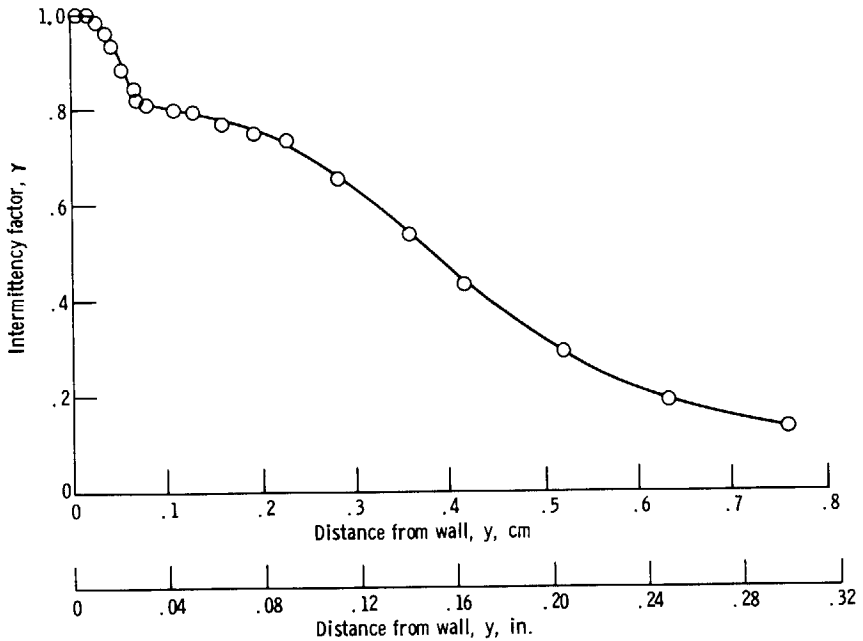

Figure 16. - Distribution of intermittency factor in 30^0-15^0 nozzle operating with 16.51-centimeter- (6.50-in.-) diameter uncooled inlet (inlet 2, table I). Free stream stagnation pressure P_0 = 207 newtons per square centimeter (300 psia); free stream stagnation temperature $T_0 \approx 305$ K (550^0 R); Mach number M = 0.08; contraction area ratio ϵ_c = 18.98.

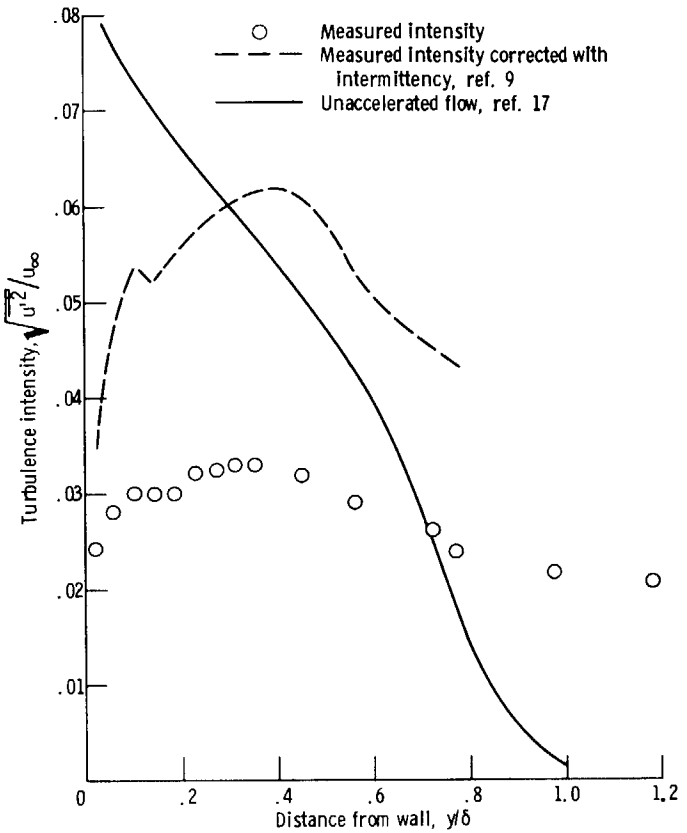

Figure 17. - Distributions of turbulence intensity in 30^0-15^0 nozzle operating with 16.51-centimeter- (6.50-in.-) diameter uncooled inlet (inlet 2, table I). Free stream stagnation pressure P_0 = 207 newtons per square centimeter (300 psia); free stream stagnation temperature $T_0 \approx 305$ K (550^0 R); Mach number M = 0.08; velocity boundary layer thickness δ = 0.061 centimeter (0.024 in.); contraction area ratio ϵ_c = 18.98.

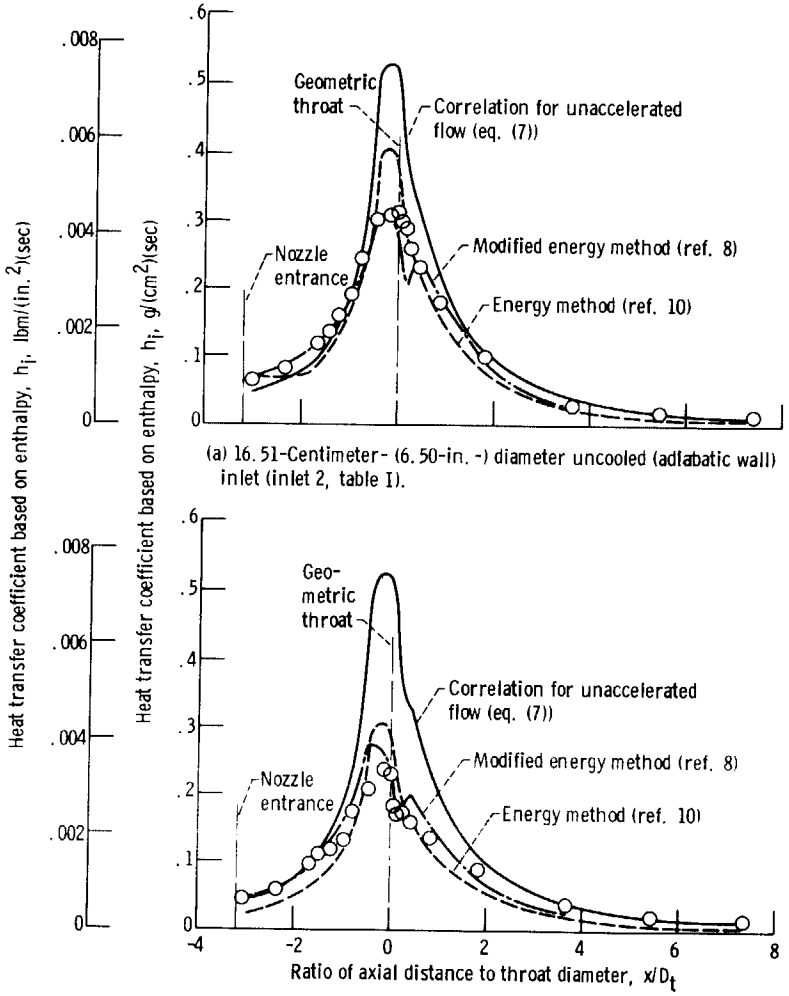

(a) 16.51-Centimeter- (6.50-in. -) diameter uncooled (adiabatic wall) inlet (inlet 2, table I).

(b) 16.51-Centimeter- (6.50-in.) diameter cooled inlet (inlet 3, table I).

Figure 18. - Comparison of predicted and experimental heat transfer in 30° - 15° nozzle. Free stream stagnation pressure P_0 = 207 newtons per square centimeter (300 psia); free stream stagnation temperature T_0 = 539 K (970° R); throat diameter D_t = 3.790 centimeters (1.492 in.); contraction area ratio ϵ_c = 18.98.

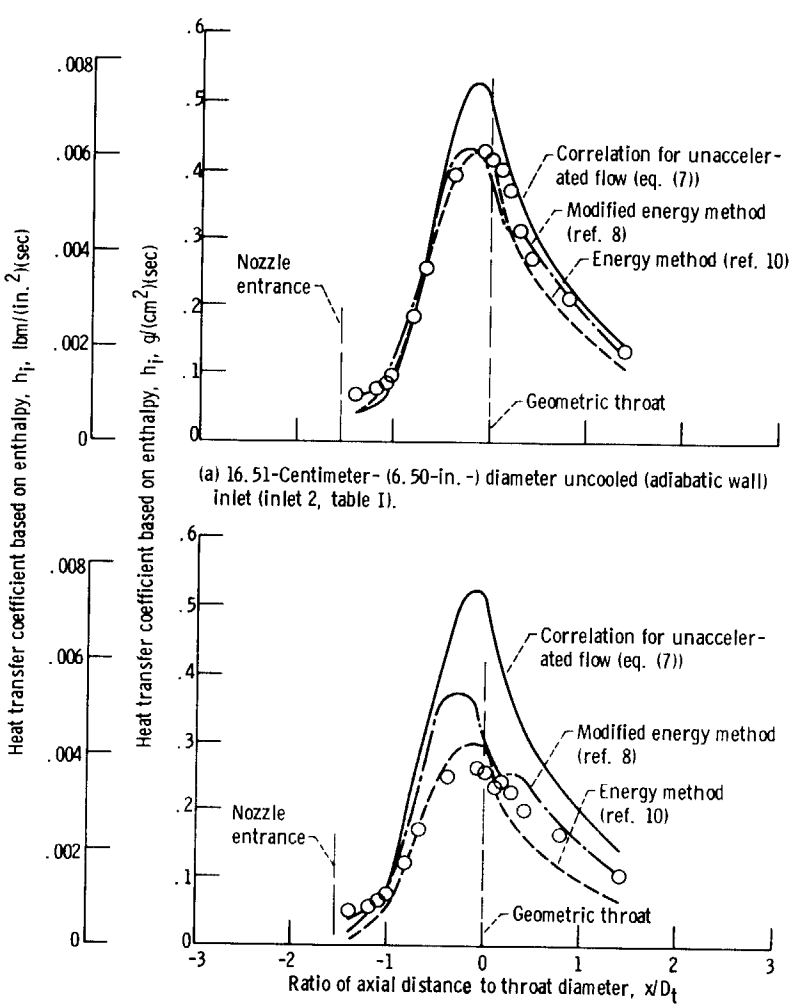

(a) 16.51-Centimeter- (6.50-in. -) diameter uncooled (adiabatic wall) inlet (inlet 2, table I).

(b) 16.51-Centimeter- (6.50-in.) diameter cooled inlet (inlet 3, table I).

Figure 19. - Comparison of predicted and experimental heat transfer in 60° - 15° nozzle. Free stream stagnation pressure P_0 = 207 newtons per square centimeter (300 psia); free stream stagnation temperature T_0 = 539 K (970° R); throat diameter D_t = 3.807 centimeters (1.499 in.); contraction area ratio ϵ_c = 18.80.

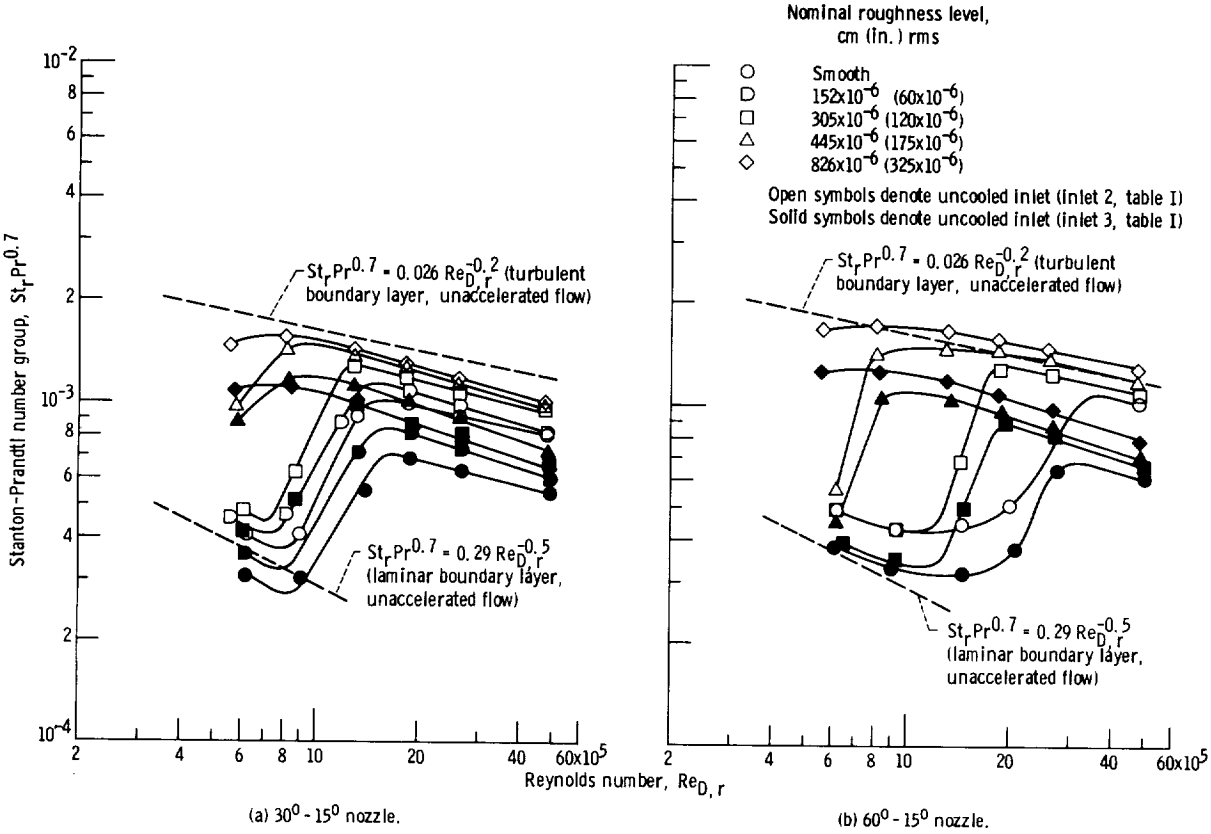

Figure 20. - Effect of surface roughness on throat heat transfer in tests with uncooled (adiabatic wall) and cooled inlets. Free stream stagnation temperature T_0 = 539 K (970° R); contraction area ratio $\epsilon_c \approx 19$.